Mechanisms of Chain Exchange in Block Copolymer Micelles

A DISSERTATION
SUBMITTED TO THE FACULTY OF THE GRADUATE SCHOOL
OF THE UNIVERSITY OF MINNESOTA
BY

Jie Lu

IN PARTIAL FULFILLMENT OF THE REQUIREMENTS
FOR THE DEGREE OF
DOCTOR OF PHILOSOPHY

Timothy P. Lodge and Frank S. Bates, Advisors

November 2015

Acknowledgements

The past five years of graduate study and life at Minnesota have been the most unforgettable and invaluable experience to me. I owe great many thanks to many people, without the support and companion of whom this thesis could never be possibly accomplished.

First of all, I want to thank my advisors, Prof. Tim Lodge and Prof. Frank Bates. Five years ago, I started with this project, knowing only very little of it. It was Tim and Frank who gave me a lot many helpful advises, and guided me through with their distinguished knowledge and experiences. Despite of the obstacles and unsolved questions I have met, my advisors have always been enthusiastic, positive, and encouraging. From them I gained not only numerous knowledge, experiences and skills of polymer research, but also the right attitude towards science and research, as well as the independency and team-work spirit. I feel the experience working with them will benefit the rest of my life.

In addition, I want to thank my colleagues, for the helpful discussions, the assistance with experiments, as well as the casual talks. Jingwen Zhang and Sangwoo Lee trained me on anionic polymerization. Carmelo Declet-Perez and Brian Habersberger taught me hydrogenation. Joe Lott, John Mcallister, Sara Arvidson, Peter Schmidt, Tim Gillard, Rob Hickey, Ron Lewis, Matt Iwin, Lucas McIntosh, Can Zhou, Yu Lei, Yuanyan Gu, Tuoqi Li, Boxin Tang, Yiming Zeng, Yuanchi Ma, En Wang, and others helped me with SANS/SAXS experiments and data analysis. Soonyong So helped me with cryo-TEM imaging. I appreciate the discussions with current and past group members, including the names above, and Sipei Zhang, Karen Haman, Tessie Panthani, Zaifei Wang, Sangwon Kim, Intaek Lee, Luca Martinetti, Chris Thurber, Sid Chanpuriya, Jun Xu, Ralm Ricate, Ajay Vidyasagar, and many others.

I am grateful for the financial support from Infineum. I thank the scientists at NIST, Oak Ridge National Lab, and Argonne National Lab for their help with SANS and SAXS experiments.

Besides research, I had a wonderful time with my friends in Minnesota. The moments we shared together are one of the best things I had when I look back.

Finally, I want to offer special thanks to my parents. Over the thousands of miles distance, their love, understanding, and encouragement are the most supportive. This project would not have been possible without them.

To My Family

Abstract

Mechanisms of equilibration in block copolymer micelles were investigated in detail using time resolved small angle neutron scattering (TR-SANS). The model polymers used in this study were polystyrene-*b*-polyethylenepropylene (PS-PEP) diblock copolymers and corresponding triblock copolymers (PS-PEP-PS, PEP-PS-PEP). When dissolved in squalane, the polymers self assembled into spherical micelles with the PEP blocks forming the solvated coronas, and undiluted PS blocks as the micelle cores. Normal and selectively deuterated equivalent polymers with controlled molecular weight, narrow molecular weight distribution and composition were synthesized by anionic polymerization of styrene and isoprene followed by the selective saturation of the polyisoprene blocks. The structure of polymer micelles were characterized using dynamic light scattering (DLS) and small angle X-ray scattering (SAXS). A contrast matching strategy was employed for the TR-SANS experiments, where separately prepared deuterated and protonated micelles were mixed at equal volume fractions in a solvent containing 42 vol% h-squalane and 58 vol% d-squalane. Chain exchange reduces the mean contrast of the micelle cores in the solvent mixture, thus reducing the SANS scattering intensity, providing a method to characterize the dynamics of the process as a function of time.

In this thesis, several aspects of chain exchange mechanisms were investigated. The hypothesis of hypersensitivity of chain exchange rate to the core block length, and the single chain exchange mechanism, were first tested and confirmed in the PS-PEP model micelle system. The chain exchange mechanisms in PEP-PS-PEP and PS-PEP-PS micelles were then investigated, and a remarkable effect of molecular architecture on the chain exchange rate is documented. In addition, this study explores the facilitating role of the corona chains in molecular exchange. It was found that adding PEP homopolymers of size comparable to the PEP blocks into dilute PS-PEP micelle solutions can significantly retard the chain exchange rate. Decreasing the corona block fraction in the PS-PEP polymers also

reduced the chain exchange rate, and the concentration dependence of the chain exchange relaxation time constant. Finally, we extended our scope to chain exchange between micelles away from equilibration, *i.e.*, micelle hybridization of two populations of PS-PEP micelles of different sizes. The results of this work suggested quantitatively different mechanisms when the micelle systems are away from equilibration, and a concentration effect was found, even when the micelles are still dilute.

Table of Contents

List of Tables

List of Figures

Chapter 1.

Introduction and Background

1.1 Introduction

Block copolymers are macromolecules composed of two or more chemically distinct chains (blocks) of homopolymers, which are linked together by covalent bonds. Due to the immiscibility between the blocks, block copolymers tend to undergo phase separation.[1] As the chemical links between blocks prevent macroscopic phase separation, microphase separation is often observed. The situation is different when solvent is present. Due to differences in polymer-solvent interactions between segments, block copolymers in solution can self-assemble into a variety of structures.[2,3] In the simplest case where the polymers contain only two distinct A and B chains (*i.e.*, an AB diblock copolymer) with A being the solvent favorable block (*i.e.*, $\chi_{SA} < \chi_{SB}$), micelles can form with relatively undiluted compact B blocks in the core surrounded by a corona of solvated A blocks. Here the polymer-solvent interaction parameter χ is defined as the exchange energy one needs to pay by substituting one site occupied by polymer segment with solvent molecule, on the Flory Huggins lattice,[4,5] normalized by the thermal energy kT. According to the Flory Huggins theory, [4,5] the mixing free energy per segment of a solution of a polymer of N segments and volume fraction φ is expressed as: $\varphi/N \times \log(\varphi/N) + (1-\varphi) \times \log(1-\varphi) + \chi\varphi \times (1$

– φ). In this mean-field description of polymer-solvent interactions, χ measures the strength of repulsive interactions between polymer and solvent segments. A smaller χ thus indicates a relatively favorable interaction. Figure 1.1 schematically illustrates the formation of a spherical micelle by the self-assembly of A-B diblock copolymers in a selective solvent, in which the red and blue chains represent the A and B blocks.

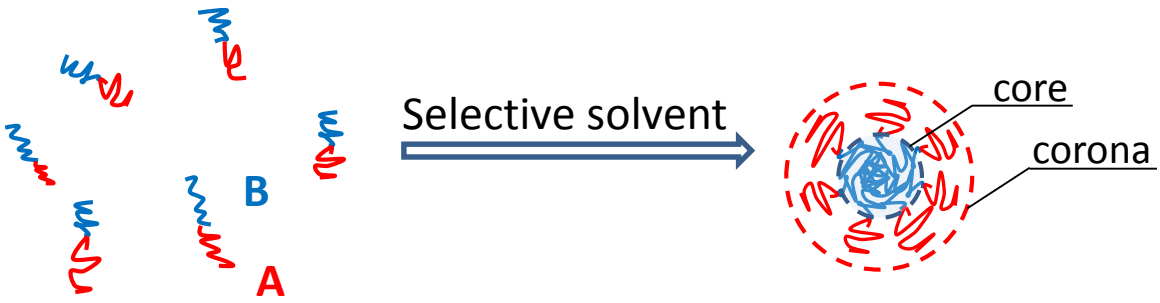

Figure 1.1. Micelle formation of A-B diblock copolymers in a selective solvent. Core and corona regions are shown as dashed circles with the same color as the corresponding blocks.

Block polymer micelles offer a host of applications including drug delivery,[6,7] viscosity modification,[8,9] toughening of plastics,[10,11] and colloidal and polymer blend stabilization.[12,13] In all these cases, chain exchange plays a vital role in establishing the self-assembled structure, including the approach to the equilibrium state, and micelle kinetic stability. Compared to typical alkyl tail surfactants (-C_nH_{2n+1}, with $n \approx 6$–20), the thermodynamic barrier to extracting a core block from a typical block copolymer micelle ($N_{core} \approx 50$–1000) can be proportionately larger. Consequently, kinetically frozen micelles, also known as path-dependent or nonergodic micelles, are commonly observed in these systems.[14–18] Understanding this molecular exchange process not only provides better insight into micelle structures, but also helps future application studies. Much less work has been done on the chain exchange mechanisms in block copolymer micelles, however, compared to the structures of block copolymer micelles, or the chain exchange between

small molecule surfactants.[19,20] Therefore this thesis mainly focuses on establishing a quantitative understanding of chain exchange kinetics in block copolymers near equilibrium.

The thesis is composed of 8 chapters. The next section in this chapter includes a literature review of micelle structure and chain exchange kinetics studies, with an emphasis on the experimental approaches. Chapter 2 describes the experimental techniques and procedures used to synthesize and characterize the polymers used in this thesis research, as well as those used to characterize micelle structure and equilibration mechanisms. Chapters 3, 4, 5, 6 and 7 each focuses on one set of experiments designed to investigate one specific aspect of chain exchange mechanism. Chapter 8 summarizes the thesis research and propose several future directions of this research project. Other related experimental results are presented in the Appendix.

1.2 Background: Formation and Structure of Block Copolymer Micelles

This section provides a concise overview of the formation and structure of block copolymer micelles, including a consideration of different experimental techniques used, as well as a more detailed literature review of the kinetic studies of block copolymer micelles near equilibration. Here we will emphasize on the experimental approaches for both, which are the primary concern of this thesis research.

Micelle Formation, Thermodynamics, and Structure Overview

Block copolymer micelles are aggregates of amphiphilic block copolymers in a selective solvent. Detailed reviews on the formation and structure of block copolymer micelles are available.[3,21–23] Briefly, the soluble block(s) are swollen by the solvent and form the micelle corona, while the insoluble blocks(s) collapse[24] to form a compact micelle core. Certain conditions are required for the formation of block copolymer micelles. Most

micelles in organic solvents have an upper critical micellization temperature (UCMT, driven by the positive temperature dependence in the χ between the insoluble block(s) and the solvent), above which micelles will dissolve into free chains. For aqueous micelle solutions, on the other hand, a lower critical micellization temperature (LCMT) often exits, and the micelles would dissolve below the critical temperature. The critical micelle concentration (CMC) is the concentration threshold for polymers to aggregate and form micelles. Below this concentration, there are only free chains dissolved in the solvent. Above a certain concentration, polymer micelles will overlap and interact with each other, leading to the close packing of micelles. In the simplest case of spherical micelles, usually BCC (body centered cubic), FCC (face centered cubic), or HCP (hexagonally close-packed) crystal structures are observed. These ordered structures will melt above the so-called order-disorder-transition temperature (T_{ODT}). Those temperature and concentration boundaries thus define the phase diagram of block copolymer micelles.

The simplest yet most commonly seen morphology of micelles is a sphere. As illustrated in Figure 1.2, one spherical micelle can be roughly divided into three parts: a compact spherical micelle core composed of collapsed solvent unfavorable blocks with radius R_{core}, a swollen corona composed of radially distributed solvent favorable blocks with a thickness L, and the interfacial layer between the micelle core and corona with a thickness σ_{int}. The number of polymer chains within a micelle is called the aggregation number N_{agg}. When $R_{core} << L$, as shown in Figure 1.2a, the micelle is called a "hairy" or "star-like" micelle. If instead, $R_{core} >> L$ as shown in Figure 2b, it is called a "crew-cut" micelle.[25]

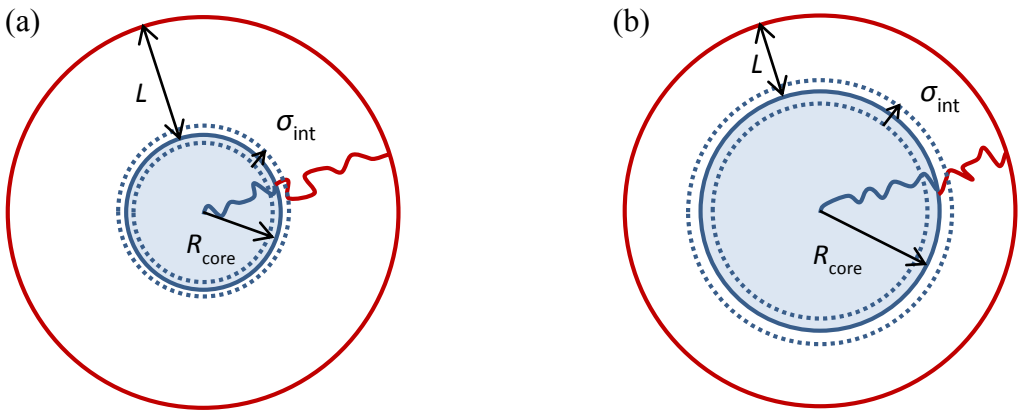

Figure 1.2. (a) Hairy and (b) crew-cut spherical micelles composed of diblock copolymer chains. The blue chain (filled circle) represents micelle core blocks B (region). The red chain (open circle) represents micelle corona blocks A (region). The dashed circles describe the interfacial layer between core and corona, which is influenced by the Flory-Higgins interaction between core and corona blocks within the solvent.

A number of theoretical studies have been done in order to establish the connection between polymer / solvent characteristics, and polymer micelle structures, especially for spherical micelles formed by linear diblock copolymers. These studies can be roughly divided into two categories, according to their methodology: those based on the scaling concepts derived from De Gennes,[26] and the others based on the mean-field theories first developed by Noolandi and Hong,[27] Leibler *et al.*,[28] Nagarajan and Ganesh[29] and Hurter *et al.*[30] In general, the total Gibbs free energy of micelle ΔG_{tot} is contributed by three parts:

$$\Delta G_{tot} = \Delta G_{core} + \Delta G_{corona} + \Delta G_{interface} \qquad (1.1)$$

Minimization of ΔG_{tot} leads to the development of different theories that correlate polymer and micellar characteristics such as the micelle core radius R_{core}, the aggregation number N_{agg}, and the corona thickness L. Detailed reviews of theoretical studies on this topic are available.[31,32]

For polymer micelles in selective organic solvents, both ΔH and ΔS in $\Delta G_{tot} = \Delta H - T\Delta S$ are negative. Here the negative ΔH mainly results from the formation of micelle cores, which is an exothermic process due to the favorable interaction between core blocks than that between one core block and solvent. The negative ΔS, on the other hand, arises from the arrangements of core and corona blocks in the micelles. Therefore as temperature increases, ΔG_{tot} also increases and the micelle system would experience a UCMT, as mentioned above. For the micellization in aqueous solution and some ionic liquids,[33–35] however, an LCMT is often observed. One typical example is PEO-PPO-PEO (poly(ethylene oxide-*b*-propylene oxide-*b*-ethylene oxide)) block copolymers in water,[36] whose LCMT phase behavior was attributed to the conformational change of the polymer as induced by the changes in hydrogen bonding when temperature increases.[37,38]

The formation of block copolymer micelles thus is analogous to classical small molecule surfactants. However, due to the complex architecture, dynamics, as well as the large molecular weights of polymer chains, block copolymer micelles offer more possibilities in their structure and functionality than small molecule surfactants. In addition to spherical micelles composed of non-ionic linear diblock copolymer chains as showed in Figure 2, some other amphiphilic polymers can also form micelles under an appropriate condition. For example, novel micelle structures can form by the self-assembly of polymers with non-linear structures such like cyclic[39] or highly branched[40] polymers under certain conditions. In addition, block copolymer micelles with electrolyte coronas are interesting candidates that are stimuli-responsive to pH and salt concentration.[41,42] Complexation of anionic amphiphilic block copolymers with DNA or drugs can also serve an promising direction for targeted gene therapy or drug delivery.[6,43–45] On the other hand, simply adding one more block C onto the diblock copolymer A-B (with A being the solvent favorable block) could greatly increase the flexibility in micelle structure. For example, when the interaction between the C block and solvent, χ_{SC}, is responsive to temperature or pH change,

the resulting polymer micelle structure is responsive as well. Typical examples of such block copolymer micelles mainly based on PNIPAM (poly(N-isopropyl acrylamide) have been described by different authors.[46–49] Due to the LCST behavior of the PNIPAM block in a block copolymer such like PEO-PNIPAM and PEG-PNIPAM (with PEG being the abbreviation of poly(ethylene glycol)) in water, the corresponding micelles form and dissolve at the CMT of the PNIPAM block. Such thermo-reversible micellization (or gelation for certain polymers) has drawn quite an amount of interest, as the LCST of PNIPAM in water is close to body temperature and tunable as well. In general, when the C block is soluble, it together with A form the micelle corona. When the C block is insoluble, it together with B forms a micelle core, and possibly molecular bridges between micelles, which could potentially lead to micelle networks and gelation.

Micelle Morphology Transition

The complexity of block copolymer micelles lies not only in the numerous types of composing polymers, but also in the fact that the morphology of micelles can be conveniently tuned by changing polymer composition or solvent selectivity without altering other characteristics of the polymer. Increasing the core block fraction in a block copolymer generally leads to morphology change from spherical micelles to cylindrical/worm-like micelles and to bilayer vesicles. This trend, as a direct consequence of the impressibility of polymer chains in the liquid state, is consistent with that for small molecule surfactants.[50] This consideration can be quantified with a dimensionless group, known as the packing parameter P, given by $P = V_{core} / (a_{int} \times l_{core})$. Here V_{core} is the volume of solvophobic core per chain, a_{int} is the interfacial area between the core and corona per chain, and l_{core} is the effective length of the core block in the liquid state. l_{core} sets a rough upper limit on the effective length of the chain, *i.e.*, large extensions beyond this limit may prevent the collection of hydrocarbon chains from being considered a liquid. For spherical

micelles, the critical packing shape (the shape defined by the core region occupied by one core block and the interfacial area per chain, see Figure 1.3a) is a cone, and therefore *P* must be less than 1/3 for the polymers to remain in spherical packing. Upon increasing the core block content in the polymers, the core blocks in the micelle core become crowded. Since the core blocks are incompressible, the interfacial area per chain must decrease to allow for more room in the core per chain, by reducing the room in corona per chain. This leads to an increase in *P* and decrease in interfacial curvature, or in other words, the morphology transition from spheres to cylinders. Similarly, increasing the core block length even more would result in the transition from cylinders to bilayer vesicles, and probably inverse micelles. He *et al.*[51] investigated micelle morphology of four amphiphilic poly((1,2-butadiene)-*b*-ethylene oxide) (PB−PEO) diblock copolymers in an ionic liquid, 1-butyl-3-methylimidazolium hexafluorophosphate ([BMIM][PF6]). Direct observation of micelle morphology transitions was made using cryogenic transmission electron microscopy (cryo-TEM), by varying the length of the corona block while holding the core block constant. The correlation of packing parameter, packing shape, and observed micelle phase transition by the authors are reproduced in Figure 1.3b.

Another factor that influences micelle morphology is solvent selectivity. Increasing solvent selectivity increases surface tension, and thus decreases interfacial area per chain, which eventually leads to the morphology transformation from spheres to cylinders and to bilayer vesicles. Solvent selectivity can be conveniently tuned by adding a co-solvent, or by changing the temperature to change the Flory-Huggins interaction parameter χ between solvent and polymer. Figure 1.3c shows cryo-TEM images corresponding to a typical phase transition in block copolymer micelles induced by changing solvent selectively, adapted from Bang, Lodge and co-workers.[52] The authors used an asymmetric poly(styrene-*b*-isoprene) diblock copolymer dissolved at 1 vol% in a series of solvents with varying selectivity for styrene: dibutyl phthalate (DBP), diethyl phthalate (DEP), and dimethyl

phthalate (DMP). The degree of solvent selectivity was adjusted by mixing DBP/DEP and DEP/DMP in various proportions. With increasing solvent selectivity, the predominant micellar shape changes from spheres to cylinders to vesicles, reflecting the changing interfacial curvature.

Interestingly, many studies of micelle morphologies reveal the non-ergodicity (path dependence) in polymer micelles. Won et al. investigated micelle structures composed of PEO based linear diblock or triblock copolymers in aqueous solution.[15] Via controlled polymer synthesis they studied the dependence of micelle structure on the molecular characteristics of the polymers. Different micelle morphologies (spheres, cylinders, vesicles, and many hybridized structures) were found to coexist near the boundaries of micelle morphology transition conditions. This phenomenon was attributed to the slow kinetics of micelles. Similar polymers were also shown to undergo no exchange in ionic liquids, even at temperatures as high as 200 ºC.[16] This topic will be discussed in more detail in Section 1.3.

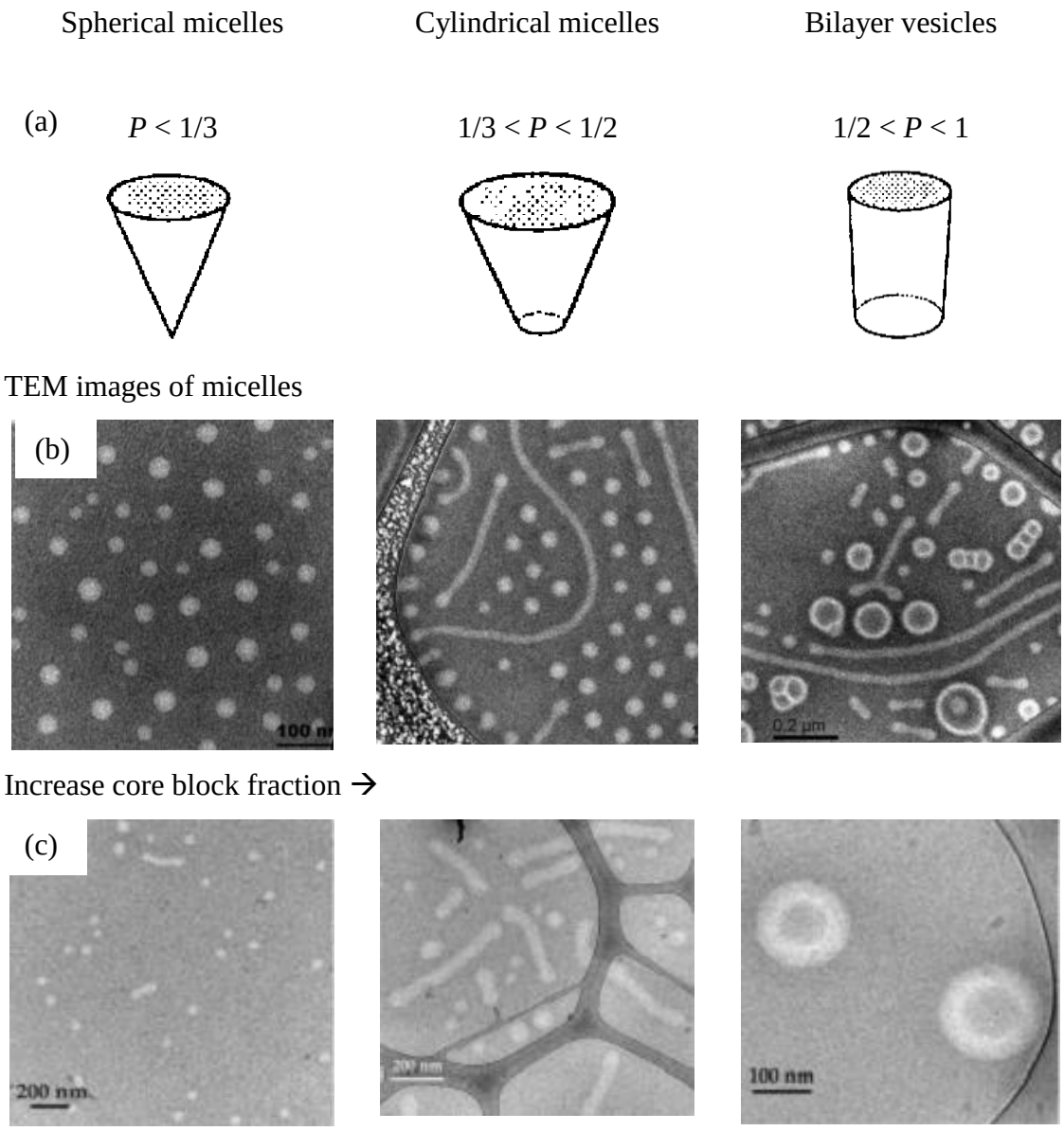

Figure 1.3. (a) Critical packing parameter *P* and packing shape for spherical micelles, cylindrical micelles and bilayer vesicles correspondingly.[50] Transmission electron microscopy (TEM) images of block copolymer micelles in an increasing order of polymer (b) core block fraction[51] and (c) solvent selectivity.[52]

Experimental Techniques

Experimentally, the micelle structure parameters can be characterized with several techniques, which can be generalized into two categories: direct imaging with microscopy, and indirect observation with scattering techniques. This section will discuss briefly the pros and cons of these techniques. To obtain a reliable quantitative evaluation of micelle structure parameters, the combined use of different techniques is necessary. Detailed experimental operations and theoretical basis of these techniques will be covered in Chapter 2.

Using transmission electron microscopy (TEM) or cryo-TEM for liquid samples, micelle size and shape can be observed. Transmission electron microscopy (TEM) is a technique in which a beam of electrons is transmitted through an ultra-thin specimen, interacting with the specimen as it passes through. It operates at the same principle as a light microscope except that electrons are used instead of light, and thus contrast in a TEM image comes from electron density difference within the sample. Due to the much smaller wavelength of electron beams, TEMs are capable of imaging at a significantly higher resolution than light microscopes. As a method of direct observation of micelles, this technique has been widely applied to study spherical or non-spherical micelles, in both aqueous solution and organic solvents, and even in polymer melts. Some typical cryo-TEM images of micelle solutions are shown in Figure 3b and c. The interpretation of micelle structure based on the TEM images is straightforward, and does not reply on any assumption about micelle morphologies, which is an advantage over all the scattering techniques. The limitations of this technique are also obvious. Firstly and most importantly, TEM images only reflect micelle morphologies in localized regions, which could vary across the specimen. It is thus necessary to take multiple TEM images in different regions of the specimen. Secondly, for block copolymers containing only carbon and hydrogen, the electron density is low, and thus limits the image contrast. One way to improve this

situation is to use preferential staining,[53] in which a staining agent with high electron density (*e.g.* RuO_4 and OsO_4) stains selectively on the micelle cores / coronas, and thus improves in the image contrast. Thirdly, sample preparation usually requires more time and practice in TEM, and especially cryo-TEM, where liquid state solutions are freezed to produce a thin film of vitrified sample on the holding grid, than other scattering experiments.

Scattering techniques, including dynamic light scattering (DLS), static light scattering (SLS), small angle neutron scattering (SANS) and small angle X-ray scattering (SAXS) are the other category of commonly used methods to investigate micellar structures in solution. A typical experimental setup for light scattering experiments (Figure 1.4a) and neutron / X-ray scattering experiments (Figure 1.4b) are illustrated schematically. Briefly, an incident beam (light, neutrons, or X-ray) is scattered by particles (or micelles) in the samples and the scattered beam from different scatterers or inner structure of one scatter interference with each other to generate a specific scattering intensity, which is a function of the observation angle θ. The scattering intensity is thus a reflection of the size, shape, optical properties, and as well as the relative position of the scatterers. Mathematical models are available to connect the observed scattering intensities with these properties for some systems, micelles, as an examples.[54–56] Therefore scattering techniques, compared to microscopy techniques such as TEM, are indirect investigations of sample microstructures: pre-assumptions of sample microstructures (*e.g.* micelle morphologies in solution, or crystal structures) are often necessary. On the other hand, scattering experiments are capable of providing averaged structure information across a sample, compared to the local information a TEM image can provide. The sample preparation is simpler than that in a TEM experiment.

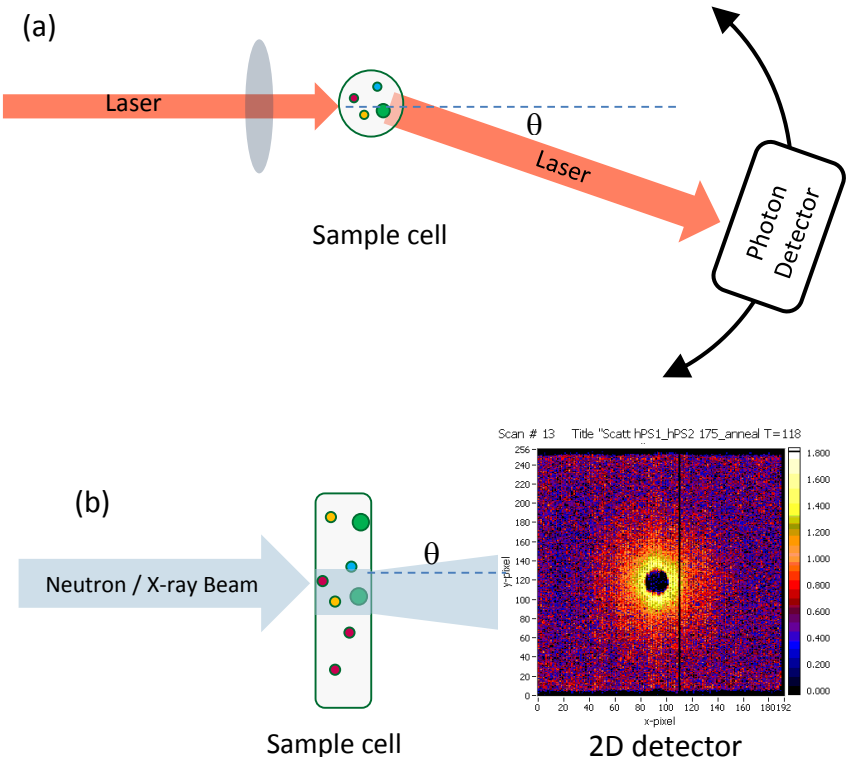

Figure 1.4. (a) Schematic top view of a typical light scattering instrument using a movable 1 D detector, which shows different components and the definition of θ. A sample tube containing a dilute solution of scatterers is also shown, where the filled small circles of different colors represent the particles (micelles). (b) Schematic side view of a typical neutron or X-ray scattering experiment using a static 2D detector. A sample 2D neutron scattering pattern of dilute micelle solution is included, which was taken in one SANS experiment at the Oak Ridge National Laboratory, Oak Ridge, Tennessee. The scattering angle θ and the solution in sample cell are illustrated in the same way as in Figure 1.4(a).

While both DLS and SLS use laser light as the incident beam, the way the scattering intensity is analyzed is different between them. In SLS, the time-averaged total intensity is measured as a function of the scattering angle. The molecular weight and a characteristic linear dimension of the particle may be determined for some systems from SLS, and therefore information on the internal structure and shapes of the particles as well as interparticle structure can be deduced.[57–59] In contrast, in DLS the temporal variation of the scattering intensity is measured and is represented usually through what is known as the

intensity autocorrelation function. The diffusion coefficients of the particles, particle size, and size distribution can be deduced from such measurements.[60–62] To acquire reliable results, it is often necessary to avoid multiple scattering by using dilute solutions of scattering particles (micelles) in a standard static or dynamic light scattering experiment. Detailed reviews on light scattering techniques and data analysis are available.[63–65]

When X-ray or neutrons are used in place of light as the incident beam, multiple scattering can be avoided, and in addition, because of their smaller wave length, detailed structure at shorter length scales can be probed. As a result, small angle X-ray and neutron scattering have become valuable adjuncts to light scattering in block copolymer micelles.[54,55,66] The scattering intensity in a SAXS experiment is proportional to the square of electron density difference between scatterers and their surroundings. For organic materials containing only carbon, hydrogen, oxygen and nitrogen, the electron density difference is usually not significant, which limits the application of SAXS in some amorphous polymer systems. The scattering intensity of SANS, on the other hand, depends rather on the scattering length density ρ difference (*i.e.* the contrast) between scatterers and their surroundings, which is determined by the interaction of the nuclei of each atom and the neutrons. As a result, isotopes, such as hydrogen and deuterium atoms possess different scattering length densities. Therefore by simply varying the isotope content in scattering objects or solvent molecules the contrast and thus scattering intensity can be tuned. In addition, this allows for the so-called "contrast matching" for complex structures. For some core-shell structured micelle systems, the scattering length density of solvent can be tuned by mixing with isotope equivalents (*e.g.* D_2O) within a certain range to contrast match either the micelle cores or coronas, which allows for an individual and thus more precise evaluation of the core and corona dimensions. Alternatively, this idea can be applied to time-resolved SANS experiments to monitor dynamic phenomena, such as the

equilibration dynamics in micelles, in a quantitative way. This will be discussed in more detail in Chapter 2.

1.3 Background: Equilibration in Block Copolymer Micelles

Compared to the structure of block copolymer micelles, there are significantly smaller number of studies on their dynamic process. Due to the relatively long chains being subject to additional thermodynamic and dynamic constraints (*e.g.*, entanglements, crystallinity, vitrification), block copolymer micelles exhibit significantly slower equilibration kinetics than small molecule surfactants.[2,3,15] As a result, unlike the exchange kinetics between small molecule surfactant micelles that has been intensively studied decades ago,[19,20] certain details of the mechanism(s) of equilibration in block copolymer micelles remain unclear. Understanding the block copolymer molecular exchange process represents a critical step in establishing a unified approach to dealing with self-assembly of amphiphiles of all sizes, from classical small surfactants[67] and lipids[68] progressing up in molecular weight through the enormous parameter space afforded by macromolecular architectures.[69] This section will provide a literature review of the progress made in understanding the mechanisms of block copolymer micelle equilibration, both theoretically and experimentally. We will go from the facts already known about micelle kinetics to the unknowns.

Two Chain Exchange Mechanisms

Two primary mechanisms have been addressed for micelle equilibration kinetics: unimer exchange or single chain extraction-diffusion, and micelle fusion/fission (Figure 1.5). The first attempt to investigate micelle kinetics was made by Aniansson and Wall,[19,70] with dilute low molecular weight surfactant solution. Due to steric hindrance, only the

unimer exchange mechanism was initially considered. The other mechanism, micelle fusion/fission, was later re-examed by Kahlwei, Lessner, and Teubner.[71,72]

(a) Unimer exchange, or single chain extraction-diffusion

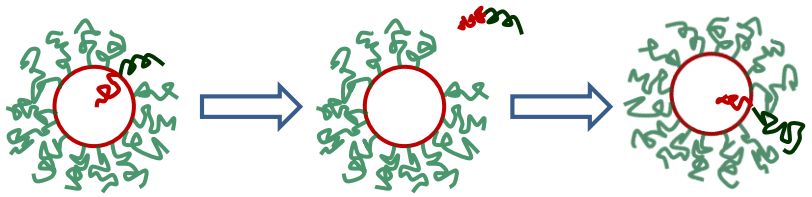

(b) Micelle fusion/fission

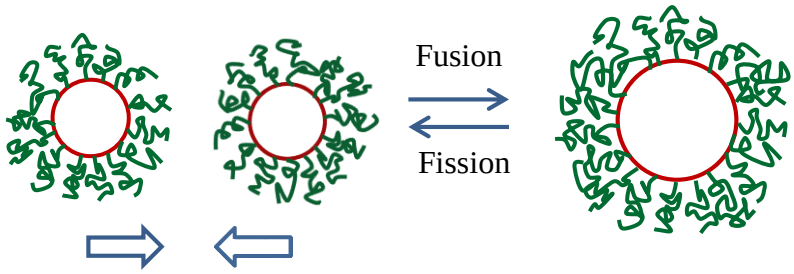

Figure 1.5. Two primary mechanisms of molecular exchange: (a) unimer exchange, and (b) micelle fusion/fission.

Later on, Halperin and Alexander[73] examined exchange kinetics of block copolymer micelles and claimed that the Anniasson-Wall model also applies in the macromolecular case for both star-like and crew-cut micelles. The authors argued that the exchange process is unimer exchange mechanism dominated, and that the primary energy barrier to overcome comes from exposing the collapsed core block to the corona/solvent matrix. Accordingly, a unimolecular rate constant k was expressed as a single exponential decay where the enthalpic penalty term is reflected by $N_{core}^{2/3}\gamma a^2$, with γ being the interfacial tension between core blocks and the matrix, and a being the monomer size. The authors also

suggest that the slight chain stretching of corona blocks in block copolymer micelles, especially the star-like micelles where the corona region is significant, could possibly act as an accelerating component in the chain extraction step (see Figure 1.5a).

On the other hand, Dormidontova[74] studied the kinetics of micelle evolution in block copolymer micelles using a scaling approach, and also concluded that single chain exchange is favored over micelle fusion/fission when the system is close to its equilibrium state. Furthermore, micelle equilibration rates in different systems have been experimentally observed to be largely independent of micelle concentration within the dilute regime,[75–78] suggesting that micelle fusion/fission is insignificant. By assuming single chain exchange, fitting models have been established and successfully described the relaxation kinetics in block copolymer micelles.[76,77,79–83] In agreement with this, a recent fluorescence study[84] found that the micelle fusion/fission rate is 10^6 times slower than chain expulsion-insertion in symmetric triblock copolymer (poly(ethylene oxide-*b*-propylene oxide-*b*-ethylene oxide)) micelle solutions. In addition, our TR-SANS study of the chain exchange kinetics in hybridized micelles have conclusively demonstrated the single chain exchange mechanism, which will be discussed in detail in Chapter 4.

Experimental Approaches

The earliest attempt to characterize chain exchange was to employ size exclusion chromatography SEC.[85–87] The observations of separate peaks for single chains and micelles above certain temperatures provided evidence of chain exchange and insight into micelle formation. However, due to the limitation of the technique itself, no quantitative examination was made.

Many other characterization techniques are documented since then, including fluorescence quenching,[88–94] sedimentation,[95,96] and small angle neutron scattering

(SANS).[75–83,97–100] In kinetic studies, one of the major problems is to match the relaxation timescale with the time range that experimental techniques are capable of observing. Generally speaking, in all of these experiments a detector is used to measure the change of a particular property as a sign of the exchange between differently labeled block copolymer chains. For example, intensity is monitored in fluorescence quench spectroscopy and SANS, and the elution time in sedimentation. In general, it is found that block copolymer micelles exhibit very slow chain exchange rates, and that under many circumstances they are completely frozen.[9,15,89,101,102] This phenomenon can be rationalized by considering the two aspects that limit the chain exchange rate: the kinetic barrier resulted from the glass transition of the core and corona block chains (T_g), and the thermodynamic barrier resulted from the incompatibility between core blocks and the solvent ($\chi_{core/solvent}N_{core}$). Detailed quantitative relations between the polymer / solvent properties and micelle dynamics is, however, not understood.

Fluorescence quenching has been widely used in studying micelle kinetics since the 1990s. This technique requires the use of a pair of equivalent block copolymers tagged with different fluorescent labels, so that the mixing of the labeled chains can induce time dependent fluorescence intensity. Due to the limitation of this technique and the perturbation of the experiment as a result of the florescence tags, many of the reported results are controversial, and no quantitative conclusions were made. For example, the chain exchange process between several different diblock copolymer micelle systems were found to have more than one relaxation time constant,[88,90,91,93,103] assuming the rate of chain exchange follows the same exponential dependence as small molecule surfactants. The reason was not clear and two hypothesis were proposed, one being the bulky fluorescence label,[90,93] while the other being the possible coexistence of micelle fusion-fission together with the single chain exchange mechanism.[104]

Recent TR-SANS Studies and Future Challenges

Time-resolved small-angle neutron scattering (TR-SANS) has recently drawn attention as a clean and universal way of investigating micelle kinetics quantitatively, for it requires only deuterium labeling and accordingly minimizes experimental perturbations. The detailed experimental setup for a TR-SANS experiment in measuring micelle equilibration dynamics will be described in Chapter 2. Applying the TR-SANS technique, Lund et al. quantitatively investigated the equilibrium chain exchange kinetics of a poly(ethylene-*alt*-propylene-*b*-ethylene oxide) (PEP-PEO) micellar system in water/ dimethylformamide (DMF) mixture.[75,78] A broad logarithmic relaxation was observed, with the longest relaxation time consistent with the Halperin and Alexander theory.[73] However, contradictory to this logarithmic relaxation result, the same Halperin and Alexander theory suggests that the chain exchange kinetics in block copolymer micelles should follow the same principle as in small molecule surfactants, *i.e.*, a single exponential relaxation, with the rate constant $k \sim \exp(-E_a / kT)$. A similar logarithmic relaxation decay was found in a hydrocarbon system of PS-PB (poly(styrene-*b*-butadiene)) diblocks and PB-PS-PB triblocks dispersed in n-alkane solvents, which was again not explained sufficiently.[98,105] A standard relaxation function $R(t)$, which describes the relative changes in the concentration of deuterated equivalent polymer chains in the micelles, was introduced by the authors as:[78]

$$R(t) = \left(\frac{I(t) - I(\infty)}{I(0) - I(\infty)} \right)^{1/2} \qquad (1.2)$$

where $I(0)$ and $I(\infty)$ are the scattering intensities of the unmixed core samples and the mixed core samples, respectively, at each value of scattering wave vector q ($q = 4\pi\lambda^{-1}\sin(\theta/2)$).

More recently, Choi *et al.* successfully described the logarithmic relaxation quantitatively by taking into consideration the polydispersity of polymer segments in micelle cores.[76] With the aid of TR-SANS, they studied the molecular exchange between

dilute (1 vol%) poly(styrene-*b*-ethylene-*alt*-propylene) (PS-PEP) diblock copolymer micelles in squalane. They also showed that the data collected at different temperature can be shifted onto an individual $R(t)$ master curve, with a single a_T function, analogous to the WLF equation, which is well-known in rheology.[106,107] The double exponential relaxation function of $R(t)$ (Equation 1.2) was established as:

$$R(t) = \int_0^\infty P(N)K(t,N)dN \qquad (1.3)$$

$$P(N_i) = \frac{z^{z+1}}{\Gamma(z+1)} \frac{N_i^{z-1}}{N_n^z} \exp(-\frac{zN_i}{N_n}) \text{ , and } K(t,N) = \exp\left[-t \frac{6\pi^2 kT}{N^2 b^2 \zeta} \exp(-\alpha\chi N) \right] \qquad (1.4)$$

Here $K(t, N)$ is the time correlation function for the extraction of PS core blocks, where the thermal activation barrier is expressed as $\tau_{\text{Rouse}}\exp(\alpha\chi N_{\text{core}})$, and α is an unknown O(1) prefactor.[108–110] Taking into consideration of the polydispersity, $K(t, N)$ is modified with a Schulz-Zimm distribution function $P(N_i)$, where $z = [(N_w/N_n)\text{-}1]^{-1}$, Γ is the gamma function, N_w and N_n are the weight average and number average degree of polymerization respectively. The two parameters adjusted to obtain best fit are N_w/N_n and $\alpha\chi$. The monomeric friction factor $\zeta(T)$ was estimated to be 1.71×10^{-8} [N×s×m^{-1}],[111] and the statistical segment length b was taken to be 0.67 nm.[112]

This model was developed subject to the following assumptions: (i) single chain expulsion/insertion is the dominant mechanism; (ii) extraction of a core block is the rate limiting step; (iii) motions of the unentangled core blocks are governed by Rouse dynamics; (iv) the energy barrier E_a for ejecting a block copolymer into the solvent/corona matrix is proportional to the core block length. The successful application of Equations 1.2, 1.3 and

1.4 to describe the chain exchange rate in several different block copolymer micelle systems[76,80,81] therefore confirms the hypersensitivity to core block length. There are, yet, more questions left to be answered. In the following few paragraphs, we will discuss several questions that currently remain about micelle chain exchange kinetics, with some of them being explored in the next few chapters.

First, it is not clear how corona blocks are involved chain exchange. If assumption (ii) holds and the activation energy E_a for chain exchange comes soly from the core block / solvent incompatibility, then the corona blocks should not affect chain exchange rate. However, both early theoretical considerations by Halperin[73] and experimental works by Choi *et al.*[79] using TR-SANS measurements suggest the opposite. At an elevated concentration where corona blocks overlap and micelles pack into bcc lattice, Choi *et al.* found the chain exchange rate of PS-PEP in squalane is reduced by approximately one order of magnitude. Since the core block length was not altered, this result suggests that more factors are involved in micelle chain exchange, with the corona overlapping being one possible explanation, as the corona blocks may accelerate the chain extraction process by experiencing a relief of chain stretching upon escaped into the solvent. Following their work, Halperin[113] analyzed this situation theoretically and proposed an alternative explanation: the chain insertion barrier increases due to the enlarged micelle core size and greater corona density, which is a consequence of micelle overlapping. This point is further explored in Chapters 5, 6, and 7.

Second, almost all the current studies have been limited to spherical micelles composed of only diblock copolymers, while the diversity in polymer architecture and micelle morphology has not yet been addressed. As discussed in Section 1.2, block copolymers of complex architecture, such as multi-blocks copolymers, graft or branched copolymers can all form micelles, and depending on the core / corona block ratio as well as the interfacial tension different micelle morphologies can be obtained. Using TR-SANS, Lund and

coworkers compared the molecular exchange dynamics of a PB-PS-PB (10K-20K-10K) triblock copolymer with those of a PB-PS (10K-10K) diblock copolymer in dodecane (C_{12}) and tetradecane (C_{14}), both of which favor the PB blocks.[98] While both solutions were dilute and the polymer micelles had comparable sizes, the triblocks exchanged at a rate about 10 times slower than the diblocks. Another piece of pioneering work by these authors[114] examined the exchange kinetics in block copolymer micelles across the cylinder-to-sphere transition in exactly the same solution and total concentration, by millisecond TR-SANS. A slight but clearly measurable increase in the exchange kinetics of the spherical micelles was found.

Another interesting question is the core block repeat unit N_{core} dependence of E_a. As discussed earlier, according to Aniansson and Wall,[19,70] and Halperin and Alexander[73] the chain exchange rate time constant should scale with exp (E_a / kT). If we further assume that the core block extraction step is rate-limiting, the activation energy can be expressed $N_{core}^{2/3}\gamma a^2$, with γ the interfacial tension between core blocks and the matrix, and a the monomer size. This suggests an $N_{core}^{2/3}$ dependence, while equations 1.2 and 1.3 use N_{core}^{1}. Since the experimental measurements from different micelle system could be explained by either the $N_{core}^{2/3}$ or the N_{core}^{1} relation,[76,77,79,83,114] the exact form of N_{core} dependence in the activation energy term of $R(t)$ is not clear. Halperin hypothesized that[113] the difference in observed N_{core} dependence comes from the different micelle shapes (*i.e.*, star-like vs. crew-cut), yet this point calls for future examination.

In summary, this chapter serves as the introduction and background literature review of this thesis, which focuses on the chain exchange mechanisms of block copolymer micelles. Section 1.1 provides an overview of this topic and the chapter organization of this thesis. Section 1.2 and 1.3 provide a concise literature review on polymer micelle structure / formation and equilibrium mechanisms respectively, both focusing on the

experimental approaches. In addition to that, the pros and cons of different experimental techniques used in this study are discussed in general in the Section 1.2, and the current findings as well as remaining challenges in exploring the chain exchange mechanisms of block copolymer micelles are summarized in Section 1.3.

Chapter 2.

Polymer Synthesis and Characterization

The block copolymer poly(styrene-*b*-(ethylene-*alt*-propylene)) (PS-PEP) and squalane ($C_{30}H_{62}$, selective for PEP) were selected as the model polymer and solvent for the study of polymer equilibration dynamics. The low vapor pressure of squalene, as well as the thermostability of both PS and PEP polymer chains, allow for a relatively wide temperature window in the experiments. More importantly, the PS chains are kinetically frozen at room temperature: $T_{g,PS} \approx 70$ °C,[115] which is below the CMT of PS-PEP in squalane, and is a feasible temperature experimentally as well. In addition, the compatibility of PS and squalane is appropriate so that the dynamics of micelles can be tuned within experimental detection limits.

In this section, experiments performed to synthesize and characterize several different polymers, including PEP, PS-PEP, PS-PEP-PS, and PEP-PS-PEP are described in detail. Both the why and how of doing the experiment are discussed. A combination of experimental techniques, including various scattering methods, were employed to provide a full investigation of polymer and micelle characteristics.

2.1 Polymer Synthesis: Overview

The PEP homopolymers, PS-PEP diblock and triblock copolymers were synthesized using anionic polymerization of isoprene and styrene, followed by the selective saturation of the polyisoprene (PI) block, producing a more stable PEP block while not altering the PS block. Using anionic polymerization, the molecular weight distribution and polymer composition can be precisely controlled. As discussed briefly in Chapter 1, the chain exchange kinetics in block copolymer micelles is very sensitive to core block length and possibly the corona block length too. Therefore anionic polymerization, although somewhat tedious compared to other synthesis methods, is the most appropriate synthetic method for this study.

A general synthetic scheme is illustrated in Figure 2.1, using PEP-PS-PEP as an example. Since sequential anionic polymerization is employed, the synthesis procedures for preparing PEP, PS-PEP, and PS-PEP-PS are nearly identical. For deuterated equivalent polymers (to be used in TR-SANS experiments), perdeuterated styrene (Polymer Source, Inc.) was used instead of normal styrene monomer. In order to maximize the scattering intensity change during a chain exchange TR-SANS experiment, all the PI blocks were saturated using deuterium instead of hydrogen gas. All chemicals were purchased from Sigma-Aldrich, unless noted otherwise. Detailed experimental procedures will be described in the following sections.

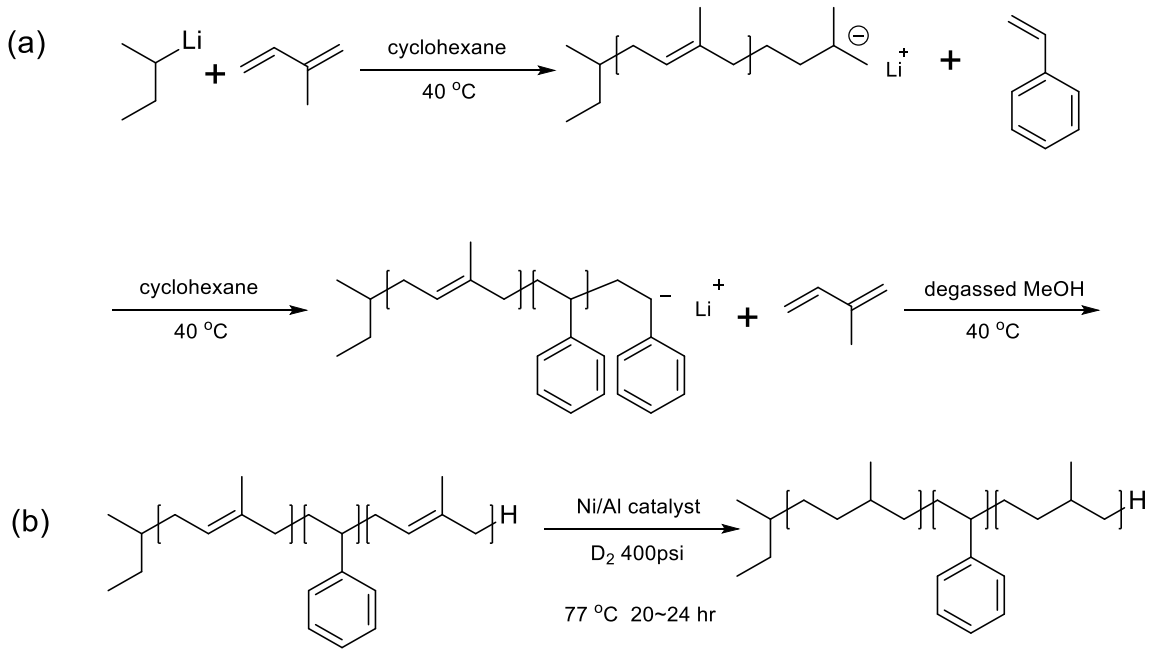

Figure 2.1. Synthesis scheme of PEP-PS-PEP triblock copolymers, by performing (a) sequential anionic polymerization of isoprene and styrene, followed by (b) selective saturation of the double bonds in the PI blocks with high pressure deuterium gas (D_2).

2.1 Polymer Synthesis: Anionic Polymerization

A living polymerization is one that proceeds in the absence of irreversible transfer and termination reactions, and therefore control over the distribution as well as composition of the resulting polymers are made possible.[116–119] Anionic polymerization has been the most important mechanism of living polymerization, since the 1950s.[120] As an ionic polymerization, termination by combination is avoided. In addition, the reagents for anionic polymerization need to be carefully purified to remove water and air, which helps the active sites (*i.e.*, carbanions) stay alive for a sufficiently long time, making it possible to control the molecular weight, structure, and distribution of resulting polymers. Assuming 100% conversion of monomers, the number average molecular weight M_n of resulting polymer can be predicted as $M_n = M_0 \times$ monomer concentration / initiator concentration, with M_0 being the molecular weight of one repeat unit. In an ideal case

where no impurities exist and all the chains are initiated at roughly the same time, the distribution of polymers synthesized by anionic polymerization can be estimated by the Poisson distribution as $Đ = M_w / M_n = 1 + N_n / (N_n + 1)^2 \approx 1 + 1 / N_n$, where M_w is the weight-average molecular weight and N_n is the number average polymerization degree. A broad selection of block copolymers and branched copolymers with controlled architecture can be prepared.

The monomers for performing anionic polymerization need to be carefully purified to remove impurities and inhibiters before use. The monomers were degassed by performing freeze-pump-thaw cycles at least three times. In each cycle, the monomers were first frozen in a sealed round bottom flask immersed in liquid nitrogen and vacuum was pulled, while the flask was isolated under vacuum, the monomers were thawed in warm water (~40 ºC) for styrene and ice water bath for isoprene. This procedure drives most of the dissolved gas in the monomers to the vapor phase and then removes the gas by pulling vacuum when the monomers were frozen. Then the thawed monomer liquid was transferred in the gaseous state through a short path glass tube under vacuum to another round bottle flask to mix with purification agent (dibutyl-magnesium for styrene and n-butyl-lithium for isoprene). The transfer of monomer was facilitated by immersing a second round bottom flask in liquid nitrogen, and at the same time warming up the monomer flask with 40 ºC water for styrene or 0 ºC ice bath for isoprene. After the transfer, monomers were mixed with purification agent in the second flask, sealed under vacuum, and stirred for 30 min to 1 hour, while maintained in 40 ºC water bath for styrene or 0 ºC ice bath for isoprene. This step was repeated to ensure the complete removal of the inhibitor and impurities in the monomers. Purified monomers were collected in a burette and sealed under vacuum. Typically the burette can be stored at 4 ºC in the fridge for up to 3 days before use.

The solvent was also purified before use. For the particular anionic polymerization reaction in this study, cyclohexane was selected as the solvent in order to produce a 1,4 PI

microstructure, which then can be saturated to become PEP. Cyclohexane was degassed by argon bubbling, and then passed through a column of activated alumina followed by a column of copper redox catalyst (CU-0226S, Engelhard) to remove residual water and oxygen.

The reaction was performed in a sealed Pyrex glass reactor (1–3 L). Typically, a 3 L reactor was used to synthesize 30 g of PEP-PS-PEP, in 1.5 L of cyclohexane. The spherical reactor was assembled by attaching 5 or 6 pieces of glassware onto each port (size 5, Ace Glass). Typically a thermocouple holder, one or two 1 L solvent flask(s), and two monomer burettes, one for styrene and one for isoprene, and a three-port connector are used. The reactor was assembled, sealed, and typically six cycles of vacuum/argon/torch-flaming are performed to remove air and moisture from the glass surfaces. After checking for leakage, the reactor was charged with 3 psi argon prior to the reaction.

The solvent was first released into the reactor, and stirred while immersed in a 40 ºC water bath. A measured amount of initiator, sec-butyl-lithium (1.3M solution in cyclohexane), was transferred from the glove box using an air-tight glass syringe and injected into the reactor through a septum-sealed port of the three port connector. Monomers were then added from each burette sequentially. Each block was given 6-8 hours to grow before adding the next aliquot of monomer. The reaction was terminated with degassed methanol, and the unsaturated triblock copolymer was precipitated by slow addition to excess methanol, and then dried under vacuum at room temperature. For block copolymers with high molecular weights (>100 kDa in total), it was difficult to fully remove the methanol by the conventional drying method, due to the high viscosity of polymers as well as the limitation of the vacuum pump. The residual methanol was found in this study to have big impact on the following selective hydrogenation of block copolymers, as discussed in Section 2.5. Therefore, for these polymers, it is necessary to

re-dissolve the polymers in benzene after the normal drying step, and freeze-dry the solution, to remove the residual methanol.

2.3 Polymer Synthesis: Hydrogenation/Deuteration with Heterogeneous or Homogeneous Catalyst

The hydrogenation/deuteration reactions were performed in a sealed stainless steel reactor[121] charged with high pressure hydrogen or deuterium gas. Different catalysts and thus different reaction procedures were used for saturating the double bonds in polyisoprene (PI) blocks and PI homopolymers.

For polyisoprene homopolymers, a Pt-Re/SiO_2 heterogeneous catalyst (provided by Dow Chemical) was used. A 0.2 g/mL solution of polyisoprene in cyclohexane was prepared, and 1 g of catalyst was added per 5 g of polymer. The reaction was performed in a sealed stainless steel reactor charged with high pressure D_2 (~ 500 psi) at 170 ºC for 24 hours with continuous stirring. Subsequently the solution was cooled down, the catalyst was removed by filtration though a pressurized filter, and the polymer was recovered by precipitation in methanol, and dried in a vacuum oven at room temperature. ^{1}H-NMR spectroscopy was used to verify that the resulting polymer is fully saturated and to determine the average number of deuterons per repeat unit, which was found to be 2.3 using an internal standard, pyridine, due to slight H/D exchange.[122,123]

The polyisoprene blocks in both PS/PI diblock and triblock copolymers, on the other hand, were saturated using a homogeneous Ni/Al catalyst in cyclohexane.[124,125] This catalyst can selectively saturate the PI blocks without altering the PS blocks, because of higher solubility and less possibility of catalyst poisoning, and is widely used for selectively saturating alkanes.[126,127] The Ni/Al catalyst, unlike Pt-Re/SiO_2, is sensitive to air and water. Therefore extra care should be taken in preparation for this reaction. The

catalyst solution was prepared by combining triethyl-aluminum and nickel 2-ethylhexanoate in cyclohexane. 2 g of 2-ethylhexanoate was first mixed with 60 mL purified cyclohexane under argon in a sealed round bottom flask, and then 20 mL was taken out with a plastic syringe and injected into a 100 or 50 mL round bottle flask with one of its ports sealed with a rubber septum under argon. Three vacuum/argon/torch flaming cycles were performed to this flask before adding the 2-ethylhexanoate solution, in order to remove air and moisture. The injected solution was kept in an ice bath, in order to reduce the heat generated during the mixing of 2-ethylhexanoate with triethyl-aluminum. 6 mL triethyl-aluminum (1.0 M in cyclohexane) was taken from the glove box with an air-tight syringe, and slowly injected into the cold 2-ethylhexanoate solution in cyclohexane. A black emulsion of Ni/Al catalyst in cyclohexane was then formed. The polymer solution was also prepared in a round bottle flask under argon. Typically 5 g of polymer were dissolved in 500 mL of purified cyclohexane. The polymer and catalyst solutions were injected into the stainless steel reactor purged with low pressure argon to avoid exposure to air, through the inlet of the reactor, which was sealed by a small rubber septum. The reactor was then purged with argon again, and charged with deuterium gas (Cambridge Isotope Laboratories) to 400 psi at room temperature. Then the temperature was raised to 77 °C and the reaction was allowed to progress for 24 hr. In cases where the polymers contained large polyisoprene blocks, the catalyst was added twice on the next day after the first hydrogenation reaction was done, in order to fully saturate the double bonds in polyisoprene blocks. Sometimes it was necessary to lower the temperature to 70 ºC and / or add BHT (butylated hydroxytoluene) as a stabilizer to prevent degradation of the polyisoprene blocks during reaction.

After the reaction was complete, the reactor was opened and the solution was taken out to mix with sufficient 8 wt% citric acid in water to deactivate the remaining catalyst. A complete reaction should render the solution colorless. The solution mixture easily

separated in a separation funnel, where the catalyst mainly stays with the inorganic phase (water) and the saturated polymers stay with the organic phase (cyclohexane). The organic phase was then filtered through activated alumina to remove residual water and residual catalyst. The final polymers were recovered by precipitation in methanol, followed by room temperature drying in a vacuum oven. The quality of selective saturation and the degree of D/H exchange were characterized using size exclusion chromatography (SEC) and ^{1}H-NMR.

2.4 Polymer Characterization: Size Exclusion Chromatography (SEC)

SEC, sometimes referred to as GPC (gel permeation chromatography), is a method commonly used to characterize the molecular weight distribution of polymers. Like other liquid chromatography techniques, SEC separates a mixture of solutes with an appropriate column. The column for an SEC instrument is packed with porous particles with a distribution of pore sizes. Solutes (polymer chains) of larger size come off the column in less time than smaller solutes, as the number of pores they can enter is smaller. Therefore the SEC column separates polymer chains by their hydrodynamic volume ($\sim R_g^3$) for a range of sizes corresponding to its pore size. The eluting liquid is monitored by a detector that responds to the polymer concentration. Commonly used devices include the refractive index (RI) detector, the UV-vis detector, and the light scattering (LS) detector. An RI detector provides information of relative solute content distribution as a function of elution time based on the refractive index change, and an UV-vis detector supplies the concentration information for certain species that absorb at certain wavelength, as a function of elution time. The UV-vis detector is less commonly used than the RI detector, but offers advantages over the latter for certain samples that contain a mixture of polymers with different UV absorbing activities. Both these two detecting methods require proper calibration to translate the size distribution as a function of elution time of the sample into

its molecular weight distribution as a function of calibrated molecular weight. The simplest yet most commonly used calibration method involves the use of a series of nearly monodispersed polymer standards of known molecular weights, in order to relate the elution time to molecular weight. Since the elution time is directly related to the hydrodynamic volume of the polymer, not its molecular weight, this calibration only provides the relative molecular weights of the polymer sample in terms of the standards. The chemical species, composition and architecture (especially nonlinearity and branching), which all can affect the hydrodynamic volume of the polymer samples, are not distinguished by the detection and calibration methods. SEC also has a tendency to overestimate the distribution width of polymer samples of narrow dispersity ($Đ < 1.05$). On the other hand, a light scattering detector has the ability to obtain an absolute molecular weight for each slice of molecular weight distribution, without any column calibration. The scattering intensity of a dilute polymer solution is directly related to the concentration fluctuation in the solution, which can be characterized by the refractive index increment, $\partial n/\partial c$, for a constant pressure and temperature. This quantity can be measured precisely using a differential refractometer. Or, if the composition of the polymer sample (which can be obtained using NMR, see next section) is known, the $\partial n/\partial c$ of the polymer can be estimated from the weighted average of the $\partial n/\partial c$ of each compounds, which are often documented in published tables.

Figure 2.2 summarizes the SEC traces for all the polymers synthesized and used in this thesis research: (a) / (b) PEP-d/hPS-PEP, (c) / (d) d/hPS-PEP-d/hPS triblock copolymer, (e) / (f) d/hPS-PEP diblock copolymer, and (g) PEP homopolymers, before and after hydrogenation, respectively. As discussed above, the polymer chains with relatively smaller hydrodynamic volume elute later, as they explore more pores than the ones with larger hydrodynamic volume. The small peak appearing before the primary peak thus indicates small amounts of chain coupling in the reaction. In Figures 2.2a and 2.2b, the two

peaks appearing sequentially after the primary peak correspond to diblock copolymers and homopolymers, which resulted from incomplete addition of the last and second block, respectively. Similarly, the small shoulder appeared around 21 mL in Figure 2.2e corresponds to a small amount of PI homopolymers resulting from the incomplete addition of styrene. After saturating the polyisoprene blocks, the SEC trace of each polymer shifts towards the left, while the general shape of the traces are retained and thus the molecular weight distribution is generally unchanged. The presence of diblock and homopolymers in the triblock copolymer samples (Figure 2.2a to 2.2d) does not significantly affect the chain exchange experiments, as discussed in Chapter 5. The quality of the selective hydrogenation reaction and the absolute molecular weight of each block is discussed in the next section.

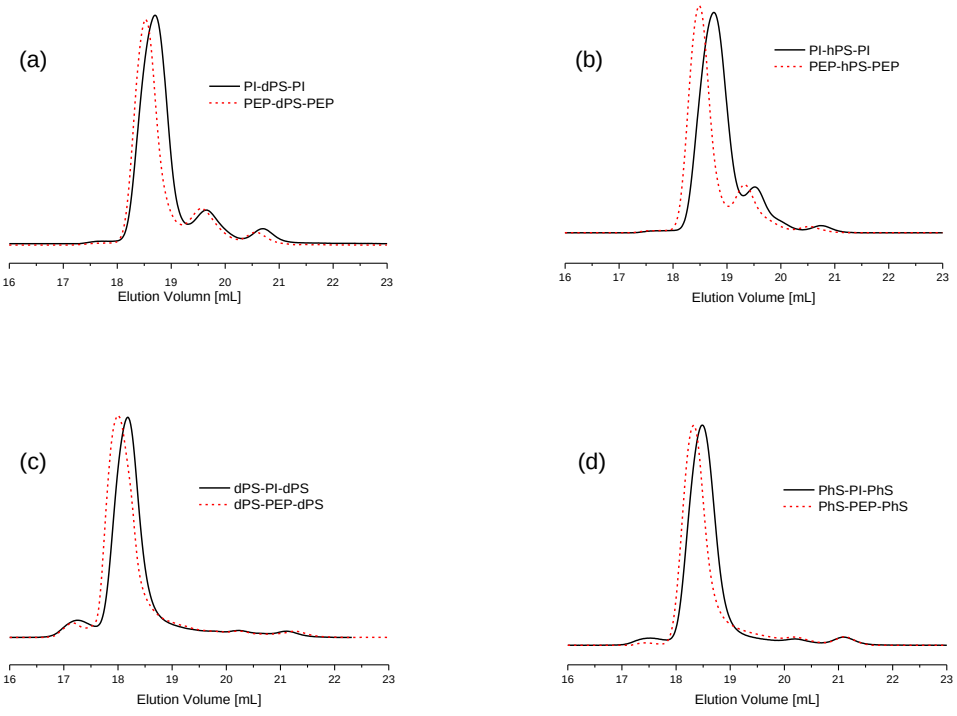

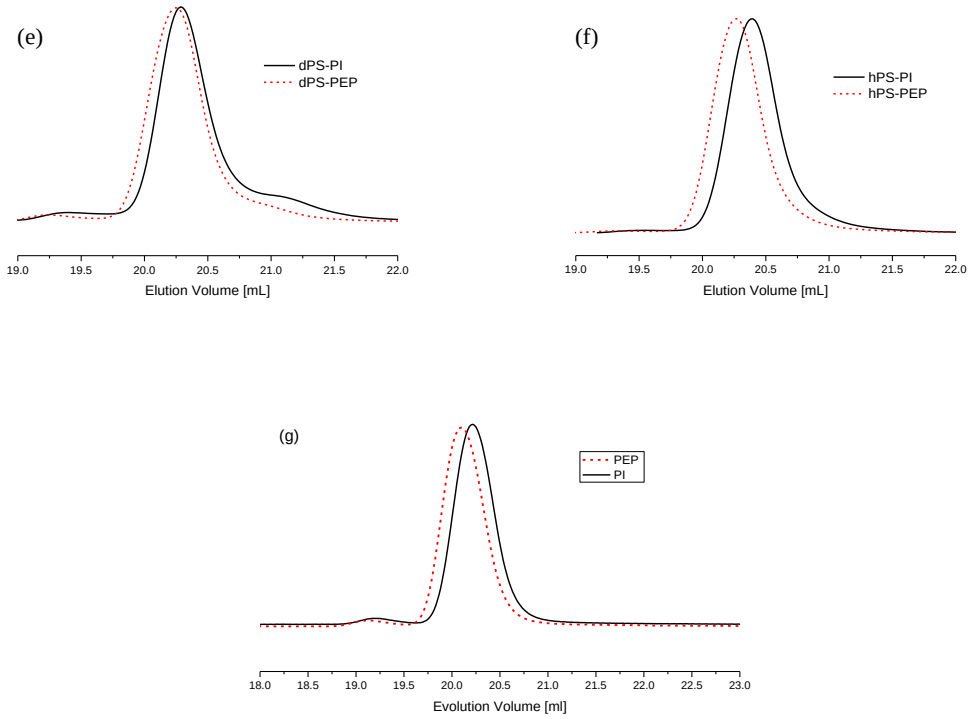

Figure 2.2. SEC of all the polymers synthesized and used in this study, before and after selective saturation of the polyisoprene block: (a) PEP-dPS-PEP, (b) PEP-hPS-PEP, (c) dPS-PEP-dPS, (d) hPS-PEP-hPS, (e) dPS-PEP, (f) hPS-PEP, (g) PEP homopolymers. Red dashed lines and black solid lines represent saturated and unsaturated triblocks, respectively.

2.5 Polymer Characterization: Proton Nuclear Magnetic Resonance (^{1}H NMR)

^{1}H NMR was used to characterize the PI/PS ratio of the PI-PS-PI and PS-PI-PS triblock copolymers, and the quality of selective hydrogenation/deuteration reactions. This section provides an example of how the PI/PS ratio is calculated in one PS-PI-PS triblock polymer using ^{1}H NMR spectra, followed by a discussion of the quality of selective hydrogenation / deuteration reaction as affected by the residual methanol in unsaturated PI-PS or similar polymers (as mentioned in Section 2.2). Table 2.1 summarizes the molecular weights M_n, number of repeat unites N_n, volume fraction of the PS core blocks f_{PS} (assuming bulk

densities of PS and PEP homopolymers) and distribution of all the polymers synthesized and used in this thesis research. The corresponding SEC traces are shown in Figure 2.2.

Table 2.1. Polymer molecular characteristics of all the polymers synthesized and used in this thesis, including a comparison with the polymers synthesized by SooHyung Choi,[76,125] which are also used in some of the chapters.

Sample	M_n [kDa]	N_n	f_{PS}	$Đ$
PEP-hPS-PEP[a]	72-24-72	940-230-940	0.129	1.06[*]
PEP-dPS-PEP[a]	67-24-67	871-218-871	0.132	1.06[*]
hPS-PEP-hPS[a]	45-144-45	433-1867-433	0.360	1.04[*]
dPS-PEP-dPS[a]	49-133-49	455-1729-455	0.390	1.05[*]
hPS-PEP[b]	28-40	273-550	0.376	1.05
dPS-PEP[b]	30-41	269-560	0.368	1.07
PEP[c]	65	895	0	1.07
hPS-PEP-1[d]	26-70	250-970	0.238	1.05
dPS-PEP-1[d]	29-71	260-985	0.243	1.07
hPS-PEP-2[d]	42-64	400-880	0.378	1.04
dPS-PEP-2[d]	47-71	423-926	0.357	1.10

[a] The corresponding SEC traces are shown in Figure 2.2a to 2.2d. [*] These dispersities were calculated for the primary peaks appeared in Figure 2.2a to 2.2d only. [b] The corresponding SEC traces are shown in Figure 2.2e and 2.2f. [c] The corresponding SEC traces are shown in Figure 2.2g. [d] Reproduced from Choi *et al*.[76]

Example Calculation of a Triblock Copolymer Composition and Molecular Weight

A typical ^{1}H NMR spectrum of dilute PS-PI-PS triblock copolymer solution in deuterated chloroform CCl_3D (98%, Cambridge Isotope) before and after selective deuteration is shown in Figure 2.3, together with the chemical structure of the polymer. The colored dots correlate the chemical shift peaks to the corresponding protons on the chemical structure of the polymer sample. In Figure 2.3b, the horizontal axis is chemical shift in ppm, and the vertical axis is signal intensity in arbitrary units. The ^{1}H NMR trace of the corresponding polymers are shifted vertically for a clearer view.

In Figure 2.3b, the sharp peak at about 7.2 ppm corresponds to the small amount of (2%) CCl_3H in the solvent CCl_3D. The two adjacent broad peaks (7.15 ~ 6.2 ppm) correspond to the chemical shifts of the protons on the benzene ring in the polystyrene block, as illustrated by the orange and green dots. The one mid-sized peak at 5.1 ppm together with the following two twin peaks (~ 4.7 ppm) correspond to the protons associated with the double bonds in the PI blocks, which result from the 1,4- and 3,4-addition of isoprene monomers during the anionic polymerization, as illustrated by the red and blue dots in the Figure 2.3a. The disappearance of the peaks associated with the PI double bonds, and the retention of the PS peaks after selective saturation of the PS-PI-PS triblock copolymer, indicate the selective saturation of the PI block. An enlarged plot of the polymer after saturation is shown in the inset for the range of 6 ppm to 4 ppm, to confirm the complete saturation (> 99.9 %) of PI double bonds. The rest of the protons in the polymer generate the broad multi-peak region in the ^{1}H NMR spectra from 2.3 ~ 1.2 ppm before saturation of the PI block and 2 ~ 0.8 ppm after saturation. From the integrated peak area under the PS peaks and PI peaks, the ratio of PI/PS in the triblock copolymer can be calculated, as shown below.

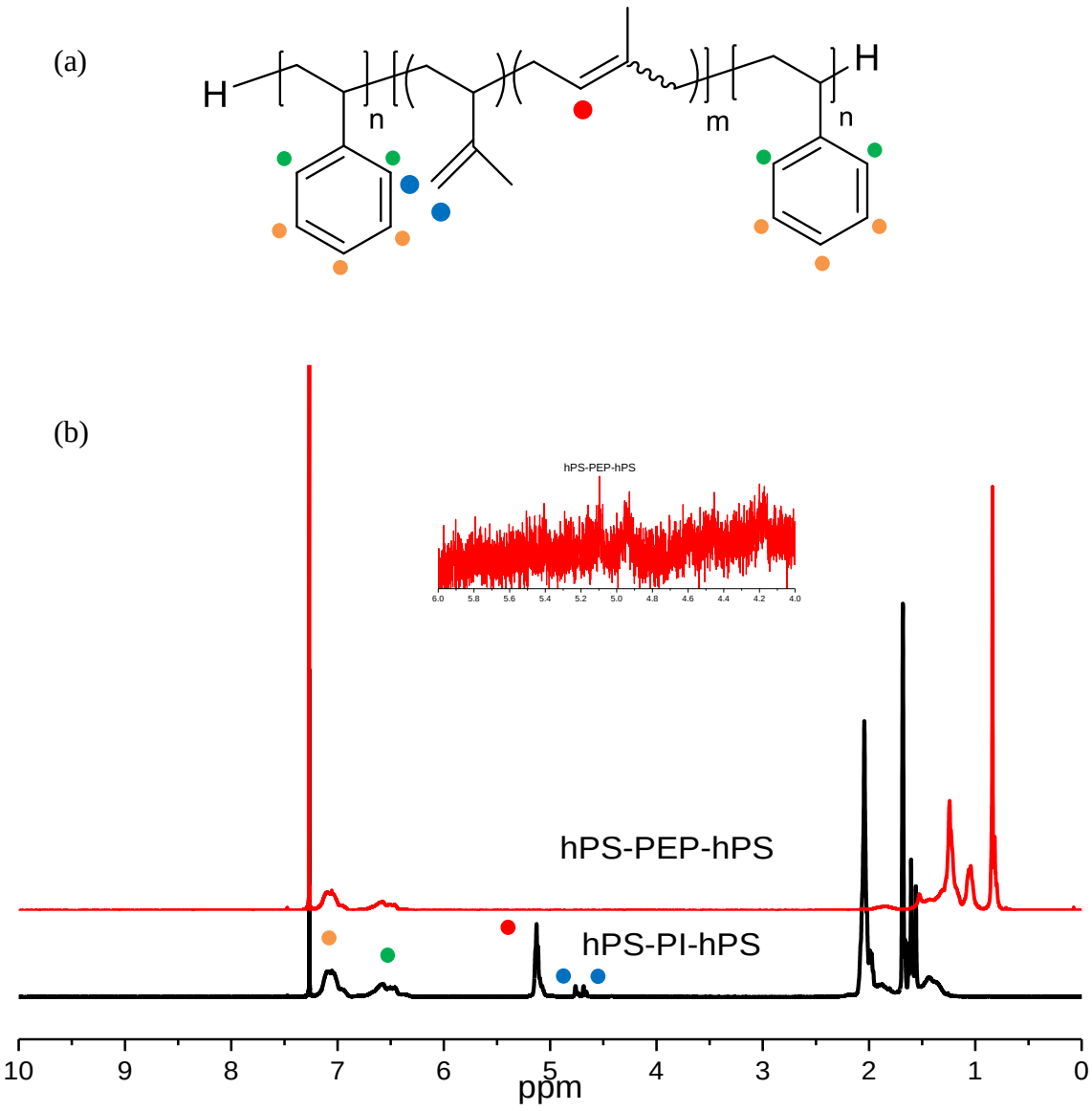

Figure 2.3. (a) The chemical structure of PS-PI-PS triblock copolymer, and (b) the ^{1}H NMR spectra of the same polymer before (black line) and after (red line) selective saturation of the PI block. The red and blue dots illustrate the two kinds of protons and their corresponding chemical shift peaks associated with double bonds in the PI blocks. Similarly, the orange and green dots represent the two kinds of protons and their corresponding chemical shift peaks associated with the benzene ring in the PS blocks. The inset shows an enlarged plot of the ^{1}H NMR spectrum of the saturated polymer, in a region of the peaks associated with the double bonds of polyisoprene blocks.

First, the content of 1, 4- structure in the PI blocks can be calculated from the area under the peaks, at 5.7 ppm (A, red dots) and the twin peaks at 4.7 ppm (B, blue dots), as:

$$\text{mol\% of 1, 4- structure} = \frac{A}{A+B/2} \times 100\% \quad (2.1)$$

For this particular PS-PI-PS triblock copolymer, this value is calculated to be 91.1 %.

Second, in a similar way, the mole fraction of PS in the block copolymer can be calculated from the integrated area under the peaks at 7.02 ppm (C, orange dots), 6.6 ppm (D, green dots), 5.7 ppm (A, red dots), and the twin peaks at 4.7 ppm (B, blue dots) as:

$$\text{mol\% of PS block} = \frac{(C+D)/5}{\frac{(C+D)}{5}+A+B/2} \times 100\% \quad (2.2)$$

For this particular PS-PI-PS triblock copolymer, this value is calculated to be 30.5%. In making this triblock copolymer, equal amounts of isoprene monomer was added to make the first and last block. Therefore by assuming 100% conversion, the PS-PI-PS triblock copolymer should be symmetric. Since the molecular weight of the first PS block was characterized by SEC to be 45 kDa, the molecular weight of the PI block can be calculated as:

$$M_{0,I} \times \left[\frac{2\times M_{PS}/M_{0,S}}{\left(mol\%PS/_{1-mol\%PS}\right)}\right] = 68 \times \left[\frac{2\times 65kDa/104}{\left(30.5\%/_{1-30.5\%}\right)}\right] = 134\ kDa \quad (2.3)$$

To calculate the molecular weight of the saturated PI block, the degree of deuterium substitution in the PI block due to H/D exchange needs to be estimated. To exclude the complication of the protons on styrene, this value is estimated by comparing the ^{1}H NMR

spectra of PEP homopolymers before and after the same selective saturation reaction. Following the similar protocol as above and using pyridine as an internal standard, the number of deuterium atoms in the PEP homopolymers can be calculated to be approximately 2.3, which is slightly higher than 2, the ideal number of deuterium atoms due to saturation of double bonds, indicating slight H/D exchange. Since this selective hydrogenation reaction should not affect the polystyrene blocks (as suggested by the ^{1}H NMR spectrum), the number of deuterium atoms in the PEP blocks of the block copolymers should also be approximately 2.3. The identical number can be obtained by simply comparing the peak area under the broad multi-peak region in between 2.3 ~ 1.2 ppm before saturation of the PI block and 2 ~ 0.8 ppm after saturation (Figure 2.3b), using the styrene peaks (7.15 ~ 6.2 ppm) as an internal standard. This result is consistent with the reported value of deuterium substitution in PS-PEP diblocks,[125] synthesized and saturated using the same method. The molecular weight of the corresponding PS-PEP-PS is then determined to be 45-143-45 kDa. This polymer is used in triblock micelle chain exchange experiments, as discussed in Chapter 5.

^{1}H NMR Used to Characterize the Quality of Selective Saturation

As discussed in Section 2.2, the selective hydrogenation/deuteration reaction was found to be sensitive to the residual methanol in the unsaturated polymer. The polymers dried in a vacuum oven sometimes contain a small amount of the precipitant methanol, especially when their molecular weight is higher than 100 kDa, as evidenced by a small methanol peak in the ^{1}H NMR spectra. This small amount of methanol could significantly affect the saturation reaction, and needs to be strictly removed by freeze-drying the polymer again from benzene. This conclusion was drawn by comparing the ^{1}H NMR spectra obtained from (1) a PS-PI polymer before saturation, (2) the saturated polymer using directly vacuum dried PS-PI, (3) the saturated polymer using freeze-dried PS-PI, and

(4) the saturated polymer using freeze-dried PS-PI but with 1.5 mL of methanol added. The results are shown in Figure 2.4. Obviously, the peak associated with the double bonds in PI block all have disappeared after saturation, regardless of the drying method and the addition of methanol. However, the peaks associated with the protons in the benzene rings of the PS block either disappeared or are smeared for sample 2 and 4, indicating the residual methanol left in normal dried PS-PI polymers can affect the selective saturation reaction, by possibly saturating the benzene rings of the PS block.

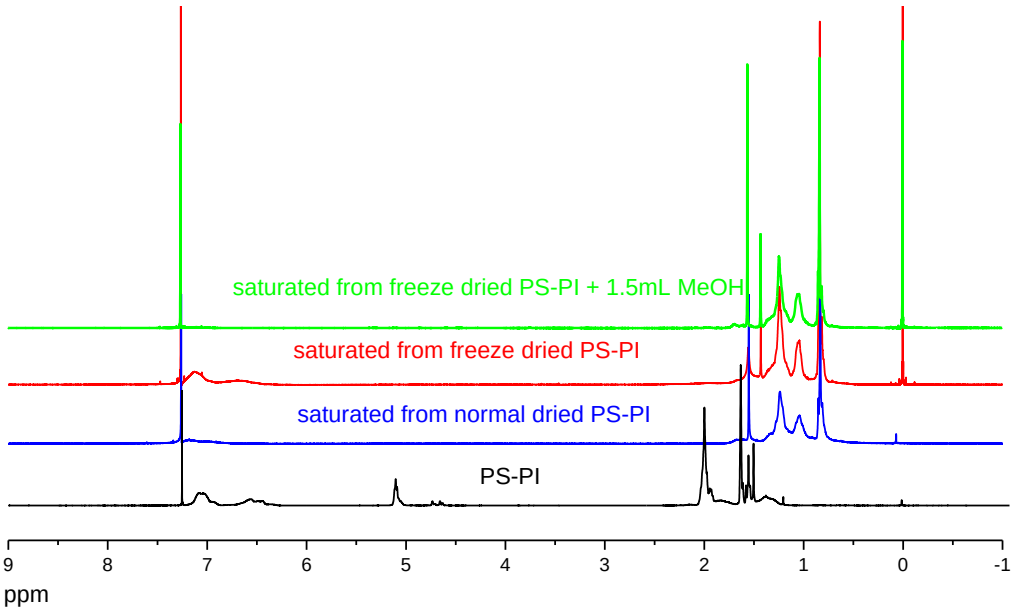

Figure 2.4. ^{1}H NMR spectra of unsaturated PS-PI (black), the saturated polymer using directly vacuum dried PS-PI (blue), the saturated polymer using freeze-dried PS-PI (red), and the saturated polymer using freeze-dried PS-PI but with 1.5 mL of methanol added into the reaction solution (green).

2.6 Micelle Preparation

The micelle solutions in squalane were prepared using a co-solvent method, followed by thermal annealing, to ensure the micelles reach a thermodynamically equilibrated structure. The block copolymers (PS-PEP, PS-PEP-PS, PEP-PS-PEP, etc.) were dissolved in squalane and dichloromethane, a co-solvent that is neutral for both the PS and PEP blocks. Typically the amount of co-solvent is comparable to or larger than the amount of squalane used. The co-solvent is used in larger amount for making a concentrated solution, in order to facilitate polymer dissolution. The dichloromethane was subsequently removed at room temperature while stirring. The solution was weighed before adding the dichloromethane (with only the glass vial, stir bar, the polymer, and squalane), and weighed again when the dichloromethane is gradually evaporating. A matching weight is taken as the sign of complete removal of dichloromethane. The solution was further dried under vacuum while stirring, to removing any residual dichloromethane and dissolved air, which could increase the risk of polymer/squalane degradation during thermal annealing. Using the Riedel equation and the parameters given by VonNiederhausern and co-workers,[128] the vapor pressure of squalane can be estimated to be 1.7×10^{-9} kPa at room temperature. The low vapor pressure of squalane thus ensures that it will not be removed during short time vacuum (~10 min). The solution was then annealed at 180 °C for 30 min and gradually cooled in air.

2.7 Dynamic Light Scattering (DLS)

As briefly discussed in Section 2.4, light scattering in a dilute polymer solution arises from fluctuations in concentration. This fluctuation over time generates time dependent scattering intensity, which is monitored in a DLS experiment. Under some circumstances, the intensity fluctuation can be analyzed to extract a characteristic relaxation time, which contains information about the hydrodynamic size of individual polymer chains in the

solution. This makes DLS a powerful tool to characterize polymer solutions and other small particle dispersions undergoing Brownian motion. Detailed reviews on DLS experiments and data analysis are available.[62,63,65] Briefly, it is necessary to translate the scattering intensity fluctuation information into the fluctuation of spatial distribution of particles. When the solution is sufficiently dilute so that the mutual (D_m) and tracer diffusion coefficients (diffusion at zero concentration, D_t) are approximately the same, the hydrodynamic radius of the particles is related to the diffusion coefficient D_m, and solvent viscosity η_s via the Stoke-Einstein relation:

$$R_h = \frac{kT}{6\pi\eta_s D_m} \qquad (2.4)$$

.

By making proper assumptions on the particle size distribution function, the diffusion coefficient D_m can be connected with the time autocorrelation function, which characterize the degree of correlation of the fluctuation of scattering intensity I_s, at a certain observation time t, over a period of experiment of time T. The time autocorrelation function C_t is defined as:

$$C_t = \lim_{T\to\infty} \frac{1}{T}\int_0^T I_s(t')I_s(t'+t)dt' \qquad (2.5)$$

.

A useful method to measure particle size and distribution, when the particle sizes are narrowly distributed, is the cumulant method, and is used in this study to characterize polymer micelle sizes. Alternatively, one can also use the Laplace inversion programs CONTIN or REPES[129] to estimate the actual distribution of particle sizes.

In this study, DLS is employed to characterize the temperature dependent hydrodynamic radius of block copolymer micelles in squalane, complementing small angle X-ray scattering experiments described in the next section. The micelle solutions (0.2 % to 1 %) were prepared following the procedures described above, followed by passing through a 0.2 μm syringe filter to remove dust. The sample solutions were loaded into glass tubes of 1 cm diameter and degassed by pulling vacuum. A Brookhaven BI-200SM goniometer and a Brookhaven BI-9000AT correlator at λ = 637 nm were used to make DLS measurements over a range of angles (60°~120°) at room temperature. For high temperature DLS experiments, a home-made goniometer equipped with a silicon oil index-matching bath, an electric heater (25 ~ 200 ºC), a Brookhaven BI-DS photomultiplier, a Lexel 95-Ar+ laser operating at 488 nm and a Brookhaven BI-9000 correlator were used. For each temperature, samples were annealed for at least 10 minutes, and then measurements were taken for about 10 min. Figure 2.5 shows a typical hydrodynamic radius plot as a function of temperature for 1 vol% PEP-PS-PEP triblock copolymer micelles in squalane, obtained from DLS measurements using cumulant analysis. The observed slight increasing in R_h of the micelles with temperature is a result of the intermicellar interactions and the incorporation of solvent in micelle cores as temperature approaches the CMT, and is consistent with the reported results of PS-PEP diblock copolymer micelles in squalane.[125] The red and blue circles in Figure 2.5 illustrate the measured R_h of the micelles during the heating and cooling temperature ramp, respectively. The heating and cooling ramps produce identical R_h results within experimental error, suggesting that the micelle preparation method yields equilibrated micelle structures.

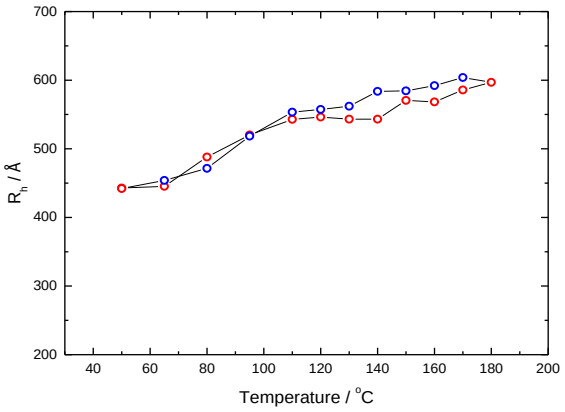

Figure 2.5. Hydrodynamic radius R_h of 1 vol% PEP-PS-PEP micelles in squalane, upon heating (red open circles) and subsequent cooling (blue open circles).

2.8 Small Angle Scattering and Fitting Model

General Small Angle Scattering

Small angle scattering techniques, including small angle X-ray scattering (SAXS) and small angle neutron scattering (SANS), are powerful tools to obtain detailed inter- and intra- micellar structure information. Compared to DLS, small angle scattering techniques are suitable for both dilute, semi-dilute, concentrated, and ordered polymer micelle systems. In addition, due to the different scattering power of different blocks (electron density in SAXS, and scattering length density in SANS, as discussed in Chapter 1), it is possible to obtain detailed information such as micelle core size, corona length, and micelle to micelle distance, with the aid of appropriate fitting models.

Figure 2.6 schematically illustrates the elastic scattering by two particles separated by a distance $\vec{r}_{jk}$. The incident and scattering beam can both be described as a traveling electromagnetic wave in general: $\vec{E} = \vec{E}_0 \cos(\omega t - \vec{k} \cdot \vec{r})$, where $\vec{E}_0$ is the amplitude of the electric field, ω is the frequency, t is the time, $\vec{k}$ is the wave vector, and $\vec{r}$ is the position. The amplitude of the incident wave vector and scattered wave vector are both $2\pi/\lambda$. The

scattering wave vector $\vec{q}$ is thus defined as the difference between the incident and scattering wave vectors: $\vec{q} = \vec{k}_i - \vec{k}_s$. For elastic scattering where no energy is exchanged between the scattering medium and the wave, $\lambda_i = \lambda_s$, and from Figure 2.6 the amplitude of $\vec{q}$ can be obtained as: $q = 4\pi/\lambda \times \sin(\theta/2)$, which has units of inverse length.

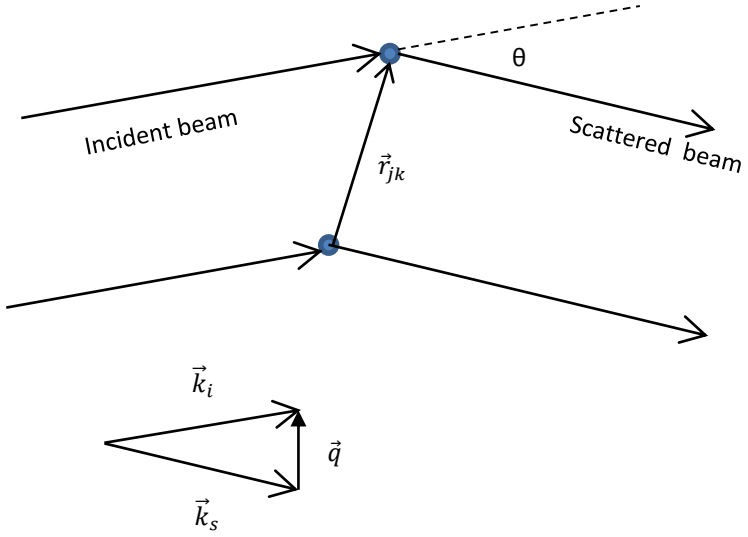

Figure 2 6. Illustration of elastic scattering by two particles and the definition of $\vec{q}$.

The total scattering from a polymer system contains two parts: the incoherent scattering resulting from random fluctuations that are independent of θ (and thus $\vec{q}$), and the coherent scattering coming from the spatial correlation of monomers and polymer, which is a function of θ (and thus $\vec{q}$). Experimentally the incoherent scattering usually can be subtracted with a background sample (*e.g.* solvent sample scattering). Due to the destructive interference of scattered beams from both interior and external structures (*e.g.*, the scattering from polymer chains within a micelle, and the scattering from different micelles), the overall coherent scattering intensity is reduced. For dilute and isotropic objects, the coherent scattering intensity from a small angle scattering experiment can be expressed as:

$$I(q) = P(q) \times S(q), \qquad (2.6)$$

where the $P(q)$ and $S(q)$ are the form factor and structure factor. For polymer micelle solutions, $P(q)$ describes the internal structure of one micelle (*e.g.*, micelle core and corona size, aggregation number, etc.), while $S(q)$ describes the spatial correlation between micelles, which approaches unity in dilute solution and increases as concentration increase.

The Hard Sphere Fitting Model

In this study small angle X-ray scattering (SAXS) and small angle neutron scattering (SANS) experiments were performed with both dilute and concentrated spherical polymer micelle solutions. The structural characteristics of the micelles were obtained using a hard sphere fitting model with polydispersity correction for the micelle core radius. A detailed description of the hard sphere model has been documented elsewhere.[125] Briefly, the model assumes that a micelle consists of a spherical homogeneous core with Gaussian distribution in radius and Gaussian corona chains attached to the core surface, and that the intermicellar interaction can be approximated by the interaction of hard spheres with an effective radius R_{hs}. A schematic illustration of the model and fitting parameters is shown in Figure 2.7. In the model, the coherent scattering intensity is expressed as:

$$I(q) = \int D(R_c)\left(P_{mic}(q) + A_{mic}(q)^2[S(q) - 1]\right)dR_c . \qquad (2.7)$$

Here the micelle form factor $P_{mic}(q)$ is the sum of four parts: the form factor of spherical micelle core,s the form factor of Gaussian micelle corona chains, the cross term between

core and corona chains, and the cross term between corona chains. The function $P_{\mathrm{mic}}(q)$ is therefore written as:

$$P_{mic}(q) = N_{agg}^2 \beta_{core}^2 A_{core}^2(q) + N_{agg} \beta_{corona}^2 P_{chain}$$
$$+ 2N_{agg}^2 \beta_{core} \beta_{corona} A_{core}(q) A_{corona}(q) + N_{agg}(N_{agg} - 1) \beta_{corona}^2 A_{corona}^2, \qquad (2.8)$$

In this equation, the N_{agg} is the aggregation number (or the number of chains) of one micelle. β_{core} and β_{corona} are the excess scattering length of core and corona blocks, defined as $v_{\mathrm{block}} \times (\rho_{\mathrm{block}} - \rho_{\mathrm{solvent}})$, with v_{block} being the volume of the corresponding block, and ρ being the scattering length density for the corresponding component. The origin of ρ differs for SAXS and SANS, and will be discussed later. Here the core form factor is expressed as:

$$A_{core}^2(q) = \Phi^2(qR_c) \exp(-q^2 \sigma_{\mathrm{int}}^2) \qquad (2.9)$$

with

$$\Phi(x) = 3[\sin x - x \cos x] / x^3 , \qquad (2.10)$$

with R_{c} being the core radius and σ_{int} being the interfacial thickness. The Debye function for Gaussian chains:

$$P_{chain}(q) = \frac{2[\exp(-q^2 R_g^2) - 1 + q^2 R_g^2]}{q^4 R_g^4} \quad , \qquad (2.11)$$

is used for the corona chain form factor with R_g being the radius of gyration of the corona chains. The form factor amplitude of corona chains is given as the normalized Fourier

transform of the radial density distribution function of the corona chains, $\rho_{corona}(r)$,[130] which is chosen as the linear combination of two spline functions $\rho_1(r)$ and $\rho_2(r)$, following previous studies[131,132] (see Figure 2.7b):

$$A_{corona} = \frac{4\pi\int \rho_{corona}(r)\frac{\sin(qr)}{qr}r^2 dr}{4\pi\int \rho_{corona}(r)r^2 dr}\exp(-q^2\sigma_{int}^2/2), \qquad (2.12)$$

$$\rho_{corona}(r) = \frac{\rho_1(r) + a_1\rho_2(r)}{1+a_1}. \qquad (2.13)$$

Returning to Equation 2.7, the form factor amplitude of the radial scattering length distribution of the micelle $A_{mic}(q)$ is expressed as

$$A_{mic}(q) = N_{agg}(\beta_{core}A_{core}(q) + \beta_{corona}A_{corona}(q)), \qquad (2.14)$$

where N_{agg}, β_{core} and $A_{core}(q)$ are as described above. The Percus-Yevick approximation is used to obtain the monodispersed hard sphere structure factor $S(q)$, which is a function of q, R_{hs}, and the volume fraction of hard spheres η_{hs}. Lastly, the Gaussian distribution of core radii R_c is expressed in terms of the mean core radius $<R_c>$ and the standard deviation σ_R:

$$D(R_c) = \frac{1}{\sqrt{2\pi}\sigma_R}\exp\left[-\frac{\left(R_c - \langle R_c\rangle\right)^2}{2\sigma_R^2}\right]. \qquad (2.15)$$

Therefore, a total of nine fitting parameters are required by the model: N_{agg}, R_c and σ_{int} as in $P_{mic}(q)$ and $A_{mic}(q)$, R_g as in $P_{mic}(q)$, a_1 and s as in $A_{mic}(q)$, R_{hs} and η_{hs} as in $S(q)$, σ_R as in $D(R_c)$.

(a)

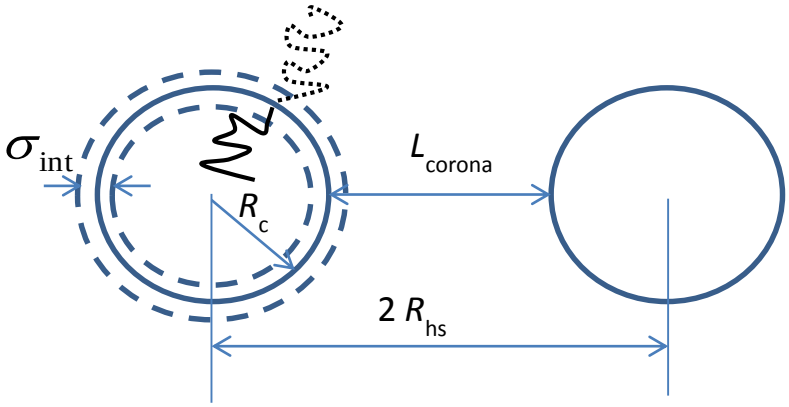

(b)

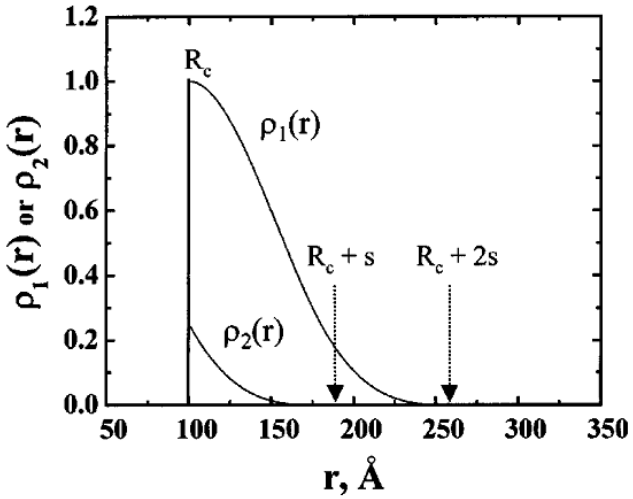

Figure 2.7. (a) Schematic illustration of the micelle characteristics used in the hard sphere model fitting function. The two blue circles are two adjacent micelles, while the dashed circles illustrates the interfacial region between micelle core and corona. The curved solid line and dashed line are example core and corona blocks of the micelle. The micelle has a core size R_c, interfacial thickness σ_{int}, the distance between adjacent micelles $2R_{hs}$, and the corona thickness L can be estimated as $R_{hs} - R_c$. This figure is reproduced from the dissertation by SooHyung Choi.[133] (b) The two spline functions of corona chain radial density $\rho_1(r)$ and $\rho_2(r)$ are plotted against the distance to micelle center r. The position $R_c + s$ and $R_c + 2s$ are where corona chain density reaches zero (*i.e.*, the fringe of micelle corona) in $\rho_1(r)$ or $\rho_2(r)$, respectively. Therefore, the radial distribution of corona chains starts from $r = R_c$ and ends between $r = R_c + s$ and $r = R_c + 2s$. This plot is reproduced from Bang *et al.*[130]

SAXS and SANS Experiments

As briefly discussed in Chapter 1, while SAXS and SANS experiments are both widely used to investigate the structure of polymer samples, and the *q* range they are capable of providing is similar, they differ in several aspects. In a SAXS experiment, the scattering power of an atom is determined by its electron density and thus the atomic number. In a SANS experiment however, the scattering power of an atom depends on the interaction between neutrons and its nuclei, and does not follow a simple relation with the atomic number. Isotopes with different numbers of neutrons in the nuclei but the same number of electrons will scatter the same in SAXS but can be very different in SANS. This allows for the isotope labeling in SANS experiment, which will be exploited in the following chapters. The scattering length density is simply the total scattering length per unit volume, which is the sum of the scattering length of each atom contained in a specified component (*e.g.* a repeat unit), divided by the component volume. Table 2.2 summarizes the calculated electron densities and coherent neutron scattering length densities of the materials used in this study. Here the volume of PS and PEP repeat units, and that of squalane molecules, are estimated from the bulk homopolymers densities: ρ_{hPS} = 1.047 g/cm^3, ρ_{PEP} = 856 g/cm^3, $\rho_{hsqualane}$ = 0.81 g/cm^3. The volume of H and D atoms are assumed to be the same.

Table 2.2. Electron densities and coherent neutron scattering length densities of selected chemicals.

	Formula	ρ_e[a] (mol e^-/cm^3)	υ[b] (10^{-22} cm^3)	b[c] (10^{-12} cm)	ρ_n[d] (10^{10} cm^{-2})
h-PS	C_8H_8	0.565	1.65	2.33	1.41
d-PS	C_8D_8	0.565	1.65	10.66	6.46
PEP	$C_5H_{7.7}H_{2.3}$	0.463	1.36	1.98	1.46
h-squalane	$C_{30}H_{62}$	0.437	8.65	–3.24	–0.374
d-squalane	$C_{30}D_{62}$	0.437	8.65	61.30	7.08

[a]electron density, [b]volume of one repeat unit in polymer chain or the solvent molecule, [c]coherent neutron scattering length, [d]coherent neutron scattering length density, calculated as $\rho_n = b/\upsilon$.

The SAXS experiments were conducted using equipment maintained by the DuPont-Northwestern-Dow Collaborative Access Team at Argonne National Laboratory, using 4 keV radiation (wavelength $\lambda = 0.886$ Å) and a sample-to-detector distance of 6 m. Sample solutions were isolated in 1.5 mm quartz capillaries using a high-temperature silicone-based sealant. A 2–20 s exposure to the X-ray beam was employed for individual measurements. Scattered X-rays were collected with a 2-D MAR-CCD detector, and azimuthally averaged to the one-dimensional form of intensity $I(q)$ (arbitrary units) versus the magnitude of the scattering wave vector q. Background scattering was subtracted based on the powder pattern obtained from a quartz cell containing only solvent.

The SANS experiments were performed on the NG-7 30 m beamline at the Center for Neutron Research of the National Institute of Standards and Technology (NIST), or the CG-2 General-Purpose SANS instrument at the High Flux Isotope Reactor (HFIR) facility

of Oak Ridge National Laboratory (ORNL). For NG-7 at NIST, a sample-to-detector distance (SDD) of 13 m and a wavelength λ = 7 Å were used. For CG-2 at ORNL, SDD = 14 m, and λ = 4.75 Å. For both instruments, sample solutions were loaded into quartz cells of 1 mm thickness at room temperature. For high temperature measurements, the sample holders were pre-heated to a designated temperature with a precision temperature controller (±0.2 °C) prior to the experiment. After inserting the sample cell into the heated holders, it took approximately 10 min for the temperature to equilibrate. The temperature inside the cell was monitored with a calibrated thermocouple, with its tip inserted into a reference cell loaded with squalane and located adjacent to the sample cell in the heating block. The 2-D scattering data were corrected for empty cell scattering, transmission, and detector sensitivity and reduced to absolute intensity using procedures established by NIST.[134]

In summary, this chapter discussed in detail the synthesis procedures and experimental techniques used in this study. The block polymers were synthesized using sequential anionic polymerization of isoprene and styrene, followed by the selective saturation of the polyisoprene blocks for better thermal stability. The polymers were characterized by SEC and ^{1}H NMR to obtain the molecular weights, dispersity, and compositions. The polymer micelles in squalane were prepared using a co-solvent method followed by thermal annealing. DLS experiments were performed to characterize the hydrodynamic radius of polymer micelle in dilute solution at various temperatures. The detailed micelle characteristics can be extracted from small angle scattering experiments, using a hard sphere core-shell model for polydispersed micelles. The TR-SANS experiments used to investigate micelle chain exchange kinetics are discussed in the following chapters.

Chapter 3.

Molecular Exchange in Diblock Copolymer Micelles: Bimodal Distribution in Core-Block Molecular Weights

* Reproduced in part with permission from Lu, J.; Choi, S.; Bates, F. S.; Lodge, T. P., *ACS Macro Lett*ers **2012**, 1, 982–985.

3.1 Introduction

As briefly discussed in Chapter 1, the pioneering experiments by Lund, et al. based on time-resolved SANS (TR-SANS) with poly(ethylenepropylene-*b*-ethylene oxide) diblock oligomers in water,[75,78] and poly(styrene-*b*-butadiene) diblock copolymers as well as poly(styrene-*b*-butadiene-*b*-styrene) triblock copolymers in various *n*-alkane solvents[98,105] have shown that the associated dynamics of molecular exchange are approximately logarithmically dependent in time, as opposed to the intuitive exponential form.[73] TR-SANS measurements with relatively high molecular weight poly(styrene-*b*-ethylenepropylene) (PS-PEP) diblock copolymers dissolved in squalane ($C_{30}H_{62}$) revealed that the origins of this behavior can be traced to a finite distribution in core (PS) block molecular weight.[76] Remarkably, even a relatively small spread in the distribution of PS core block sizes ($Đ = M_w/M_n < 1.1$) was shown to produce dramatic broadening of the rate

of molecular exchange, both in disordered (1% by volume block copolymer)[76] and ordered (15%)[79] spherical micelles. In a recent publication Zinn and coworkers[77] have shown that molecular exchange in aqueous solutions of n-alkyl-PEO diblocks (n = 18, 24 and 30) containing strictly monodisperse ($Đ$ =1) core blocks is exponential in time, consistent with the theoretical model proposed by Choi *et al.*[76]

Here we report a new TR-SANS study that quantitatively confirms the predicted form of the molecular exchange dynamics in spherical micelles prepared with an intentionally broadened distribution in core block molecular weights.

3.2 Experiments

Materials

We have blended pairs of relatively monodisperse PS-PEP diblocks, where the PS block molecular weights differ by a factor of 1.6. Normal (hPS-PEP-1 and hPS-PEP-2) and selectively deuterated (dPS-PEP-1 and dPS-PEP-2) diblocks were synthesized by sequential anionic polymerization of styrene and isoprene, followed by homogeneous catalytic saturation of the poly(isoprene) blocks with deuterium, as described previously by Choi *et al.*.[125] The molecular weight distribution of the individual diblocks is relatively narrow ($Đ \leq 1.1$) and the average degree of polymerization of the PS blocks fall into two categories: $<N_{PS}> \cong 255$ and 412. (see Table 2.1)

Time Resolved Small Angle Neutron Scattering

Figure 3.1 illustrates the contrast matching strategy underlying the TR-SANS experiment. A solution containing equal volume fractions of micelles with protonated (hPS) and deuterated (dPS) cores (referred to as a "post-mixed" specimen, see below) is rapidly heated to a target temperature and a series of SANS patterns are recorded over time under

isothermal conditions. The isotopic composition of the solvent is chosen so as to match the neutron scattering length density (ρ) of the micelle cores after complete molecular exchange, $\rho_{solvent} = f_{h\text{-}squalane} \times \rho_{h\text{-}squalane} + (1 - f_{h\text{-}squalane}) \times \rho_{d\text{-}squalane} = (\rho_{d\text{-}PS} + \rho_{h\text{-}PS})/2$. Here the values of $\rho_{h\text{-}squalane}$, $\rho_{d\text{-}squalane}$, $\rho_{d\text{-}PS}$, and $\rho_{h\text{-}PS}$ can be found in Table 2.2. Solving the above equation for the volume fraction of normal squalane in the solvent mixture $f_{h\text{-}squalane}$, we get $f_{h\text{-}squalane} \approx 42\%$. Therefore, the solvent should contain a mixture of 42% h-squalane and 58% d-squalane by volume. Since the intensity of neutrons scattered by a micelle core is proportional to the contrast factor, $I \sim (\rho_{solvent} - \rho_{PS\ core})^2$, the SANS intensity associated with the micelle scattering affords direct access to the extent of molecular exchange. The contrast between corona chains ($\rho_{PEP} = 1.46 \times 10^{10}$ cm^{-2}) and the solvent mixture ($\rho_{solvent} = 3.935 \times 10^{10}$ cm^{-2}) is relatively less compared to that between the deuterated and normal micelle cores (1.41×10^{10} cm^{-2} and 6.46×10^{10} cm^{-2}) and the solvent mixture.

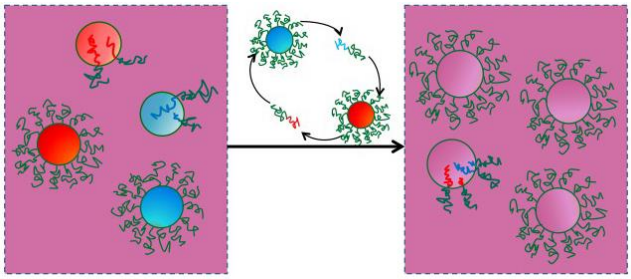

Figure 3.1. Chain exchange in a post-mixed sample of spherical micelles formed by mixing pairs of hPS-PEP (blue PS cores) and dPS-PEP (red PS cores), containing two different molecular weight PS blocks. Complete chain exchange results in a uniform distribution of the four types of PS blocks, which contrast matches the isotopically labeled squalane solvent.

Micelle solutions containing 1% by volume diblock copolymer were prepared using the co-solvent method described in Chapter 2. Two types of solutions were prepared for SANS analysis: "pre-mixed" and "post-mixed." Premixed specimens were formed by mixing all four polymers in squalane and dichloromethane followed by evaporation of the

volatile component and annealing, resulting in a solution of micelles containing equal volume fractions of both dPS and both hPS blocks. The isotopic composition of the squalane (42 vol% $C_{30}H_{62}$ and 58 vol% $C_{30}D_{62}$; Sigma-Aldrich and C/D/N Isotopes, respectively) was selected to contrast match the pre-mixed micelle cores. Preparation of the (1% by volume polymer) post-mixed solutions began with the formation of two isotopically pure mixtures, one with hPS-PEP-1 and hPS-PEP-2 (50% by volume of each hPS block type) and a second with dPS-PEP-1 and dPS-PEP-2 (also with equal volume fractions of each dPS block type). Equal portions of these isotopically pure solutions were then combined at room temperature. Because the PS cores are glassy at room temperature, no molecular exchange occurs with the post-mixed specimens until they are heated above the core (PS) glass transition temperature, $T_{g,PS} \cong 70$ °C.[115]

TR-SANS experiments were performed with the CG-2 General-Purpose SANS instrument at the High Flux Isotope Reactor (HFIR) facility of Oak Ridge National Laboratory (ORNL) using a sample-to-detector distance of 14 m and neutrons with wavelength $\lambda = 4.75$ Å^{-1}. Data reduction was performed using the Igor package provided by ORNL. Polymer solutions (1 vol%) were loaded into quartz cells (1 mm sample thickness) and inserted into a preheated and temperature controlled (± 0.2 °C) copper block fitted with two quartz windows for thermal stability. The actual temperature was calibrated using a thermocouple immersed in oil in a separate quartz cell. About 5 minutes was required for a specimen to stabilize within 1 °C of the set temperature, at which point SANS data acquisition was initiated; 2-D scattering patterns were recorded in 5 minute increments for up to 3 hours.

3.3 Results and Discussion

TR-SANS results obtained at several temperatures are shown in Figure 3.2. The systematic decrease of scattering intensity over time is a result of the mixing of isotope labeled chains. Comparing the panels in Figure 3.2, it can be seen that as the temperature

increases, the scattering intensity from a post-mixed specimen decreases in a more rapid manner towards the mixed core scattering from a pre-mixed specimen, indicating the chain exchange rate increases at higher temperatures.

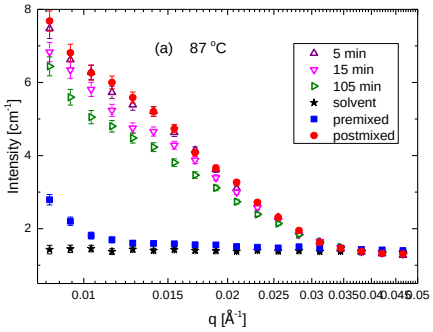

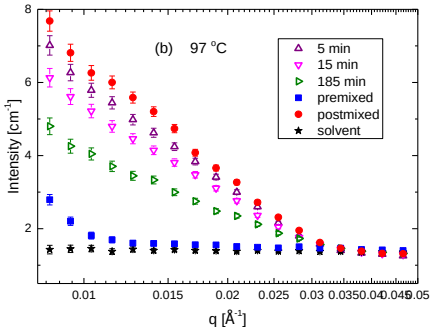

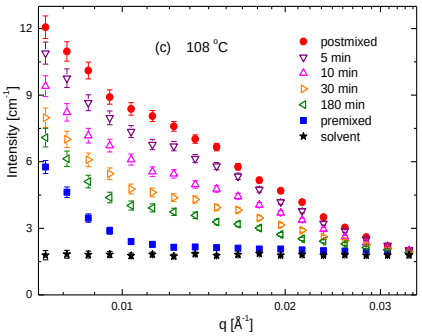

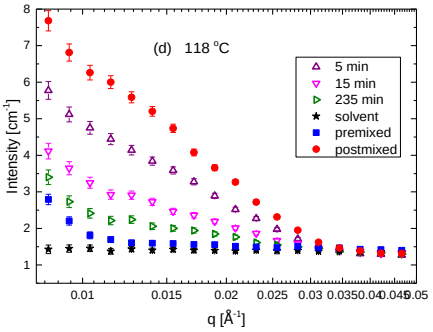

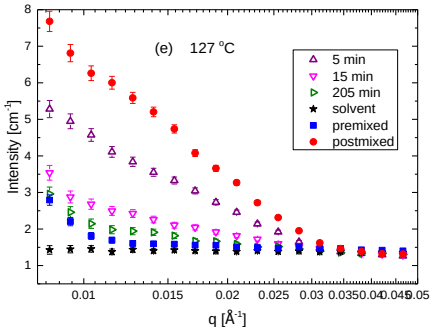

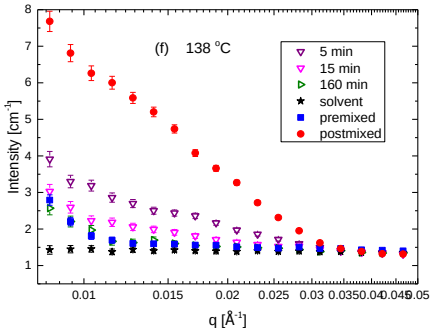

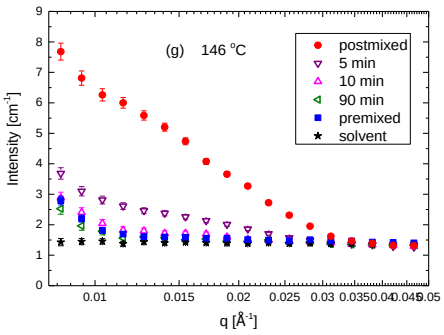

Figure 3.2. Representative TR-SANS patterns recorded in 5 minute increments during molecular exchange of PS-PEP in squalane at (a) 87 °C, (b) 97 °C, (c) 108 °C, (d) 118°C, (e) 127 °C, (f) 138 °C, and (g) 146 °C. The scattering patterns associated with the post-mixed specimen before chain exchange (red solid circles), that from the pre-mixed specimen (blue solid squares) and that from the solvent specimen (black stars) are shown in each panel for comparison.

Changes in the SANS intensity were monitored as a function of time at constant temperature over the range $0.01 \leq q \leq 0.04$ Å^{-1}, where $q = 4\pi\lambda^{-1}\sin(\theta/2)$. Relative changes in the concentration of dPS blocks in the micelles can be related to the dimensionless molecular relaxation function $R(t)$,[78] as described in equation 1.2.

The relaxation functions acquired at seven different temperatures are presented in Figure 3.3. At the lowest measurement temperature, 87 °C, approximately 15% of the initial intensity recorded for the post-mixed sample is lost over 100 minutes of time. At the highest temperature, 146 °C, $R(t)$ dropped by more than 90% over a comparable period. TR-SANS experiments conducted at all seven temperatures provided access to a wide range of molecular exchange, $0.1 \leq R(t,T) \leq 0.95$, as shown in Figure 3.3.

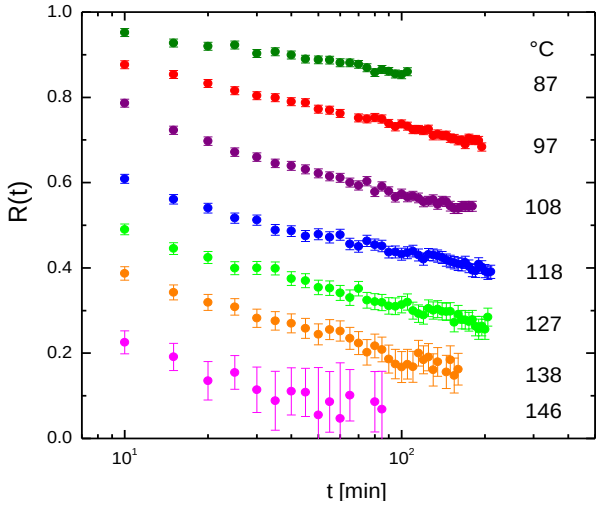

Figure 3.3. $R(t,T)$ determined by TR-SANS for post-mixed solutions of binary dPS-PEP and hPS-PEP mixtures. The spherical micelle cores were formed with equal amounts by volume of two PS blocks that differ by 60% in degree of polymerization.

In an earlier publication that dealt with molecular exchange between equal molecular weight diblock copolymers (dPS-PEP-1/hPS-PEP-1 and dPS-PEP-2/hPS-PEP-2) Choi *et al.*[76] demonstrated that master curves could be constructed from $R(t,T)$ data using the time-temperature superposition principle,[107] *i.e.*, $R(t/a_T, T_{ref}) = R(t,T)$, where a_T and T_{ref} are the shift factor and reference temperature, respectively.[76,79] Figure 3.4a illustrates application of this technique to the results shown in Figure 3.3; the corresponding $\log[a_T(T)]$ is plotted versus T in Figure 3.4b. Significantly, within experimental uncertainty the a_T values determined with the binary blends match those associated with the individual components, consistent with the assumption that the temperature dependence of the exchange dynamics is controlled primarily by polystyrene segmental motion, *i.e.*, free-volume.

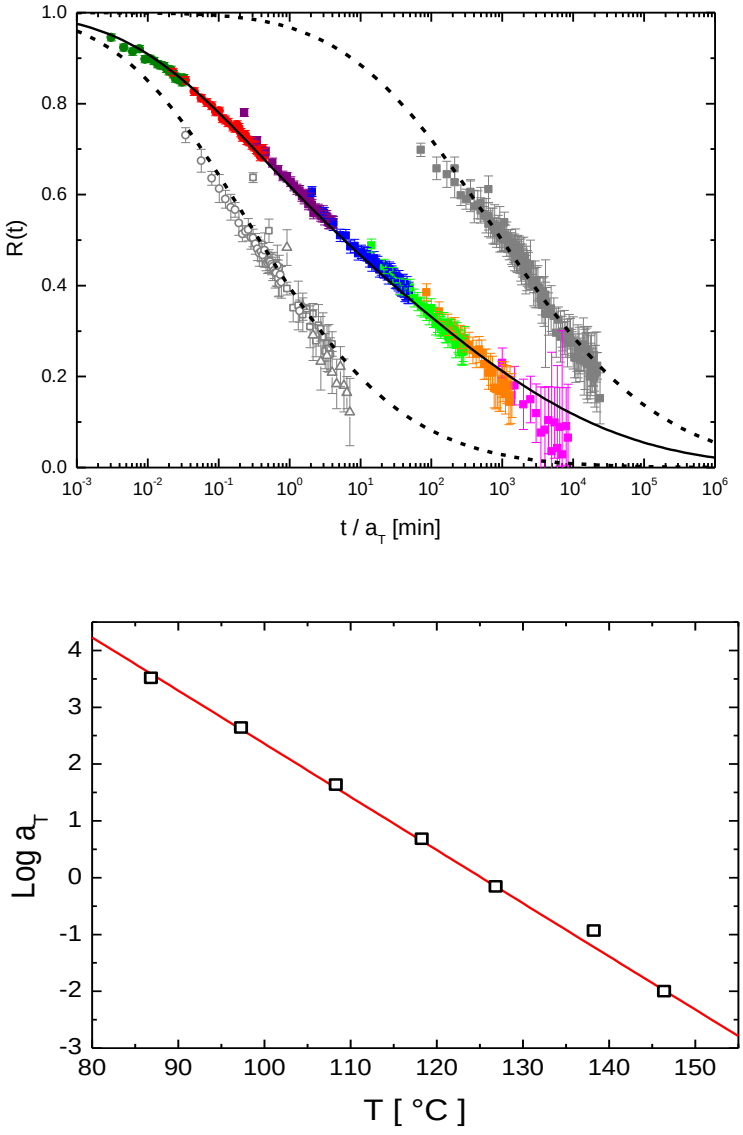

Figure 3.4. (a) Master curve for the TR-SANS results shown in Figure 3.3 following time-temperature superposition with T_{ref} = 125 °C. Colored symbols identify the measurement temperatures as shown in Figure 3.3. Gray symbols and dashed curves represent the master curves and model fits, respectively, reported earlier for the individual low and high molecular weight PS-PEP constituents used in the blended specimens.[76] The solid curve is calculated using Equation 3.4 and the two dashed curves without any adjustable parameters. (b) Time-temperature shift factors (open symbols) extracted from the time-temperature shifted data for the binary blends in (a). The solid curve represents $a_T(T)$ reported earlier for the individual (monomodal) components.[76]

Choi, *et al.*[76] modeled the molecular exchange dynamics of the monomodal diblock copolymer based micelles, as described in Equations 1.3 and 1.4. A first-order relaxation function for the extraction of an individual core block with degree of polymerization N_i subject to Rouse dynamics with a longest relaxation time τ_{Rouse} yields

$$K(t,N_i) = \exp(-t / \tau(N_i)), \tag{3.1}$$

$$\text{where } \tau(N_i) = \tau_{\text{Rouse}}(N_i) \times \exp(E_a(N_i)/kT). \tag{3.2}$$

In order to account for a distribution of chain lengths $K(t, N_i)$ is multiplied by a Zimm-Schulz distribution function $P(N_i)$ and the product is integrated over all N_i, yielding:

$$R(t) = \int_0^\infty P(N_i)K(t, N_i)dN_i \tag{3.3}$$

Only two parameters were adjusted in arriving at the model fits shown by the dashed curves in Figure 3.4a: the core block dispersity ($Đ$) and the combination parameter $\alpha\chi$, which accounts for the enthalpic penalty of exposing core segments to the solvent/corona matrix, where χ is the Flory-Huggins parameter and α is an O(1) constant.[108–110] The values of $Đ$ were 1.08 and 1.04 for PS-PEP-1 and PS-PEP-2, respectively, which are close to the dispersities determined by SEC (Table 2.1). The values of $\alpha\chi$ were 0.041 and 0.042 for the two polymers, which compare favorably with the reported value of χ for PS-PEP of 0.07.[135]

This model assumes that the overall rate of molecular exchange represents the sum of individual core block expulsion events. Hence, $R(t)$ for a binary mixture of two monomodal

populations of core blocks should be represented by the weighted sum of the component relaxation functions,

$$R(t)_{\text{binary mixture}} = \nu_1 R_1(t) + (1-\nu_1) R_2(t) \qquad (3.4)$$

where ν_1 and $R_1(t)$ are the mole fraction and relaxation function, respectively, for species 1. We have calculated the model prediction for the blend master curve (solid curve in Figure 3.4a) based on the previous model results for PS-PEP-1 and PS-PEP-2 (dashed curves in Figure 3.4a) with $\nu_1 = 0.61$ (see Table 2.1). Here we emphasize that this result, which accounts for the experimental data over nearly seven orders of magnitude in reduced time, was obtained without any adjustable parameters.

3.4 Summary and Conclusions

These results, obtained by intentionally broadening the distribution in core block molecular weights in spherical diblock copolymer micelles, provide conclusive support for the hypersensitivity of chain exchange rate to core block length, as suggested by the single chain exchange dynamics model proposed by Choi, *et al.*[76] Our findings compliment the recent study by Zinn, *et al.*[77] on rigorously monodisperse oligomeric diblocks. Whereas the elimination of dispersity drives the relaxation function to an exponential form, $R(t) \sim K(t,N) = \exp(-t / \tau(N))$, a bimodal mixture of relatively narrow distribution core blocks greatly expands the spectrum of exchange times, as demonstrated by Figure 3.4a. These findings suggest that exchange of polymers between micelles can be precisely tailored through blending strategies, including post-mixing populations of micelles with different core block molecular distributions.

Chapter 4.

Confirmation of the Independent Chain Hypothesis in the Chain Exchange of Diblock Copolymer Micelles

4.1 Introduction

As briefly discussed in Chapter 1, two primary mechanisms have been considered for micelle exchange kinetics: unimer exchange or single chain expulsion-diffusion, and micelle fusion/fission. The former was described by Aniansson and Wall[19,70] in the context of dilute low molecular weight surfactants. Halperin and Alexander (H&A)[73] later examined the exchange kinetics of block copolymer micelles and concluded that, due to the unfavorable interactions between micelle coronas, the Aniansson-Wall process should dominate in the case of macromolecular micelles at equilibrium. Dormidontova[74] studied the kinetics of micelle evolution in block copolymer micelles using a scaling approach, and also concluded that single chain exchange is favored over micelle fusion/fission when the

system is close to its equilibrium state. Furthermore, micelle equilibration rates in several different systems have been experimentally observed to be largely independent of micelle concentration within the dilute regime,[75–77,136] suggesting that micelle fusion/fission is insignificant for the micelle system near equilibrium. For the micelle systems away from equilibrium, on the other hand, the fusion/fission mechanism can become dominant, as suggested by the studies of Epps, Sullivan and co-workers.[99,100] By assuming single chain exchange, fitting models have been established and successfully described the relaxation kinetics in block copolymer micelles.[76,77,80] In agreement with this, a recent fluorescence study[84] found that the micelle fusion/fission rate is 10^6 times slower than chain expulsion-insertion in symmetric triblock copolymer (poly(ethylene oxide-*b*-propylene oxide-*b*-ethylene oxide)) micelle solutions.

Time-resolved small-angle neutron scattering (TR-SANS) has recently drawn attention as a clean and quantitative way of investigating micelle kinetics. Separately prepared deuterated core and protonated core micelles are "post-mixed" in a solvent of intermediate scattering length density. As chain exchange proceeds, the average core becomes contrast-matched to the solvent, and the scattered intensity decays to the background. Micelles prepared with previously blended deuterated and protonated chains (a "premixed" sample) provide a reference for the fully exchanged limit. Applying this technique, Richter and co-workers[75,77,83,98,136] reported studies on several systems, and defined a dimensionless molecular relaxation function $R(t)$ that quantifies the extent of chain exchange, which is given in Equation 1.2. Choi *et al.*[76] found that the rate of chain exchange in dilute solutions is largely independent of polymer concentration (from 0.5% to 2% by volume), which inferred a single chain expulsion mechanism. The authors proposed a model to describe the relaxation function by considering a hypersensitivity in chain exchange rate to the core block length/dispersity, which is shown in detail in Chapter 1, and supported by our observations in Chapter 3. This model is an extension of the detailed model of H&A, but

utilizes a linear N_{core} dependence ($E_a \sim N_{core}$) in the extraction barrier, rather than the $N_{core}^{2/3}$ in H&A. In particular, we investigated the influence of core block size distribution on chain exchange kinetics directly by blending copolymer chains of two different average PS block lengths in one binary micelle; the PS core block molecular weights differed by a factor of 1.6 (Chapter 3).[80] The measured relaxation curve was quantitatively accounted for by summing the weighted relaxation functions obtained from micelles formed by the individual components, consistent with the previously published model. These results complement the reported work of Zinn et al.[77] on spherical micelles with poly(ethylene oxide) corona polymers and hydrophobic *n*-alkyl head groups in the core, as these strictly monodisperse core segments yielded single exponential exchange rates. Thus it can be inferred that chain exchange is an independent, chain-by-chain event, and the barrier for one chain is not influenced by the length of the other chains in the same core; this also supports the single chain extraction hypothesis.

This argument for independent chain motion, although reasonable, still lacks direct proof. Here we report a TR-SANS study that quantitatively confirms the underlying assumption of independent, single chain exchange, independent of fitting parameters.

4.2 Experiment

Materials

Taking advantage of the TR-SANS technique and contrast matching strategy, we designed a micelle exchange system so that the same two PS-PEP diblock copolymers with different core block lengths are involved, but with separate observation of exchange kinetics of one species (*i.e.*, either "long" or "short" chains are visible). Normal (hPS-PEP-1 and hPS-PEP-2) and selectively deuterated (dPS-PEP-1 and dPS-PEP-2) diblocks with relatively narrow distribution ($Đ \leq 1.1$) were synthesized by sequential anionic

polymerization of styrene and isoprene, as previously described.[125] The poly(isoprene) blocks were then saturated with deuterium using a homogeneous Ni/Al catalyst, following the procedures described in Chapter 2. The average degree of polymerization of the two PS blocks were $\langle N_{PS} \rangle \cong 255$ ("short") and 412 ("long"), while the PEP blocks of all four polymers are comparable. The characteristics of the PS-PEP-1 and PS-PEP-2 diblock copolymers used in this study are summarized in Table 2.1.

Time Resolved Small Angle Neutron Scattering

Micelle solutions (1 vol%) were prepared using the co-solvent method described in Chapter 2. Figure 4.1 illustrates the contrast-matching strategy and includes the representations of "long-chain visible" micelles before and after exchange. For the pre-mixed samples, all four types of polymers (d-, h-PS-PEP-1, d-, h-PS-PEP-2) were co-dissolved in squalane and dichloromethane. The isotopic composition of the squalane (42 vol% normal squalane, and 58 vol% perdeuterated squalane (see Chapter 3 for the calculation of solvent composition); Sigma-Aldrich and C/D/N Isotopes, respectively) was selected to contrast-match the pre-mixed micellar cores. The post-mixed solutions, on the other hand, contains blends of separately prepared protonated micelles and deuterated micelles at room temperature, where PS chain extraction is suppressed ($T_{g,PS\ core} \approx 70$ °C in squalane[115]). To keep track of the exchange of PS-PEP-1 and PS-PEP-2 polymers individually in micelles containing both, it is necessary to prepare two different batches of post-mixed solutions: the “long chain visible” and the “short chain visible”. The “long chain visible” post-mixed samples, as depicted in Figure 4.1, contain micelles formed by pre-contrast-matched short chains (hPS-PEP-1 and dPS-PEP-1) and exclusively either deuterated long chains (dPS-PEP-2) or protonated long chains (hPS-PEP-2). Consequently, exchange of PS-PEP-1 molecules, *i.e.* the short chains, between the “long chain visible” micelles cannot be detected in TR-SANS, and only exchange of PS-PEP-2 chains is tracked.

Similarly, the "short chain visible" post-mixed solutions contain pre-contrast-matched long chains, and are monitored to characterize short chain exchange separately. In both cases, complete chain exchange leads to binary micelles, in which the four types of polymers are evenly redistributed. The pre-mixed samples approximate this scenario.

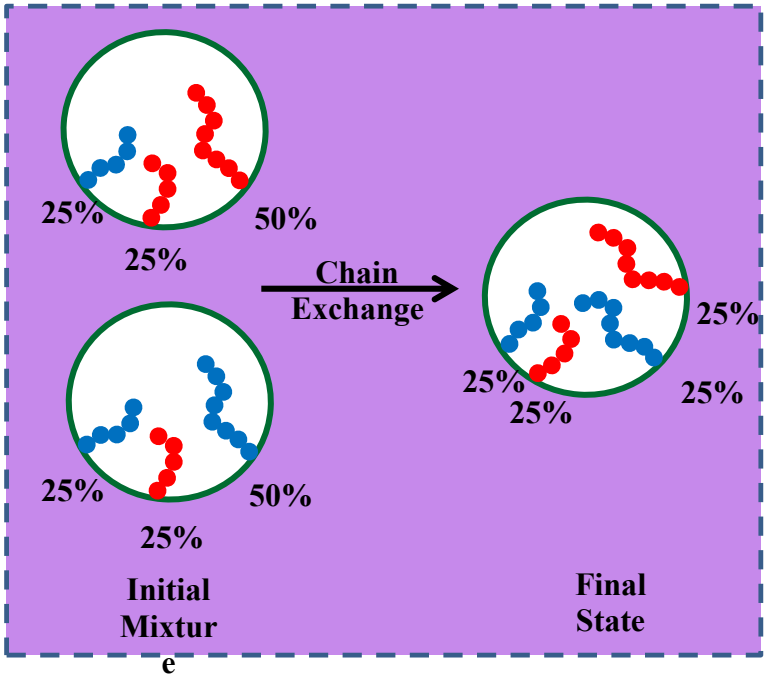

Figure 4.1. Chain exchange in a "long chain visible" post-mixed micelle solution. Micelles with protonated (blue) and deuterated (red) core blocks are blended, both containing 50 vol% contrast-matched short chains (hPS-PEP-1 and dPS-PEP-1) and 50 vol% long chains (hPS-PEP-2 or dPS-PEP-2 respectively) (the "initial mixture"). After complete chain exchange, mixed core micelles with 25% of each type by volume (the "final state") are obtained. A partially deuterated solvent is chosen (purple), to match the contrast of final state micelle cores.

TR-SANS experiments were performed with the CG-2 General-Purpose SANS instrument at the High Flux Isotope Reactor (HFIR) facility of the Oak Ridge National Laboratory (ORNL) in Oak Ridge, Tennessee. The identical instrument configurations and temperature control techniques as in the previous study described in Chapter 3 were used.[80]

Based on past experience with PS-PEP micelle equilibration kinetics, two temperatures were selected for each type of post-mixed solution (*i.e.*, long or short chain visible). The 2-D scattering patterns were acquired at 5 min intervals and were reduced and normalized using the Igor package provided by ORNL to give absolute intensities.

4.3 Results and Discussions

Figure 4.2 shows the TR-SANS results, obtained with the solvent, a pre-mixed solution and a long chain visible or short chain visible post-mixed sample at various temperatures. As the solvent squalane contrast matches the mixed cores, the mixing of isotope labeled chains can be signaled by scattering intensity reduction with exposure time at appropriate temperatures. The relaxation function $R(t)$ (Equation 1.2) is then calculated from each set of measurements at a certain temperature. To minimize experimental uncertainties, integrated intensities over a range of wave vector q (0.01 to 0.03 $Å^{-1}$ in this reported work) were used instead of that for a particular value of q. (The partially contrast-matched micelles lead to a reduction of scattering intensity as compared to our previous SANS studies in Chapter 3, and therefore a larger uncertainty in the calculated $R(t,T)$). $R(t,T)$ traces for both the long chain and short chain visible cases, each at two different temperatures, are plotted in Figure 4.3. The first point of each trace, which corresponds to scattering during the first 5 min exposure, was removed due to the time-dependent temperature.

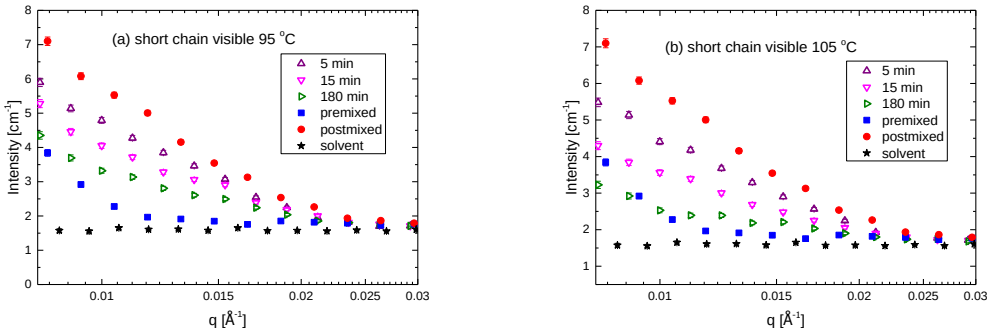

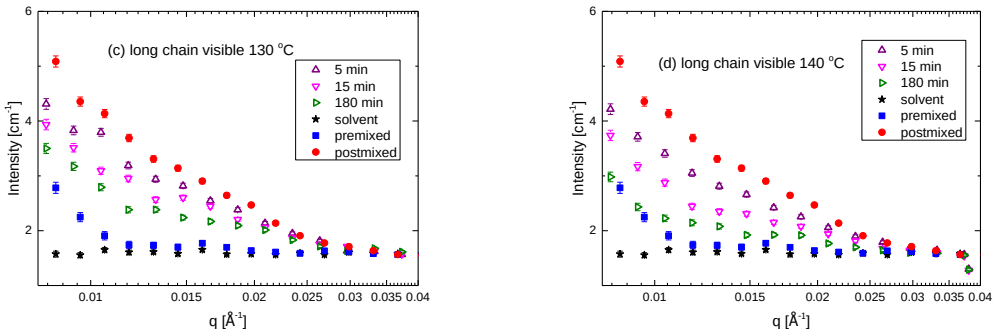

Figure 4.2. Representative TR-SANS patterns recorded in 5 minute increments during molecular exchange of PS-PEP in (a) a "short chain visible" post-mixed solution at 95 °C, (b) a "short chain visible" post-mixed solution at 105 °C, (c) a "long chain visible" post-mixed solution at 130 °C, and (d) a "long chain visible" post-mixed solution at 140 °C.

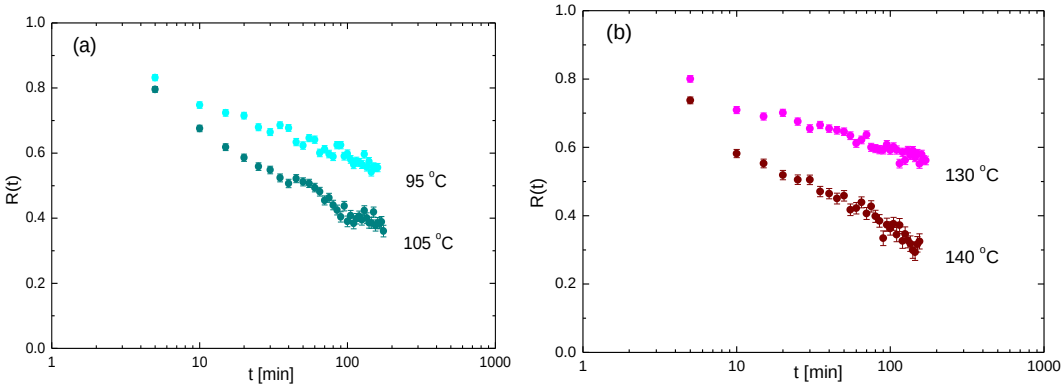

Figure 4.3. $R(t,T)$ traces determined by TR-SANS, with (a) "short chain visible" post-mixed solutions and (b) "long chain visible" post-mixed solutions, at two temperatures each.

To obtain a wider time scale in the relaxation function $R(t,T)$, the time-temperature superposition principle[107] (well-known for its application in rheological studies[106]) was applied, and the individual $R(t,T)$ traces were shifted along the horizontal axis until they visually overlap. An empirical shift factor a_T for a certain reference temperature T_{ref} is calculated according to $R(t/a_T, T_{ref}) = R(t, T)$. Figure 4.4a shows the $R(t)$ master curve from shifting individual traces measured at different temperatures (Figure 4.3) using shift factors

shown in Figure 4.4b, at a reference temperature of 125 °C. Reassuringly, within the uncertainty the shift factors (filled symbols) match those associated with single component micelle equilibration reported previously (straight line[76]), and those determined for binary polymer blends[80] (open squares, see Figure 3.4b) as well. This observation also confirms that having a different species of chains presented does not alter the micelle equilibrium mechanism.

Figure 4.4a compares the kinetics of PS-PEP block copolymer chains in the binary micelles with that of a single component. Two sets of filled symbols represent the shifted $R(t/a_T, T_{ref})$ data obtained with short chain visible (in light and dark blue) and long chain visible (in light and dark red) solutions, respectively. The dashed lines are model fits reproduced from the previous publication[76] in which single component PS-PEP micelles were investigated. The blue curve represents short chain (PS-PEP-1) micelles and the red one represents long chain (PS-PEP-2) micelles. The observation that the blue symbols fall right on the blue curve thus indicates that having long chains together in the binary micelle does not affect the exchange kinetics of the short chains. Similarly, the overlap of the red symbols and red curve implies that the long chain kinetics is independent of the presence of the short chains. These results unequivocally demonstrate that molecular exchange in block copolymer micelles is an independent event, which is consistent with the single chain expulsion mechanism predicted originally by Halperin and Alexander.[73] All the summarized earlier results suggested, but did not explicitly exclude, the possibility of micelle fission-fusion. For example, if the fission-fusion mechanism operated in parallel with single chain exchange, there might not be a strong micelle concentration dependence to the overall rate, as reported. The work presented here addresses this problem by resolving the motion of shorter and longer chains, in micelles with equivalent coronas (and therefore comparable barriers to fusion). If the contribution of fission-fusion were significant, the long chains in mixed micelles should be able to exchange at a rate closer to

that of the short chains than in pure long chains, but no hint of such a trend can be discerned. Furthermore, these data show conclusively that micelle fission/fusion events are not important.

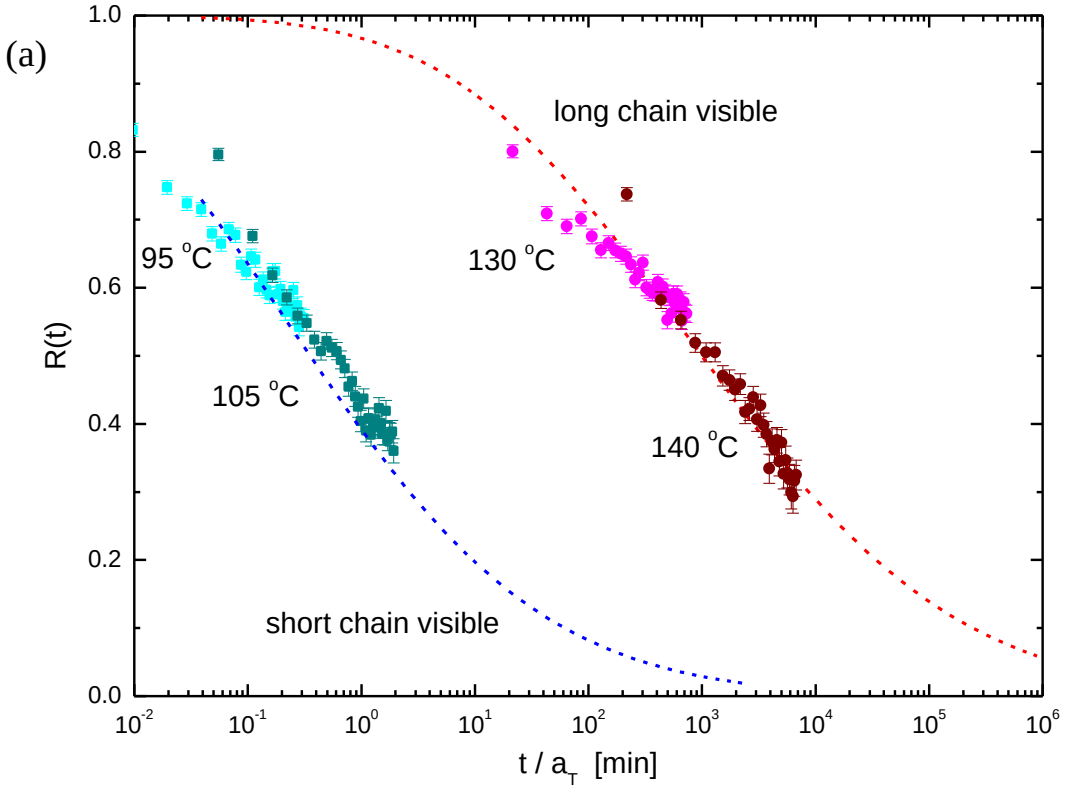

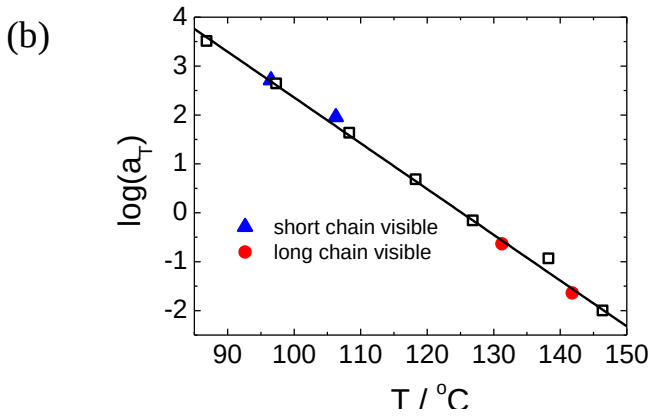

Figure 4.4. (a) Master curve for TR-SANS results shown in Figure 4.3, including a comparison with previously reported model fit[76] (the dashed curves) for single component micelles. (b) Temperature dependent shift factors (blue triangles and red circles) extracted from the relaxation function in (a). Open symbols identify shift factors associated with a core block dispersity study (Chapter 3) with blends of PS-PEP copolymers in squalane. The solid line represents a linear regression of shift factors reported for single component PS-PEP micelles.[76]

4.4 Summary and Conclusions

In this chapter we investigated micelle equilibrium kinetics of PS-PEP block copolymers in squalane using TR-SANS. The micelles contain polymers with two different PS block lengths, one of which is pre-contrast-matched so that they are invisible to SANS. Consequently, the time-dependent scattering intensity signals only the mixing of the visible species. A relaxation function $R(t,T)$ is calculated for quantitative comparison to the situation where the corresponding visible species is the only component in the micelles. Within experimental error, the two match with each other quantitatively, proving that the mixing of isotope labeled chains is an independent event, and thus the single chain exchange mechanism dominates in the described micelle solution. These results also exclude the possibility of micelle fusion/fission. In neat block copolymer melts, and in concentrated spherical domains of diblock copolymers in homopolymers, diffusion of single diblock copolymers by "activated hopping", *i.e.*, core block extraction, has also been reported. The confirmation of the single chain extraction mechanism for chain exchange between spherical diblock copolymer micelles presented here is thus in accordance with the interpretation of the reported diffusion mechanism in melts.[108,109]

Chapter 5.

Remarkable Effect of Molecular Architecture on Chain Exchange in Triblock Copolymer Micelles

5.1 Introduction

In Chapters 3 and 4, chain exchange between diblock copolymer micelles in dilute solution was investigated, using time resolved small angle neutron scattering (TR-SANS). It has been shown that the chain exchange rate is hypersensitive to core block length,[76,80] and that a single chain exchange mechanism (*i.e.*, extraction and redistribution of individual core blocks between micelles) is the rate limiting step for equilibration of hairy diblock copolymer micelle systems that are at or close to the optimal morphology.[81] Coalescence has been shown to be an operative mechanism for reorganizing an initial population of micelles with sizes far from the ideal state of aggregation under circumstances of extreme thermodynamic incompatibility, which hinders single chain

exchange.[99] Much less work has been done on the chain exchange of triblock copolymer-based micelles.

Adding an additional A or B block potentially increases the structural and dynamic complexity of the micelles. In the simplest cases involving symmetric triblocks, ABA polymers may form "hairy" micelles with B blocks looped within the core,[25] while a BAB molecular architecture accommodates the formation of "flower-like" micelles,[137] with a corona formed of A loops, and possibly clusters of micelles due to A blocks bridging between neighboring cores.

Here we report a TR-SANS investigation of micelles formed from symmetric PEP-PS-PEP and PS-PEP-PS triblock copolymers, where the structural features have been independently characterized using small angle X-ray scattering (SAXS). The results are discussed in the context of a model that describes diblock copolymer exchange well, but which is now found to be inadequate in the triblock case.

5.2 Experiment

Materials

Two sets of nearly matched PS-PEP-PS and PEP-PS-PEP triblock copolymers containing normal (hPS) and deuterated (dPS) polystyrene blocks were prepared by sequential anionic polymerization of styrene and isoprene, followed by selective hydrogenation of the polyisoprene (PI) blocks. The PI blocks in both types of triblock copolymers were saturated using deuterium gas and a homogeneous Ni/Al catalyst in cyclohexane.[124,125] Detailed experimental procedures for synthesizing the polymers used in this study have been described in Chapter 2. The SEC traces and ^{1}H NMR spectra including the calculation of the molecular weight of each block were also discussed in Chapter 2.

Molecular characteristics of the four triblocks were summarized in Table 2.1, together with those of the diblocks used previously in Chapter 3 and 4, as well as by Choi *et al.*[76,79–81] The triblocks were designed to have certain molecular weights and compositions so that they can be compared to the diblocks used previously. The PS and PEP blocks of the PEP-PS-PEP triblock polymers are of comparable degrees of polymerization to those of the PS-PEP-1 diblock, while the PEP blocks in the PS-PEP-PS triblock polymers are about twice the degree of polymerization of both PS-PEP diblocks. In other words, PEP-PS-PEP is similar to PS-PEP-1 but with one more corona block, while PS-PEP-PS is similar to a "coupled" PS-PEP-2. The dispersity $Đ$ of each polymer was obtained by SEC. Here we note that there remained a small amount of homopolymers and diblocks in the triblock materials (see Figure 2.2), which were not included in the determination of $Đ$. We do not believe the presence of these minor impurities affect the results or interpretation, as discussed below.

Small Angle X-ray Scattering (SAXS)

SAXS experiments were conducted using equipment maintained by the DuPont-Northwestern-Dow Collaborative Access Team at Argonne National Laboratory, using 4 keV radiation (wavelength $\lambda = 0.886$ Å) and a sample-to-detector distance of 6 m. The micelle solutions were prepared using the co-solvent method followed by thermal annealing, as described in Chapter 2. For this structural study, 1 vol%, 6 vol%, and 10 vol% solutions of PEP-PS-PEP, as well as 0.1 vol%, 0.5 vol%, 1 vol%, and 3 vol% solution of PS-PEP-PS were prepared. Assuming bulk densities of the PEP and PS blocks, the triblock densities were calculated and thus the volume percentages of polymers were determined. The SAXS experiments were conducted following the procedures documented in Chapter 2. The data was reduced with the Igor package Irena[138] provided by Argonne National Laboratory, and fitted with a model described below.

SAXS Fitting Model

Micelle structural features were extracted from the SAXS results using the Igor package provided by NIST.[134] A detailed description of the hard sphere model has been documented before,[125] and in Chapter 2 as well. The overall scattering intensity can be expressed as,

$$I(q) = \int D(R_c)(P_{mic}(q) + A_{mic}(q)^2[S(q) - 1])dR_c \qquad (5.1)$$

In the dilute limit $S(q) \rightarrow 1$ and equation 5.1 reduces to purely form-factor scattering,

$$I(q) = \int D(R_c)P_{mic}(q)dR_c \quad . \qquad (5.2)$$

In certain cases, such as the 3 vol%, 6 vol%, and 10 vol% PEP-PS-PEP solutions, and the 3 vol%, 6 vol%, and 10 vol% PS-PEP-PS solutions where the micelles experience some coronal overlap, micelle-micelle interactions are not properly accounted for by $S(q)$. In this situation we have found that the micelle core radius can be better estimated by fitting the data to the form factor (Equation 5.2) over the restricted q range of 0.02 to 0.13 $Å^{-1}$, where the micelle structure factor function does not contribute appreciably. For the 1 vol% PEP-PS-PEP, and the 0.1 vol%, 0.5 vol% and 1 vol% PS-PEP-PS solutions the structure factor was included in the fitting model (Equation 5.1). In this case a wider q range (0.008 $Å^{-1}$ to 0.2 $Å^{-1}$) was used.

Time-Resolved Small Angle Neutron Scattering (TR-SANS)

The contrast matching strategy is used in the TR-SANS experiments, and has been described in Chapter 3. Micelle solutions were prepared using the method described in Chapter 2. The post-mixed and pre-mixed solutions were prepared in the same way as

described in Chapter 3, which correspond to the initial and final state of chain exchange, respectively. Figure 5.1 illustrates the chain exchange between spherical micelles of (a) PEP-PS-PEP and (b) PS-PEP-PS. The detailed chain expulsion mechanisms showed in the figure are proposed based on the experimental results, and discussed later. The blue background represents the solvent squalane, the green denotes the PEP chains (coronas), and the red is PS chains (cores). Four types of micelle solutions were prepared and measured using TR-SANS: 1 vol% PEP-PS-PEP, 6 vol% PEP-PS-PEP, 0.5 vol% PS-PEP-PS, and 0.25 vol% PS-PEP-PS. The lower concentration for the PS-PEP-PS solutions was chosen to minimize the formation of molecular bridges between micelles, while still affording adequate scattering intensity.

The TR-SANS experiments were performed on the NG-7 30 m or the NG-B 30 m beamline at the Center for Neutron Research of the National Institute of Standards and Technology (NIST), Gaithersburg, MD. Data were acquired at a sample to detector distance of 13 m. The neutron beam had a wavelength $\lambda = 7$ Å and a wavelength spread of $\Delta\lambda/\lambda = 0.11$. The sample solutions were loaded into quartz banjo cells with a 1 mm specimen thickness. A 7-position temperature-controlled heating block capable of maintaining designated temperatures to within 1 °C was provided by NIST. To monitor the temperature inside a sample cell, the tip of a calibrated thermocouple was inserted in the cell next to the sample. This reference cell was filled with squalane so that the response to heating and cooling mimicked that of the actual sample. The samples were measured in the same way as described in Chapter 3. The 2-D scattering data were corrected for empty cell scattering, transmission, and detector sensitivity and reduced to absolute intensity using procedures established by NIST.[134]

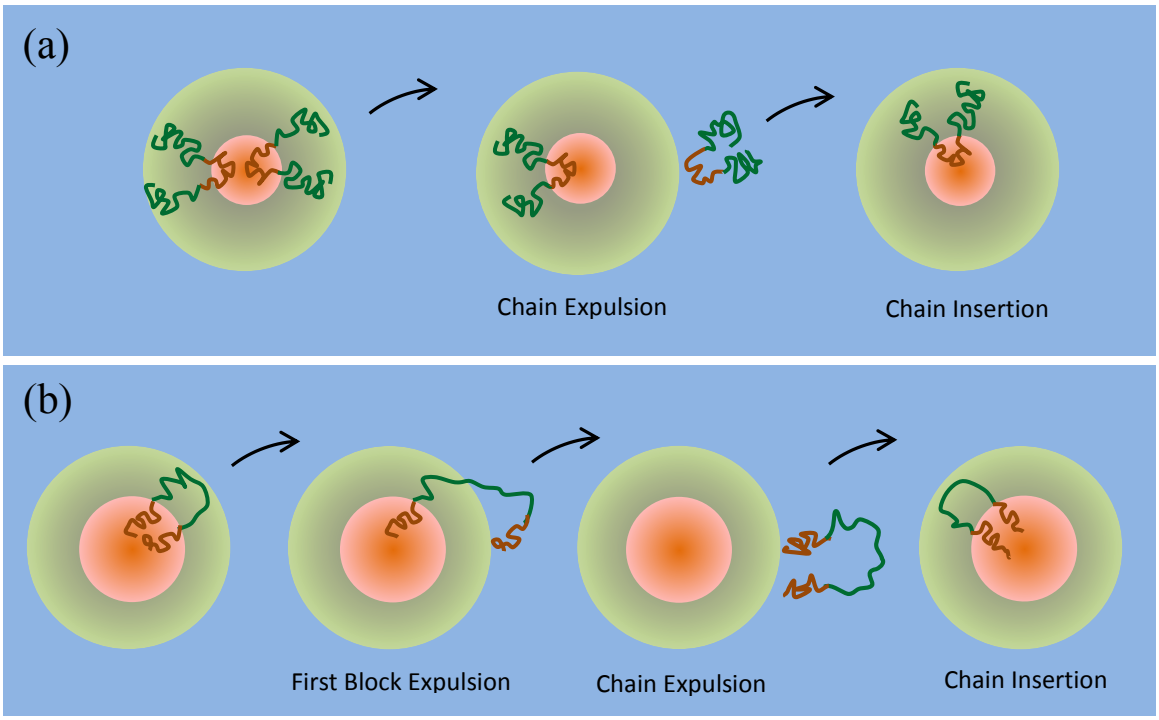

Figure 5.1. Schematic illustration of the process of chain exchange in micelles with two triblock architectures, (a) PEP-PS-PEP and (b) PS-PEP-PS. The relative micelle core sizes of PEP-PS-PEP and PS-PEP-PS were determined by SAXS; see Table 5.1. This figure is a schematic illustration of chain exchange between micelles, and does not address the detailed conformation of the PS blocks in solvent, which might be collapsed.[24]

5.3 Results

SAXS

Figure 5.2 shows SAXS patterns obtained while heating specimens containing (a) 1 vol%, (b) 6 vol%, and (c) 10 vol% PEP-PS-PEP, as well as (d) 0.1 vol%, (e) 0.5 vol%, (f) 1 vol%, and (g) 3 vol% PS-PEP-PS; data obtained while cooling were virtually indistinguishable from these results, except for the PS-PEP-PS solutions where the chain exchange is much slower (discussed below) and some hysteresis were observed (see Appendix). As the temperature is raised the broad peak associated with the micelle core form factor ($q \approx 0.08$ Å^{-1} for PEP-PS-PEP and $q \approx 0.045$ Å^{-1} for PS-PEP-PS) disappears,

indicative of dissolution at the highest temperatures. We have fit these results using equations 5.1 (Figure 5.1a, 5.1d, 5.1e, and 5.1f) and 5.2 (Figure 5.1b, 5.1c, and 5.1g); the associated core radii are listed in Table 5.1. The core dimensions of PEP-PS-PEP are essentially independent of temperature and concentration. Due to the larger PS molecular weights, PS-PEP-PS exhibits a significantly greater core radius, which may increase slightly with temperature. The 6 vol% and 10 vol% PEP-PS-PEP plot (Figure 5.2b and 5.2c, respectively) show clear evidence of interparticle interference (*i.e.*, structure factor peaks) below 200 °C, which indicate micelle-micelle interactions, and likely overlap of the corona blocks. For the 3 vol% PS-PEP-PS, the solution is visually gel like, and the corresponding SAXS plot (Figure 5.2g) shows clear structure factor peaks even at the highest temperature of 210 ºC. Some degree of structure factor scattering also can be seen in the low q region of the data obtained from the 1 % PS-PEP-PS solutions, which is qualitatively accounted for by Equation 5.1. However, the small oscillations in $I(q)$ at $q < 0.15$ Å^{-1} suggest possible micelle aggregation due to bridging of the triblock polymers.[139–141] Since the solution is a liquid at room temperature, we do not believe this is a predominant structural feature, *i.e.*, the sample is not close to gelation.

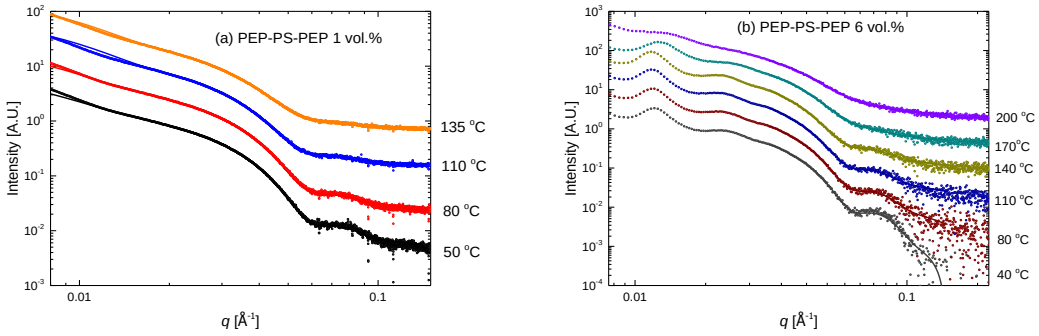

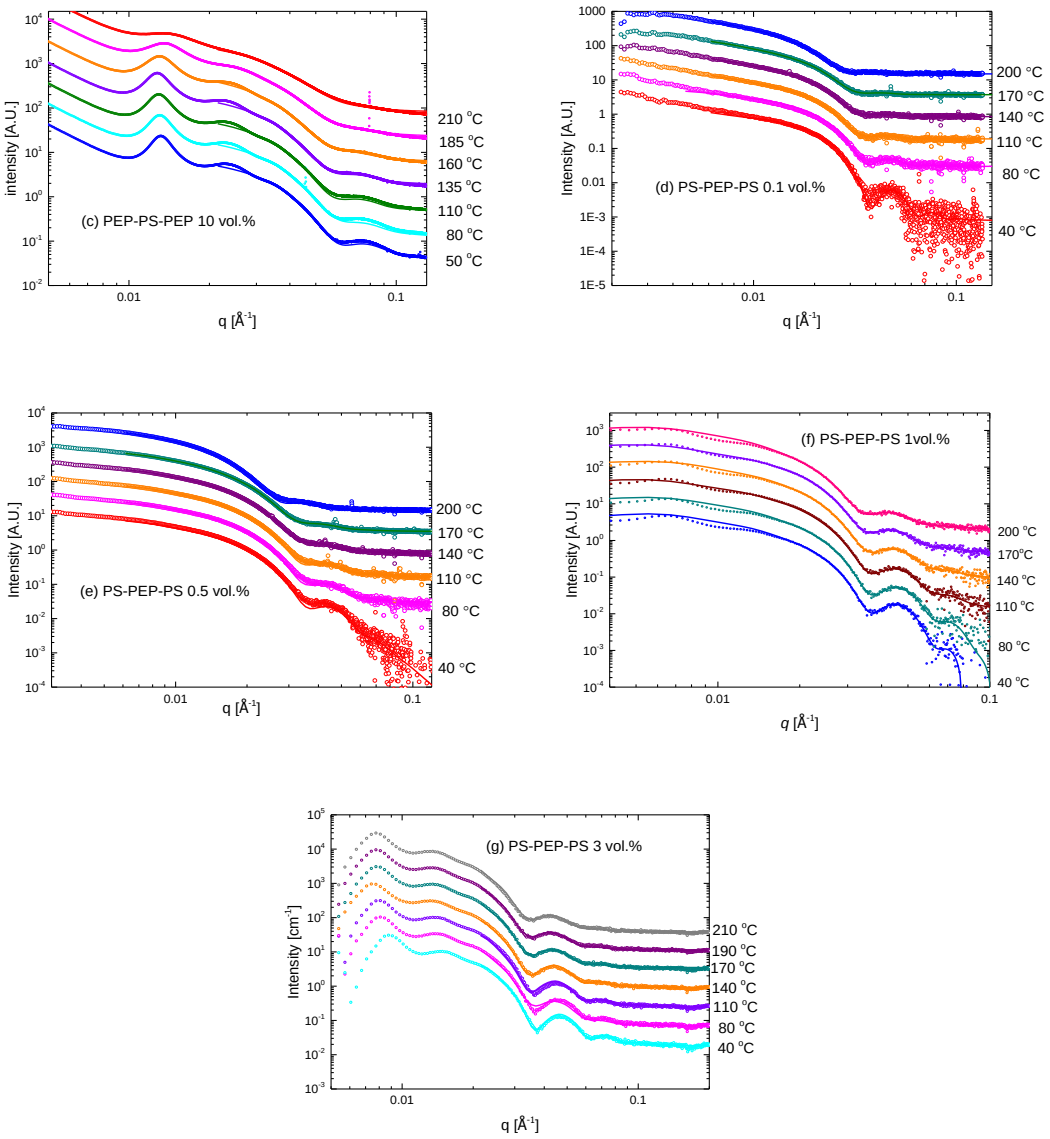

Figure 5.2. SAXS data upon heating for (a) PEP-PS-PEP 1 vol%, (b) PEP-PS-PEP 6 vol%, (c) PEP-PS-PEP 10 vol%, (d) PS-PEP-PS 0.1 vol%, (e) PS-PEP-PS 0.5 vol%, (f) PS-PEP-PS 1 vol%, and (g) PS-PEP-PS 3 vol%. Data are multiplied by powers of 3 as temperature increases. In each plot, points are SAXS data and lines are model fits in the same color.

Table 5.1. SAXS fitting results upon heating.

			1 vol% PEP-PS-PEP			
Temperature / °C	50	80	110	135	170	200
Core Radius / Å	78	79	82	76	---- *	---- *
			6 vol% PEP-PS-PEP			
Temperature / °C	40	80	110	140	170	200
Core Radius / Å	76	77	78	79	77	73
			10 vol% PEP-PS-PEP			
Temperature / °C	50	80	110	135	160	185
Core Radius / Å	76	78	80	81	84	83
			0.1 vol% PS-PEP-PS			
Temperature / °C	40	80	110	140	170	200
Core Radius / Å	120	121	129	133	137	---- *
			0.5 vol% PS-PEP-PS			
Temperature / °C	40	80	110	140	170	200
Core Radius / Å	132	134	135	140	143	---- *
			1 vol% PS-PEP-PS			
Temperature / °C	40	80	110	140	170	200
Core Radius / Å	129	128	129	131	134	136
			3 vol% PS-PEP-PS			
Temperature / °C	40	80	110	140	170	190
Core Radius / Å	128	130	132	133	133	135

* At higher temperatures form factor features in 1 vol% PEP-PS-PEP, 0.1 vol% PS-PEP-PS and 0.5 vol% PS-PEP-PS become too subtle to be fitted reliably.

TR-SANS

Sets of TR-SANS data acquired in this study are presented in Figure 5.3, one for each of the four triblock copolymer solutions studied. Each panel shows $I(q)$ recorded as a function of time at a fixed temperature. In each example, the initial patterns ($t = 0$, unmixed cores) reflect coherent scattering from equal numbers of hPS and dPS micelle cores, where the scattering length density of the solvent lies midway between that of the two isotopically pure spherical structures. Exchange of block copolymer chains with time reduces the contrast factor, virtually eliminating any discernible excess scattering intensity upon equilibration. (We attribute the minor residual scattering at $q < 0.015$ Å^{-1} for the longest recorded times to minor deviations from perfect contrast matching, particularly with respect to the corona blocks. This contribution does not impact the analysis, which relies on the relative change in $I(t,T)$ over $q > 0.01$ Å^{-1}.) These experiments were designed to reveal the rate of chain exchange over experimentally tractable times (*e.g.*, 2 to 3 hours), which represents a compromise between achieving adequate time resolution (*i.e.*, long enough to accommodate the finite time required to heat the specimens) and the 5 minute data acquisition periods necessary to acquire adequate counting statistics. This was accomplished by tuning the experimental temperature window, which is sample-dependent.

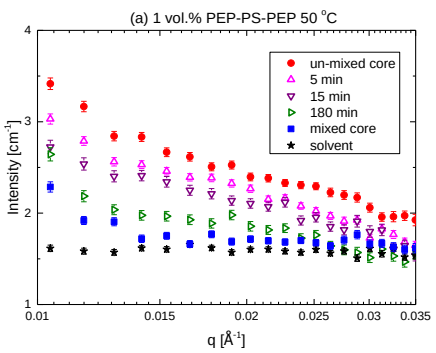

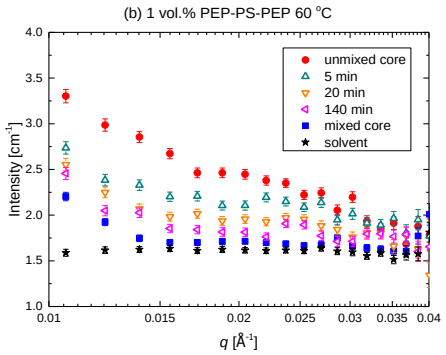

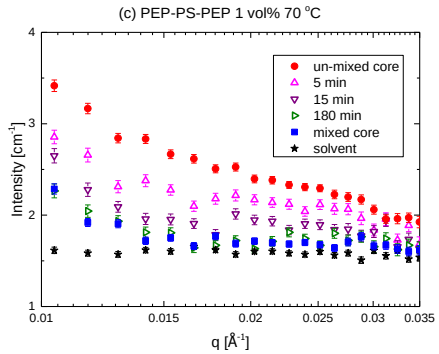
(c) PEP-PS-PEP 1 vol% 70 °C
un-mixed core
5 min
15 min
180 min
mixed core
solvent
Intensity [cm-1]
q [Å-1]

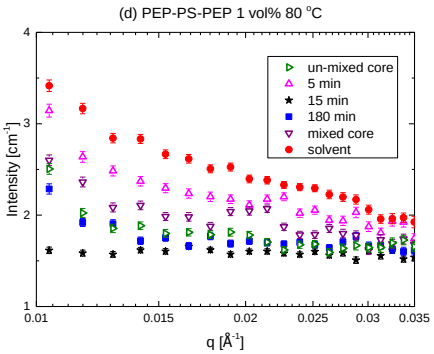
(d) PEP-PS-PEP 1 vol% 80 °C
un-mixed core
5 min
15 min
180 min
mixed core
solvent
Intensity [cm-1]
q [Å-1]

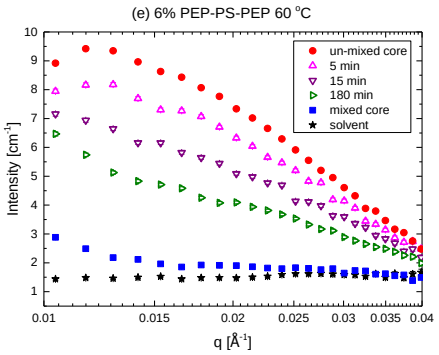
(e) 6% PEP-PS-PEP 60 °C
un-mixed core
5 min
15 min
180 min
mixed core
solvent
Intensity [cm-1]
q [Å-1]

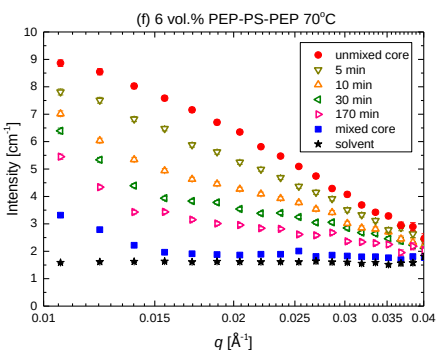
(f) 6 vol.% PEP-PS-PEP 70°C
unmixed core
5 min
10 min
30 min
170 min
mixed core
solvent
Intensity [cm-1]
q [Å-1]

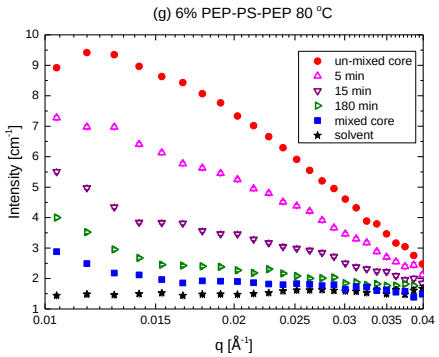
(g) 6% PEP-PS-PEP 80 °C
un-mixed core
5 min
15 min
180 min
mixed core
solvent
Intensity [cm-1]
q [Å-1]

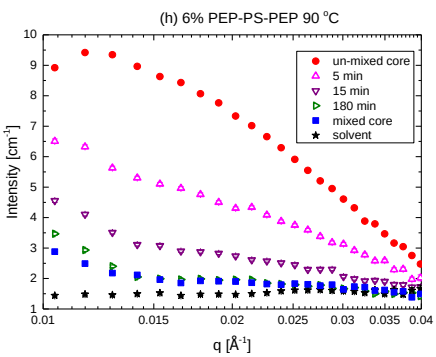
(h) 6% PEP-PS-PEP 90 °C
un-mixed core
5 min
15 min
180 min
mixed core
solvent
Intensity [cm-1]
q [Å-1]

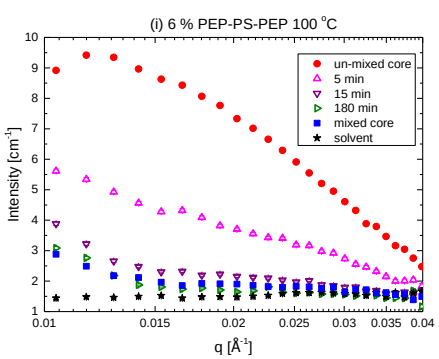
(i) 6 % PEP-PS-PEP 100 °C
un-mixed core
5 min
15 min
180 min
mixed core
solvent
Intensity [cm-1]
q [Å-1]

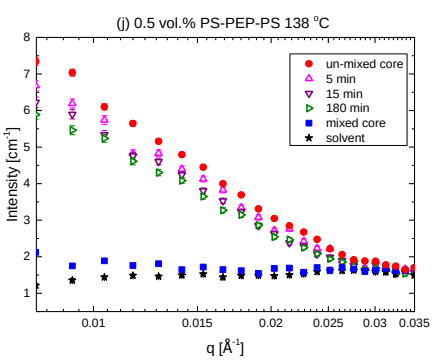
(j) 0.5 vol.% PS-PEP-PS 138 °C
un-mixed core
5 min
15 min
180 min
mixed core
solvent
Intensity [cm-1]
q [Å-1]

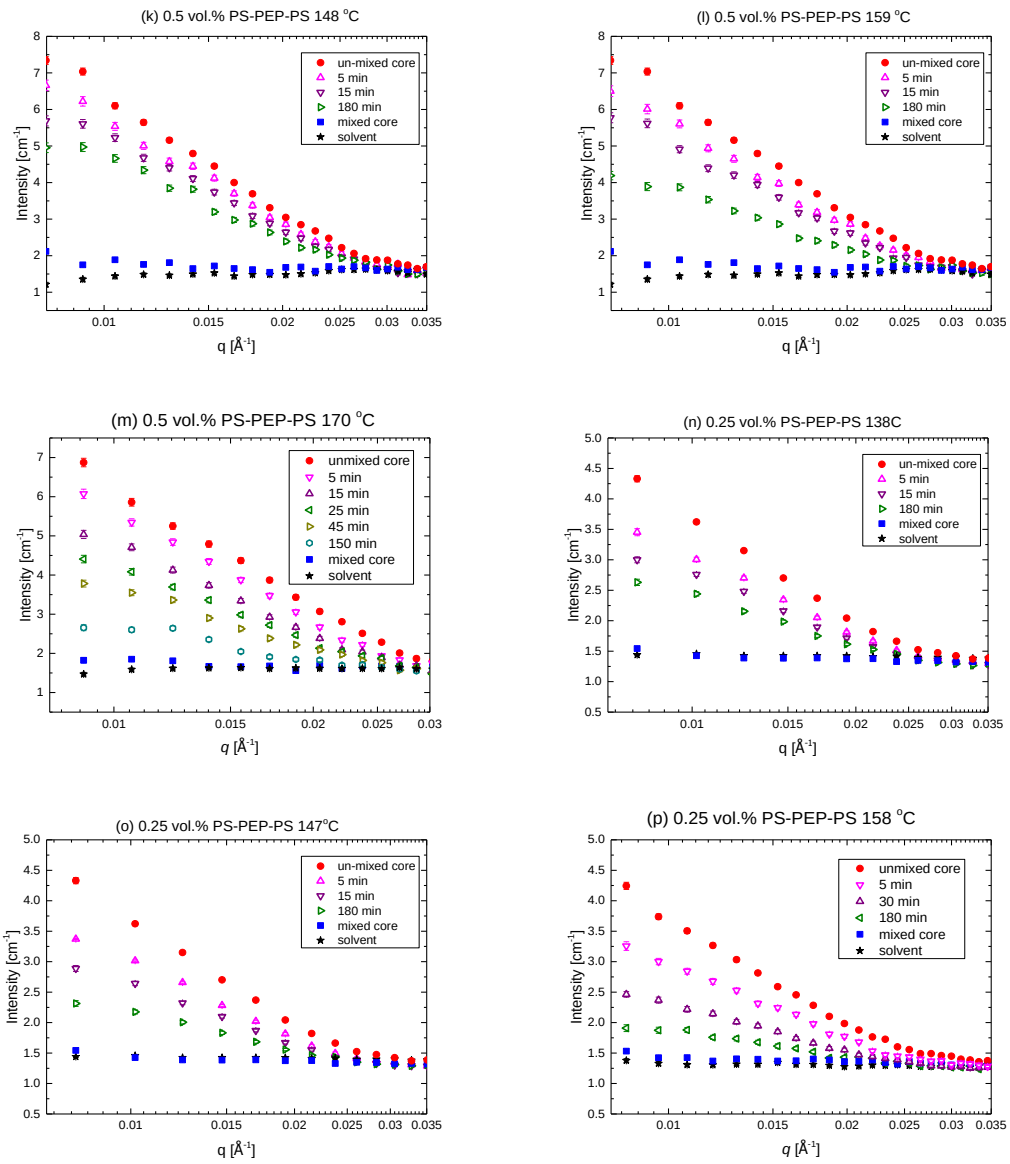

Figure 5.3. Representative TR-SANS patterns recorded in 5 minute increments during molecular exchange of: 1 vol% PEP-PS-PEP micelles at (a) 50 °C, (b) 60 °C, (c) 70 °C, and (d) 80 °C; 6 vol% PEP-PS-PEP micelles at (e) 60 °C, (f) 70 °C, (g) 80 °C, (h) 90 °C and (i) 80 °C; 0.5 vol% PS-PEP-PS micelles at (j) 138 °C, (k) 148 °C, (l) 159 °C, and (m) 170 °C; 0.25 vol% PS-PEP-PS micelles at (n) 138 °C, (o) 147 °C, and (p) 158 °C. The corresponding micelle solution used is noted in each plot. In every plot, the time resolved scattering patterns are compared to the scattering from a post-mixed specimen before chain exchange (red circles), a pre-mixed specimen (blue squares), and the solvent (black stars).

Changes in the SANS intensity were monitored as a function of time at constant temperature over the range $0.01 \leq q \leq 0.03$ Å^{-1}. The relaxation function $R(t)$ was calculated using equation 1.2. In Chapters 3 and 4, the intensity terms in equation 1.2 were calculated from an integration of the scattering intensity over the selected range of q. Alternatively, one can calculate the $R(t)$ using the invariant (*i.e.*, $\int I(q)q^2\,\mathrm{d}q$) instead of intensity integration over the same q range. The two methods generate very similar results. Figure 5.4e shows $R(t)$ for 6 vol% PEP-PS-PEP calculated using the invariant method, to compare with Figure 5.4b. $I(\infty)$ can be closely approximated using the pre-mixed specimen (mixed core). $R(t)$ is plotted for each of the measurement temperatures for the 1 vol% PEP-PS-PEP, 6 vol% PEP-PS-PEP, 0.5 vol% PS-PEP-PS, and 0.25 vol% PS-PEP-PS solutions in Figure 5.4. The first point of each trace, which corresponds to scattering during the first 5 min exposure, was removed due to the time-dependent temperature. In all four systems $R(t)$ decays more rapidly at higher temperatures.

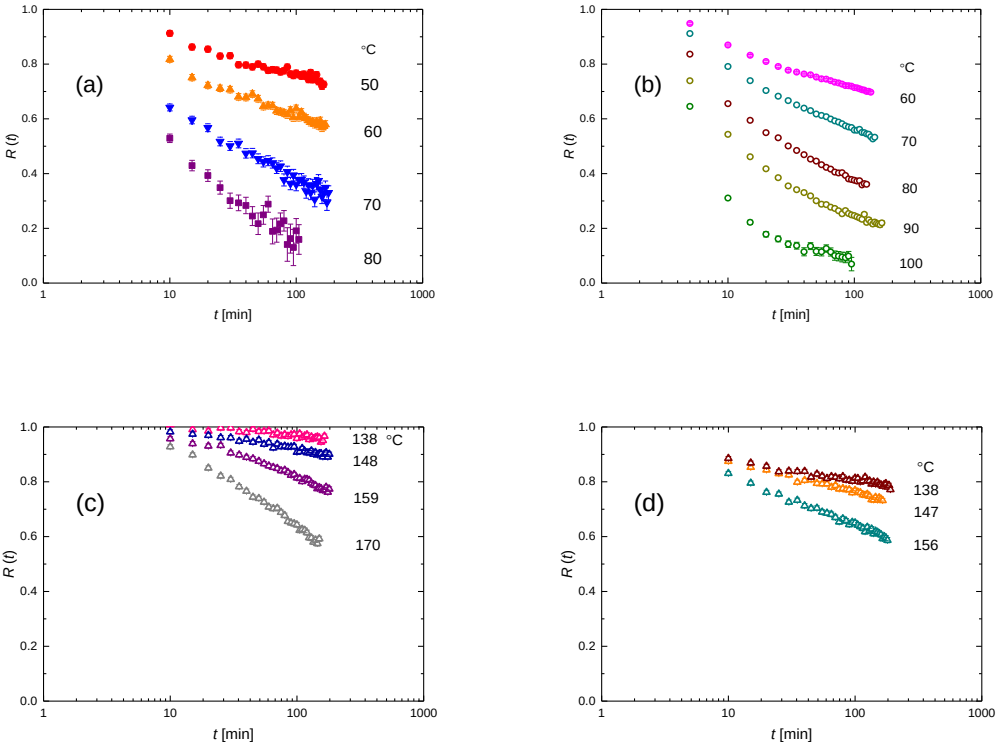

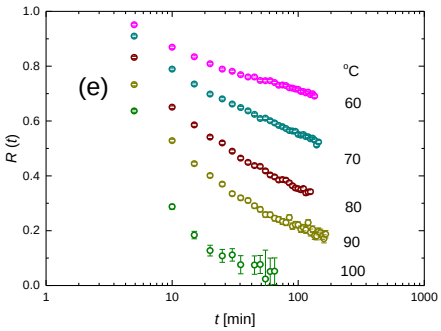

Figure 5.4. $R(t,T)$ determined by TR-SANS for post-mixed solutions of (a) 1 vol% PEP-PS-PEP, (b) 6 vol% PEP-PS-PEP, (c) 0.5 vol% PS-PEP-PS, (d) 0.25 vol% PS-PEP-PS, and (e) 6 vol% PEP-PS-PEP calculated the invariant of scattering intensity instead of the intensity integration. Temperatures are noted in each plot.

In previous publications and the previous two chapters dealing with diblock copolymer micelles,[76,79–81] it has been demonstrated that the well-known time-temperature superposition principle[106,107] can be exploited to construct master curves by shifting individual $R(t)$ traces obtained at different temperatures along the horizontal time axis. This treatment is based on the concept that the temperature dependence of the rate of chain exchange is dominated by the dynamics associated with the glass-forming PS blocks in the core. Here we apply the same principle with the four triblock copolymer micelles. Shift factors a_T were determined empirically by superposing the reduced TR-SANS data, $R(t/a_T, T_{ref}) = R(t, T)$, (Figure 5.5) where T_{ref} = 125 °C is the reference temperature. Figure 5.6 compares the values of a_T thus obtained for the triblocks with the shift factor relationship $a_T(T)$ obtained previously from PS-PEP diblock copolymer TR-SANS experiments at the same T_{ref} (solid curve).[76] Within experimental uncertainty $a_T(T)$ is independent of the molecular architecture, which strongly supports this application of the time-temperature technique. The shift factors do not follow the WLF dependence one might expect, for reasons that are not yet completely clear. However, since the use of these shift factors has been confirmed empirically, this uncertainty does not compromise the conclusions.

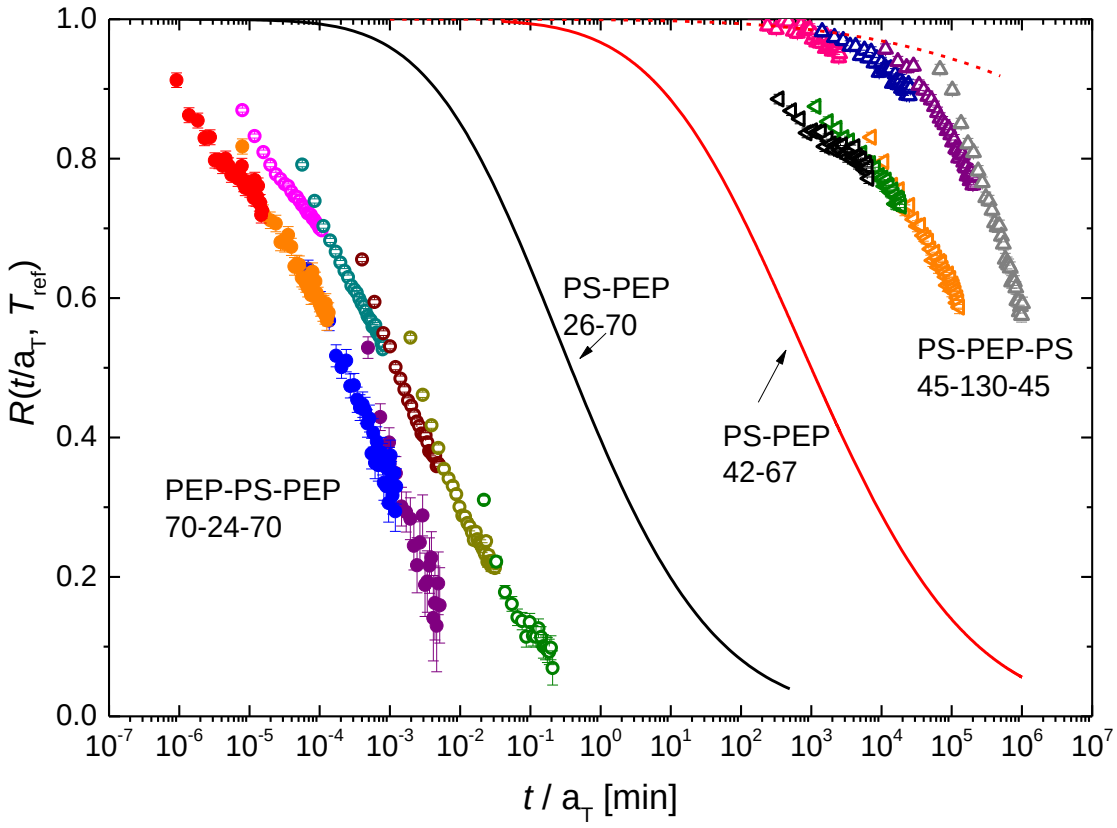

Figure 5.5. R(t) master curves (or R(t/aT, Tref) vs. t/aT curves) of four triblock micelles (left to right: 1 vol% PEP-PS-PEP, 6 vol% PEP-PS-PEP, 0.25 vol% PS-PEP-PS, 0.5 vol% PS-PEP-PS) and comparison to the diblock exchange model. The black line and red line are model fits of 1 vol% PS-PEP-1 and 1 vol% PS-PEP-2, respectively. The red dashed line is generated by the model assuming the two PS blocks in PS-PEP-PS extract independently, as discussed in the text.

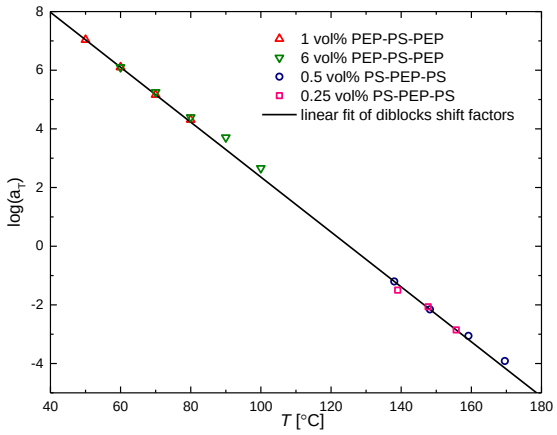

Figure 5.6. Logarithm of the shift factor a_T plotted against temperature for T_{ref} = 125 °C (open symbols, see legend). The solid line is the shift factor relationship reported earlier at the same reference temperature for diblock copolymer exchange, reproduced from Choi *et al.*.[76]

Figure 5.5 illustrates that the molecular architecture plays a pivotal role in determining the dynamics of molecular exchange in block copolymer micelles. Remarkably, the dilute PS-PEP-PS has a mean time constant that is nine orders of magnitude greater than that for the corresponding PEP-PS-PEP, and these two limiting cases bracket the results obtained previously for PS-PEP diblock copolymers, which are represented by the solid curves. We return to discuss these features below.

5.4 Discussion

Choi, *et al*. modeled $R(t)$ for PS-PEP diblock copolymers based on the hypothesis that molecular exchange is controlled by the rate of expulsion of individual core PS blocks into the solvent,[76] as described in Chapter 1 (equations 1.3 and 1.4). The core block length dependence of this model has been rigorously tested and validated for PS-PEP diblock micelles in squalane in Chapter 3, 4 and by Choi *et al.*[76,79] In particular, the extremely broad relaxation functions are fully explained by the modest dispersities associated with anionic

polymerization, and a single value of $\alpha\chi$ accounts for the orders of magnitude difference between PS-PEP-1 and PS-PEP-2. Previous workers have proposed a collapsed conformation for the PS block once outside the core, leading to $E_a \sim N^{2/3}$,[73,75,98,113,136] but our previous diblock results in Chapter 3 and 4 and those of Choi *at el*. [76,79] were quantitatively described with the aforementioned linear dependence on N.[76,79–81] Figure 5.5 summarizes the model fits to the PS-PEP diblock copolymer results reported earlier,[76] obtained with PS-PEP-1 and PS-PEP-2 at 1 vol%. Clearly, the functional form of the triblock results is quite similar to these calculated relaxation functions. In addition, the shift factors $a_T(T)$ of the triblocks are essentially the same as those of the diblocks (Figure 5.6), and therefore a convincing comparison of $R(t)$ of the triblocks to the diblock model can be made.

Starting from the left in Figure 5.5, we can first compare the 1 vol% PEP-PS-PEP master curve to the 1 vol% PS-PEP-1 model fit (solid black line). Clearly PEP-PS-PEP exchanges at a much higher rate than PS-PEP-1, while both are dilute and have comparable micelle core size (Table 5.1). These polymers have very similar core and corona block lengths, with the one obvious difference being the additional corona block attached to the PS core block in the triblock case. Clearly this additional block greatly facilities movement of the PS core block into the solvent, by a factor of about 2,000. The direction of this shift seems intuitively reasonable, but the magnitude is substantial. We emphasize that this factor is not captured by the simple model represented by Equations 5.4-5.6. If the enthalpic penalty for exposing a core block to the solvent/corona mixture were the only energetic barrier for extracting one entire molecule, adding one additional corona block should not alter the overall exchange rate, contrary to this result. Interestingly, however, this result does confirm the appropriateness of assuming Rouse dynamics apply to the core block. If the core block were forced to reptate, a corona chain would necessarily be dragged through the core, increasing the net barrier to expulsion substantially.[142] One clear conclusion from

this acceleration of chain exchange is that the corona block plays an important role; conceivably the release of a PEP block from the crowded confines of the corona into good solvent reduces the net expulsion barrier substantially, as suggested in an earlier theoretical study.[73] In such a scenario, the previously reported barriers represent a compromise between an even larger barrier to core block extraction than inferred, mitigated by a free energy gain for the corona block.

Using TR-SANS, Lund and coworkers compared the molecular exchange dynamics of a PB-PS-PB (10K-20K-10K) triblock copolymer with those of a PB-PS (10K-10K) diblock copolymer in dodecane (C_{12}) and tetradecane (C_{14}), both of which favor the PB blocks.[98] While both solutions were dilute and the polymer micelles had comparable sizes, the triblocks exchanged at a rate about 10 times slower than the diblocks. While this could be attributed to the doubled core block length,[76] or topological effects due to molecular knots in the core,[98] the fact that the PEP-PS-PEP (70K-24K-70K) triblocks exchange much faster than corresponding PS-PEP (26K-70K) as shown in Figure 5.5 clearly suggests that the core block length is not the only factor that contributes to chain exchange dynamics, likely a reflection of the role of the corona blocks as mentioned. In addition, since doubling the core block length should accordingly[76] cause the exchange dynamics to slow down by several orders of magnitude, the merely one order of magnitude difference seen by Lund *et al*. could possibly be a net effect resulting from the accelerating effect of the additional corona block in PB-PS-PB, as hypothesized above. Clearly, this issue warrants additional theoretical and experimental attention.

Next, comparing the first and second master curves in Figure 5.5, we see that increasing the concentration of PEP-PS-PEP from 1 to 6 vol% increases the exchange time constant by nearly an order of magnitude, consistent with the trend found previously with PS-PEP-1.[79] Theoretical analysis by Halperin suggests that the slower kinetics in concentrated (15 vol%) PS-PEP-1 micelles may be a result of the increased core block insertion penalty into

the corona region when escaping the micelle, due to a significantly larger micelle core than dilute micelles (1 vol%).[113] The core size of the PEP-PS-PEP micelle however, does not exhibit any noticeable change as the concentration increases from 1 vol% to 6 vol% (Table 5.1), and therefore this observation can be tentatively attributed to the crowding of corona chains above the overlap concentration.[79] In other words, for the dilute micelles, the corona chains experience a relief of chain stretching upon escaping the micelle into free solution, thereby lowering the barrier to escape, whereas at higher concentrations, the corona chains are in semidilute conditions whether in the micelle or not. This result is also suggestive of a significant role played by the corona.

A similar concentration effect on chain exchange rate is found in PS-PEP-PS solutions, as shown by the last two master curves in Figure 5.5. Increasing the concentration from 0.25 vol% to 0.5 vol% increases the exchange time constant of PS-PEP-PS by about an order of magnitude. However, unlike the case of PEP-PS-PEP, both solutions of PS-PEP-PS are quite dilute. Since the 0.5 vol% solution appears to be slightly cloudy while the 0.25 vol% solution is clear, some micelle aggregates caused by polymer chains bridging are likely to be present in the 0.5 vol% solution. As mentioned above, crowded coronas can lead to a retarded chain exchange, and therefore chain exchange in the aggregated micelles can be slower than that between the unconnected micelles in 0.25 vol% solutions. On the other hand, the unconnected micelles in 0.25 vol% solutions may contain a few dangling PS chains, *i.e.*, one of the PS end blocks remains outside of the micelle, making the expulsion of such an entire polymer molecule easier than usual.

Most importantly, Figure 5.5 suggests the remarkable effect of polymer architecture on molecular exchange dynamics. The first and third master curves in Figure 5.5, which represent the chain exchange of 1 vol% PEP-PS-PEP and 0.25 vol% PS-PEP-PS respectively, differ by about 9 orders of magnitude along the time axis, while the two polymers have comparable total size (Table 2.1) and both solutions are dilute. One can

imagine the situation of chain expulsion in the two cases as follows: for a PEP-PS-PEP molecule to leave a micelle, only the middle PS block needs to be extracted, while in the case of PS-PEP-PS both PS blocks need to escape. Once one of the two PS blocks of PS-PEP-PS reaches the solvent/corona matrix, the other PS block has to escape before the first block re-inserts into the core. Therefore the probability for an entire PS-PEP-PS molecule to leave a micelle is much lower. The very slow dynamics of PS-PEP-PS can thus be attributed to this fact, assuming that the triblocks adapt the same single chain exchange mechanism as the diblocks.[81]

Lastly, on the right of the plot in Figure 5.5, the chain exchange of 0.25 vol% PS-PEP-PS is compared with 1 vol% PS-PEP-2, a diblock with composition similar to but total molecular weight approximately half of the triblock. Crucially, the PS block sizes are very similar. It is clear that PS-PEP-PS exchanges at a much slower rate than PS-PEP-2, which can be attributed to the two connected core blocks.[76] As discussed above, if the extraction of the two PS blocks from a PS-PEP-PS triblock micelle are completely uncorrelated events, the overall molecular exchange rate would be anticipated to be controlled by the product of the probability of extracting each block independently, and that gives the dashed line besides the 0.5 vol% PS-PEP-PS data in Figure 5.5. In other words, with the further assumption that the Rouse relaxation time constant of each PS block is the same as that of PS-PEP-2, the probability of full extraction of a PS-PEP-PS molecule from a micelle would be proportional to $\exp(E_a(N_{\text{PS-PEP-PS}}/2) / kT) \times \exp(E_a(N_{\text{PS-PEP-PS}}/2) / kT)$, where N is the total number of PS repeat units in one PS-PEP-PS molecule. In the dilute limit we expect the rate of exchange to be independent of concentration, which permits a direct comparison of $R(t)$ for the 0.25 vol% PS-PEP-PS solutions to the 1 vol% PS-PEP-2 diblock results described previously.[76] Therefore Equation 5.6 can be rewritten as

$$\tau(N_{\text{PS-PEP-PS}}) = \tau_{\text{Rouse}}(N_{\text{PS-PEP-2}}) \times \exp(E_a(N_{\text{PS-PEP-2}}) / kT) \times \exp(E_a(N_{\text{PS-PEP-2}}) / kT). \quad (5.7)$$

Substituting this result into Equations 5.4 and 5.5, the complete function of $R(t)$ is expressed as:

$$R(t) = \int_0^\infty P(N)K(t,N)dN$$
$$= \int_0^\infty P(N_{PS-PEP-2})\exp\left(-t/\tau_{Rouse}(N_{PS-PEP-2}) \times \exp(E_a(N_{PS\text{-}PEP-2})/kT) \times \exp(E_a(N_{PS\text{-}PEP-2})/kT)\right)dN \cdot \quad (5.8)$$

The massive increase in τ for PS-PEP-PS relative to PS-PEP-2 (see Table 2.1) thus can be qualitatively accounted for, and is shown by the dashed (red) curve in Figure 5.5. However, while the onset of the decay in $R(t/a_T)$ is anticipated by this calculation, the actual rate of reduction in $R(t/a_T)$ is significantly smaller than predicted, suggesting that core block molecular weight and dispersity are not the only factors involved. It is certainly reasonable to expect that the extraction of the second block could be facilitated by the fact that the other PS chain end is out in free solution, beyond the corona. Experiments[143] and simulations[144] by Yokoyama and coworkers dealing with BAB triblock copolymer diffusion in BCC spherical domains suggest that this process is controlled by activation of one end block at a time ("walking" diffusion, which encounters a thermodynamic barrier (χN_B) for sequential rather than simultaneous activation ($2\chi N_B$) of both end blocks. These results are in partial agreement with ours, where the extraction of the two end blocks in PS-PEP-PS are not completely independent events.

5.5 Summary

Chain exchange of PEP-PS-PEP (1 vol% and 6 vol%) and PS-PEP-PS (0.25 vol% and 0.5 vol%) triblock copolymer micelles in squalane was investigated using TR-SANS at various temperatures, and compared with corresponding PS-PEP-1 and PS-PEP-2 diblock micelle dynamics reported previously. The observations are discussed in the context of a previously established model based on PS-PEP diblock chain exchange, and the main results are as follows. PEP-PS-PEP exchanges at a faster rate than PS-PEP-1 in dilute micelle solutions; as concentration increases from 1 vol% to 6 vol%, chain exchange rate of PEP-PS-PEP decreases; as concentration increases from 0.25 vol% to 0.5 vol%, chain exchange rate of PS-PEP-PS also decreases; PS-PEP-PS exchanges at multi-order of magnitude slower rate than PEP-PS-PEP and PS-PEP-2 in dilute micelle solutions, but somewhat faster than what is expected from the diblock model assuming uncorrelated extraction of the two PS blocks. These results indicate a remarkable effect of polymer architecture on molecular exchange between polymer micelles, and suggest a crucial role of corona blocks in molecular exchange dynamics. The contribution of corona chains to the chain exchange rate is further investigated in Chapters 6 and 7.

Chapter 6.

Addition of Corona Block Homopolymer Retards Chain Exchange in Block Copolymer Micelles

6.1 Introduction

Choi *et al*. found the chain exchange rate of 15 vol% PS-PEP in squalane to be about one order of magnitude slower than that of 1 vol% PS-PEP, implying a role of the corona blocks in the chain exchange process.[79] The detailed mechanisms of the slowed down kinetics in concentrated PS-PEP solution is not yet clear. In our recent study of triblock copolymer chain exchange (Chapter 5), an accelerating role of corona blocks was clearly indicated.[82] The rate of chain exchange in PS-PEP was compared with that for PEP-PS-PEP triblocks containing the same PS block size but with one additional PEP corona block of the same size; the latter system was found to be faster by several orders of magnitude. The hypothesis is that the corona blocks can accelerate the chain extraction step in chain exchange process, by experiencing a relief of chain stretching upon escaping into the solution, which is consistent with the earlier theoretical prediction by Halperin.[73] This result gives a clue as to the role of corona blocks in chain exchange between micelles in

concentrated solution. Namely, above the overlap concentration, the corona chains would be in a semi-dilute solution whether inside the micelles or not, and therefore the chain extraction step is less favored. On the other hand, the depletion effect of overlapped corona chains[145] leads to an increased micelle size (aggregation number) at equilibrium. This could consequentially make both the chain insertion and extraction step harder as corona chain density increases.[113] Neither of these two hypotheses has been tested yet.

Here we report a TR-SANS study of PS-PEP block copolymer micelle chain exchange in squalane/PEP mixtures. Adding PEP homopolymers of the same size as the corona block into a dilute PS-PEP diblock micelle solution introduces a controlled degree of corona overlapping/chain stretching, while keeping the Flory-Huggins interaction parameter between core blocks and matrix approximately constant. This mimics the situation in a more concentrated diblock or triblock micelle solution. Since adding the PEP homopolymers can also introduce corona chain overlap, it could also correlate the depletion effect, which could cause phase separation, and a change in the micelle size[145] Therefore in this study we carefully monitored these two issues using light scattering and small angle X-ray scattering.

Figure 6.1 schematically illustrates the overlapping of corona chains induced by adding homopolymers of the identical size and species as the corona chains or by increasing micelle concentration. In the figure, the blue circles represent micelle cores, the dark blue lines represent the micelle corona chains, the orange small circles represent solvent molecules, and the light blue lines represent homopolymers that are identical in chemical structure and size with the corona chains. For dilute micelles in solvent (Figure 6.1a), the coronas are swelled by solvent and the corona chains are not overlapping with each other, or the ones from another micelle. For concentrated micelle solution (Figure 6.1c) the corona chains form different micelles overlap with each other. A similar situation happens in dilute micelle solution with added homopolymers (Figure 6.1b), where the

homopolymers chains of the same size and chemical species overlap with the corona chains of the micelle, even though the concentration of micelle is still dilute.

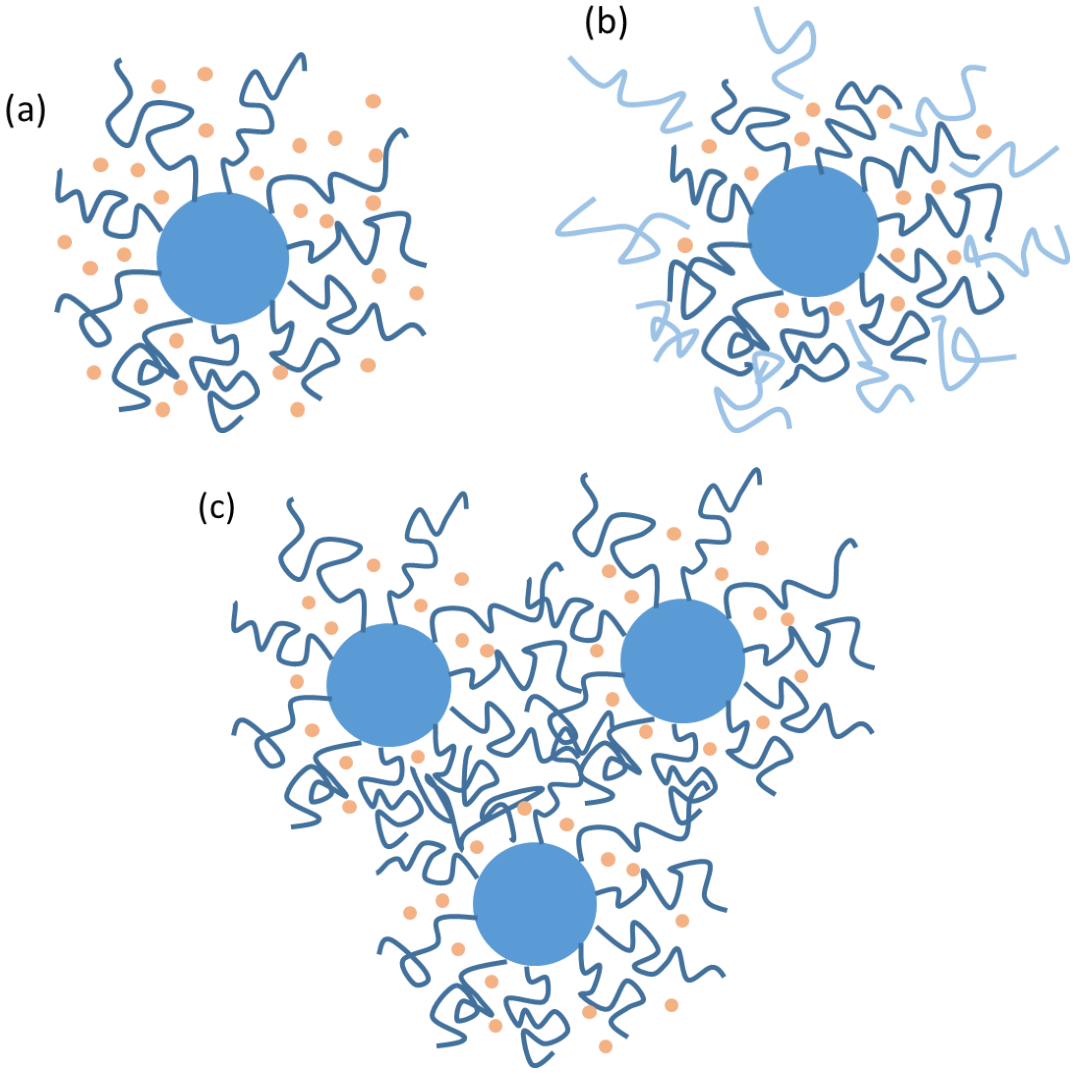

Figure 6.1. Micelle corona chains (a) swelled by solvent in a dilute solution, (b) overlap with homopolymers chains in a dilute solution, or (c) with the corona chains from another micelles in a concentrated solution.

6.2 Experimental Section

Materials

The PS-PEP copolymers (with deuterated equivalents for SANS experiments) and the PEP homopolymers of comparable size as the PEP blocks were synthesized as described in Chapter 2. The molecular weight of PEP was determined using size exclusion chromatography (SEC) with a light scattering detector (Wyatt DAWN). SEC traces of the PEP homopolymers before and after saturation were shown in Chapter 2. Table 6.1 summarizes the molecular weights, composition, and distribution of the PEP homopolymer and d- / h-PS-PEP diblock copolymers.[76] This table reproduces part of the Table 2.1, and the d- / h-PS-PEP diblock copolymers used here correspond to the "d-PS-PEP-1" and "hPS-PEP-1" polymers in Table 2.1. The PEP was designed to have the same molecular weight as the PEP block in PS-PEP diblocks, so that the overlapping of PEP chains induced by adding PEP homopolymers is comparable to that induced by increasing the concentration of PS-PEP in solution.

Table 6.1. Polymer characteristics.

	M_{PS} (kDa)	M_{PEP} (kDa)	$Đ$
dPS-PEP*	26	70	1.04
hPS-PEP*	29	71	1.10
PEP	----	65	1.07

* Reproduced from Choi *et al.*[76]

Time-Resolved Small Angle Neutron Scattering (TR-SANS)

The dPS-PEP and hPS-PEP micelles were separately prepared using the co-solvent method followed by thermal annealing, as described in Chapter 2. After the solution was cooled down to room temperature in air, PEP was added into the micelle solutions at 2 vol%, 7 vol% or 15 vol% (designated as 2PEP, 7PEP, and 15PEP samples correspondingly), and stirred until dissolved. Assuming the density of each block is the same as the corresponding bulk homopolymers, the relative amounts of d-/h-PS-PEP diblock polymers and PEP homopolymers were calculated to make the final concentration of PS-PEP 1 vol%. The solutions were then stored at room temperature and used without further thermal annealing. The glass transition temperature of the PS cores in squalane is about 70 ºC, well above room temperature.[115] Therefore the size of PS-PEP micelles in the solution mixture remain the same as those of 1 vol% micelles in pure squalane,[76] and does not depend on the concentration of PEP. The d- and h- micelles in squalane/PEP mixtures were then blended (post-mixed, thus forming unmixed micelle cores) at room temperature and loaded into sample cells for TR-SANS experiments. 1 vol% d- and h-PS-PEP micelles in pure PEP (99PEP) rather than squalane were also prepared by co-dissolving the polymers in dichloromethane, with the latter being slowly removed and the micelles being thermally annealed afterwards, as described above. The d- and h- 99PEP specimens were post-mixed by re-dissolving them in the PEP-selective solvent pentane, then dried under vacuum.

Figure 6.2 illustrates the chain exchange of dilute PS-PEP micelles in squalane and PEP. Equivalent amount of micelles composed of normal (blue core, hPS-PEP) and deuterated (red core, dPS-PEP) diblock copolymers are mixed. The PEP corona blocks are represented by the dark green lines, while the lighter green lines are PEP homopolymers. The purple matrix contains 58 vol% of d-squalane and 42 vol% of h-squalane (see Chapter 3 for the determination of isotope composition in the solvent mixture), to match the scattering length density of a 50/50 hPS/dPS mixed micelle core: $\rho_{squalane} = (\rho_{d,core} +$

$\rho_{h,core}$)/2. Therefore the exchange of isotopically labeled chains decreases the mean contrast of the micelle cores and subsequently leads to time-dependent scattering intensity. The figure schematically describes the change of corona chain concentration upon adding homopolymers of the same size as the corona blocks, due to partial penetration of homopolymers into the corona region, which allows for the examination of the impact of corona chain overlapping/stretching on the chain exchange rate.

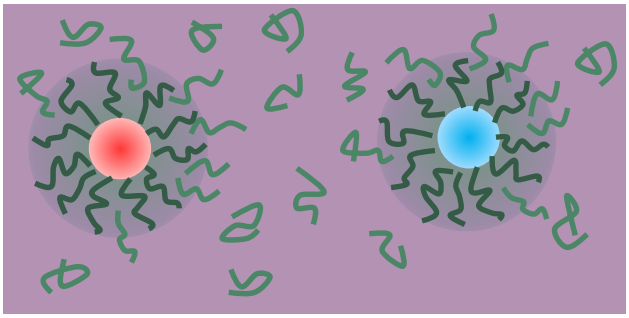

Figure 6.2. Chain exchange between deuterated (red core) and normal (blue core) PS-PEP micelles in squalane and PEP.

The SANS experiments were performed on the NG-7 30 m beamline at the Center for Neutron Research of the National Institute of Standards and Technology (NIST), or the CG-2 General-Purpose SANS instrument at the High Flux Isotope Reactor (HFIR) facility of Oak Ridge National Laboratory (ORNL). For NG-7 at NIST, a sample-to-detector distance (SDD) 13m and a wavelength λ = 7 Å were used. For CG-2 at ORNL, SDD = 14 m, and λ = 4.75 Å. For both instruments, sample solutions were loaded into quartz cells of 1 mm thickness at room temperature. 2-D SANS data was reduced and corrected using the package provided by NIST[134] and ORNL, respectively. The 99PEP samples were sandwiched between two quartz discs, confined with an aluminum washer and sealed with a silicon-based adhesive. The sample environment was described in Chapter 2. The TR-SANS experiments with a post-mixed specimen before and during chain exchange, a pre-

mixed specimen, and a solvent background specimen were conducted using the same procedures described in the previous chapters. The premixed micelle solutions were prepared by co-dissolving dPS-PEP and hPS-PEP in the micelle preparation step, followed by the same sequence of PEP addition and thermal annealing as discussed above.

Small Angle X-ray Scattering (SAXS)

The SAXS experiments were conducted on the equipment maintained by the DuPont-Northwestern-Dow Collaborative Access Team at Argonne National Laboratory, using 4 keV radiation (wavelength λ = 0.886 Å) and a sample-to-detector distance of 6 m. The sample solutions were loaded into quartz capillaries of approximately 1.5 mm in diameter. Each sample was exposed to the X-ray beam for 10-15 s at room temperature. The data were collected with a 2-D MAR-CCD detector and azimuthally averaged to provide the 1-D intensity profile. Background scattering from squalane was subtracted using the Irena package provided by Argonne.[138] Five samples were prepared and measured: (1) the 7PEP post-mixed SANS sample was directly used, *i.e.*, the PEP was added into PS-PEP micelle solutions and stirred until dissolved, with no additional thermal annealing; (2) sample 1 after annealing at 84 ºC for 180 min; (3) sample 1 after annealing at 100 ºC for 170 min; (4) sample 1 after annealing at 119 ºC for 60 min; (5) sample 1 after annealing at 180 ºC for 30 min to reach equilibrium.[125]

SAXS and SANS Fitting Models

Micelle structural features were extracted from the SAXS and SANS results using the Igor package provided by NIST.[134] The hard sphere model with a distribution of micelle core radius, and the Percus-Yevick closure approximation in the structure factor, have been successfully used in our previous studies and documented in detail.[79,82,125] A description of

the SAXS fitting model is provided in Chapter 2. All SAXS data were fitted using this model for 0.01 $Å^{-1} < q < 0.15\ Å^{-1}$, where the wave vector $q = 4\pi\lambda^{-1}\sin(\theta/2)$.

For the TR-SANS experiment, the d- and h- micelles are mixed, and as a consequence, the original form of the hard sphere model reduces to a simpler equation. Assuming a perfect contrast match is achieved (*i.e.*, the scattering length density of the solvent is exactly the mean of d- and h- micelles cores: $\rho_{squalane} = (\rho_{d,core} + \rho_{h,core})/2$) with negligible corona scattering, and that the h- and d- micelles are randomly distributed, using the hard sphere fitting model, the coherent scattering cross section for a post-mixed micelle solution can be expressed as:[79]

$$\frac{d\Sigma(q)}{d\Omega} = \left(\frac{4\pi}{3}R_{core}^3\right)\phi_s(\rho_{core} - \rho_{sol})^2 P_s(q), \qquad (6.1)$$

where R_{core} is the core radius, ϕ_s is the volume fraction of hard spheres, and $P_s(q)$ is the spherical form factor:

$$P_s(q) = \left[\frac{3(sin(qR_{core}) - qR_c\cos(qR_{core}))}{(qR_{core})^3}\right]^2 . \qquad (6.2)$$

.

Equation 6.2 was used to obtain an optimal fit of the SANS of post-mixed 2PEP and 99PEP samples.

Light Scattering (LS)

Light scattering experiments were performed at room temperature over a range of angles (60°−120°) with a Brookhaven BI-200SM goniometer at λ = 637 nm. Three types of micelle solutions in squalane were prepared: (1) 1 vol% PS-PEP, (2) 1 vol% PS-PEP + 3 vol% PEP, and (3) 1 vol% PS-PEP + 10 vol% PEP. For all three, the PEP was added to the diblock micelle solution at room temperature. The sample solutions were loaded into glass tubes of 1 cm diameter, and degassed before taking measurements.

6.3 Results

TR-SANS

SANS results obtained from the post-mixed 2PEP, 7PEP, 15PEP and 99PEP specimens at various temperatures are shown in Figure 6.3. Each panel shows a selected set of intensity traces at various chain exchange times for one post-mixed specimen while maintained at a fixed temperature. In each panel, the mixed core scattering from a corresponding pre-mixed specimen, and the background scattering from a corresponding solvent specimen (*i.e.*, squalane for the 2PEP, 7PEP, and 15PEP specimen, PEP homopolymers for the 99PEP specimen) specimen are included for comparison. The unmixed core scattering was measured with the post-mixed sample at room temperature. The sample cell was then removed, and put back in the pre-heated sample holder to measure the scattering intensity at 5 min intervals for up to 3-4 hours. A similar systematic drop of scattering intensity with the results shown in previous chapters is observed here, as a consequence of redistribution of d- and h-PS-PEP between micelles.

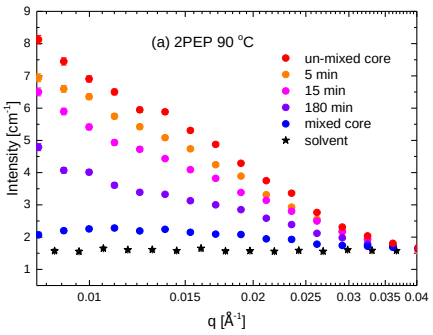
(a) 2PEP 90 °C
un-mixed core
5 min
15 min
180 min
mixed core
solvent
Intensity [cm-1]
q [Å-1]

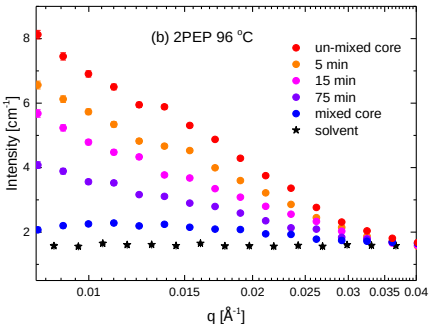
(b) 2PEP 96 °C
un-mixed core
5 min
15 min
75 min
mixed core
solvent
Intensity [cm-1]
q [Å-1]

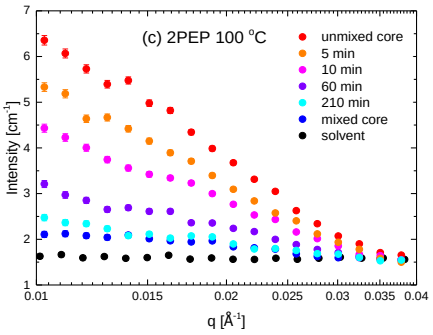
(c) 2PEP 100 °C
unmixed core
5 min
10 min
60 min
210 min
mixed core
solvent
Intensity [cm-1]
q [Å-1]

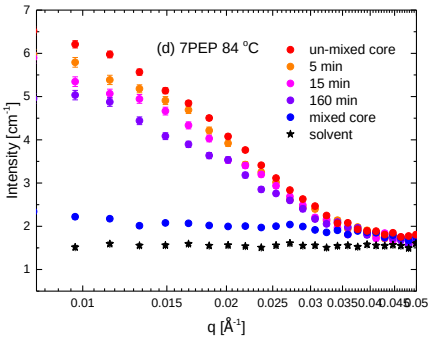
(d) 7PEP 84 °C
un-mixed core
5 min
15 min
160 min
mixed core
solvent
Intensity [cm-1]
q [Å-1]

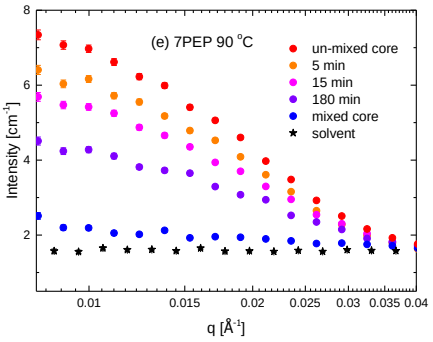
(e) 7PEP 90 °C
un-mixed core
5 min
15 min
180 min
mixed core
solvent
Intensity [cm-1]
q [Å-1]

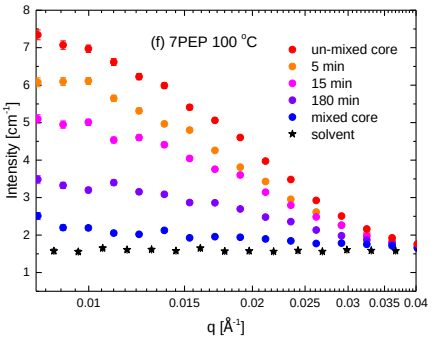
(f) 7PEP 100 °C
un-mixed core
5 min
15 min
180 min
mixed core
solvent
Intensity [cm-1]
q [Å-1]

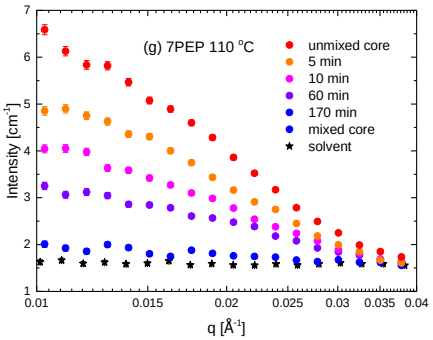
(g) 7PEP 110 °C
unmixed core
5 min
10 min
60 min
170 min
mixed core
solvent
Intensity [cm-1]
q [Å-1]

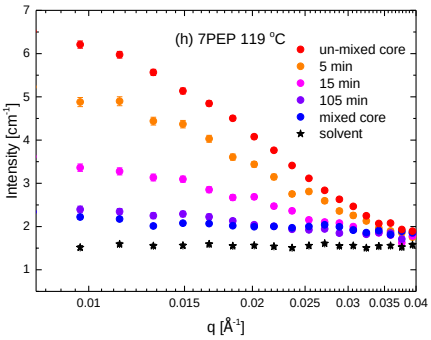
(h) 7PEP 119 °C
un-mixed core
5 min
15 min
105 min
mixed core
solvent
Intensity [cm-1]
q [Å-1]

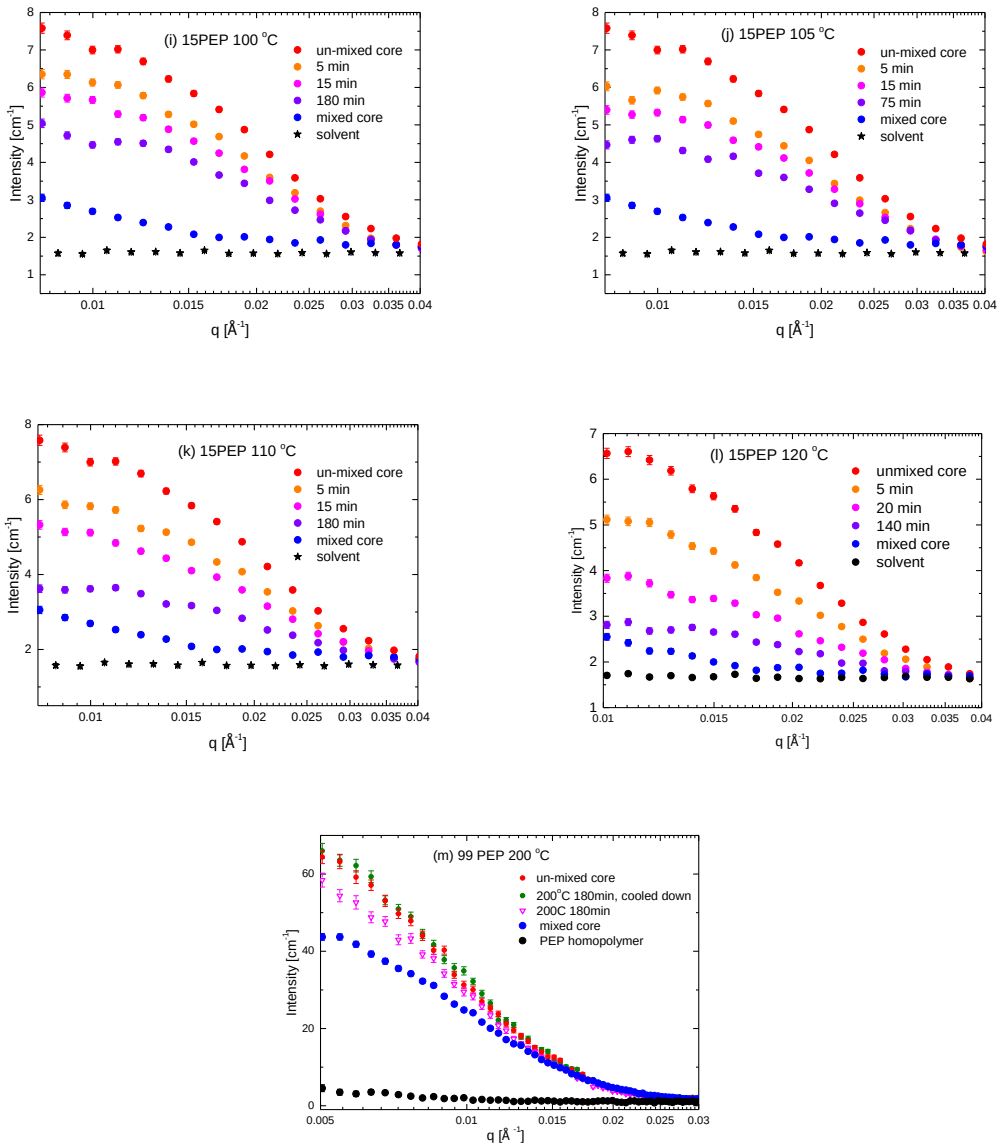

Figure 6.3. Representative TR-SANS patterns recorded in 5 minute increments during molecular exchange of: post-mixed 2PEP at (a) 90 °C, (b) 96 °C, and (c) 100 °C; post-mixed 7PEP at (d) 84 °C, (e) 90 °C, (f) 100 °C, (g) 110 °C and (h) 119 °C; post-mixed 15PEP at (i) 100 °C, (j) 105 °C, (k) 110 °C and (l) 120 °C; (m) post-mixed 99PEP at 200 °C. The corresponding sample and temperature are noted in each plot. For each plot, the scattering patterns of a post-mixed specimen before chain exchange (red), a pre-mixed specimen (blue), and a solvent specimen (black) are shown for comparison with the time-resolved scattering patterns.

As shown in Figure 6.3m, the mixed core scattering from a pre-mixed 99PEP specimen is much higher than from the premixed 2PEP, 7PEP or 15PEP specimen, due to the mismatch of the PEP homopolymers scattering length density with the 50/50 mixed h/d PS micelle cores (see Table 2.2). The open pink triangles in Figure 6.2m corresponds to the scattering pattern of a post-mixed 99PEP specimen recorded after 3 hours annealing at 200 ºC. This specimen was then taken out and cooled down, and re-measured at room temperature, and the corresponding scattering pattern is shown in Figure 6.3m. The difference between this new measurement (the green filled circles) and the previous one at 200 ºC (the open pink triangles) is a result of the decreased incoherent scattering due to thermal expansion in the specimen. Comparing the green and red filled circles in Figure 6.2, which correspond to the scattering intensity measured at room temperature using a post-mixed specimen annealed at 200 ºC for 3 hours, and a post-mixed specimen before annealing, it can be concluded that no chain exchange was observed for the 99PEP samples at 200 ºC for up to 3 hours within experimental error.

Changes in the SANS intensity were monitored as a function of time at constant temperature over the range $0.01\ \text{Å}^{-1} \leq q \leq 0.04\ \text{Å}^{-1}$. This q range was chosen to minimize the complication of corona scattering while retaining sufficient counting statistics. The extent of chain exchange as a function of time at a certain temperature can be quantitatively evaluated by the relaxation function $R(t)$ (see Equation 1.2), as discussed in the previous chapters. Since by definition $R(t)$ is independent of q, the use of $R(t)$ to describe chain exchange rate requires the assumption that micelle structure does not change over time throughout the experiment. Upon adding PEP homopolymers, however, due to the depletion of overlapping corona chains, micelles could have a tendency to increase in size when sufficient chain exchange is allowed. We therefore need to monitor the evolution of micelle size over time using SAXS, as discussed below. $R(t)$ of 2PEP, 7PEP and 15PEP

are summarized in Figure 6.3. As mentioned above, no chain exchange was observed for 99PEP specimens, for up to 3 hours at 200 °C.

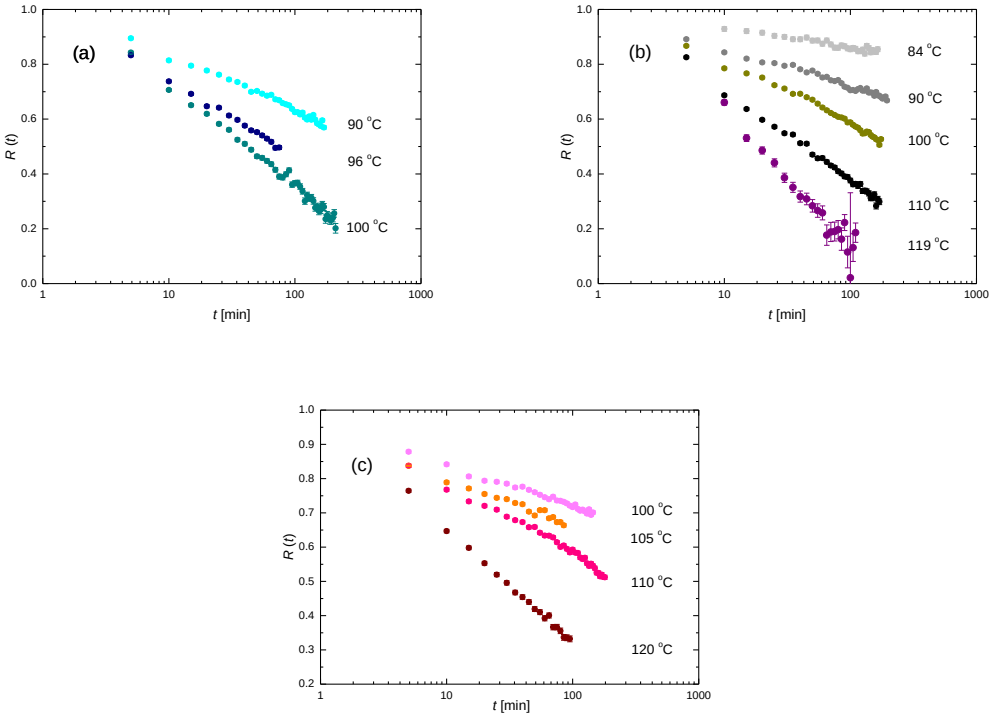

Figure 6.4. *R*(*t*,T) traces determined by TR-SANS using equation 2.1, with (a) 2PEP, (b) 7PEP and (c) 15 PEP at various temperatures.

For each of the three samples 2PEP, 7PEP, and 15PEP, the *R*(*t*,T) obtained at different temperatures can be shifted horizontally to construct a master curve, *i.e.*, $R(t/a_T, T_{ref}) = R(t, T)$, where T_{ref} = 110 ºC. This application of time-temperature superposition, which is well known in rheology,[106,107] has been successfully exploited in all our previous studies of chain exchange.[76,79–82] The shift factors a_T were determined empirically, and log (a_T) in general follows an approximately linear dependence on temperature (see Figure 6.5b for a summarized shift factor plot over temperature for all our current chain exchange studies), regardless of the concentration of PEP and PS-PEP, and numerically consistent with the earlier studies. Figure 6.5a compares the three master curves obtained here with model fits[79] of the previously reported relaxation functions for 1 vol% PS-PEP and 15 vol% PS-

PEP in pure squalane. About one order of magnitude difference in the relaxation time constant can be seen in the figure, by comparing the master curves associated with 2PEP and 7PEP, and that associated with 7PEP and 15PEP as well.

As discussed above, no chain exchange was observed with the 99PEP post-mixed specimen at 200 ºC for up to 3 hours. Assuming the shift factor for 99PEP chain exchange follows the same dependence on temperature, this result corresponds to an $R(t)$ value of 1 when $t \approx 3\times10^{10}$ min, and is shown in Figure 6.4a with the red star after the axis break.

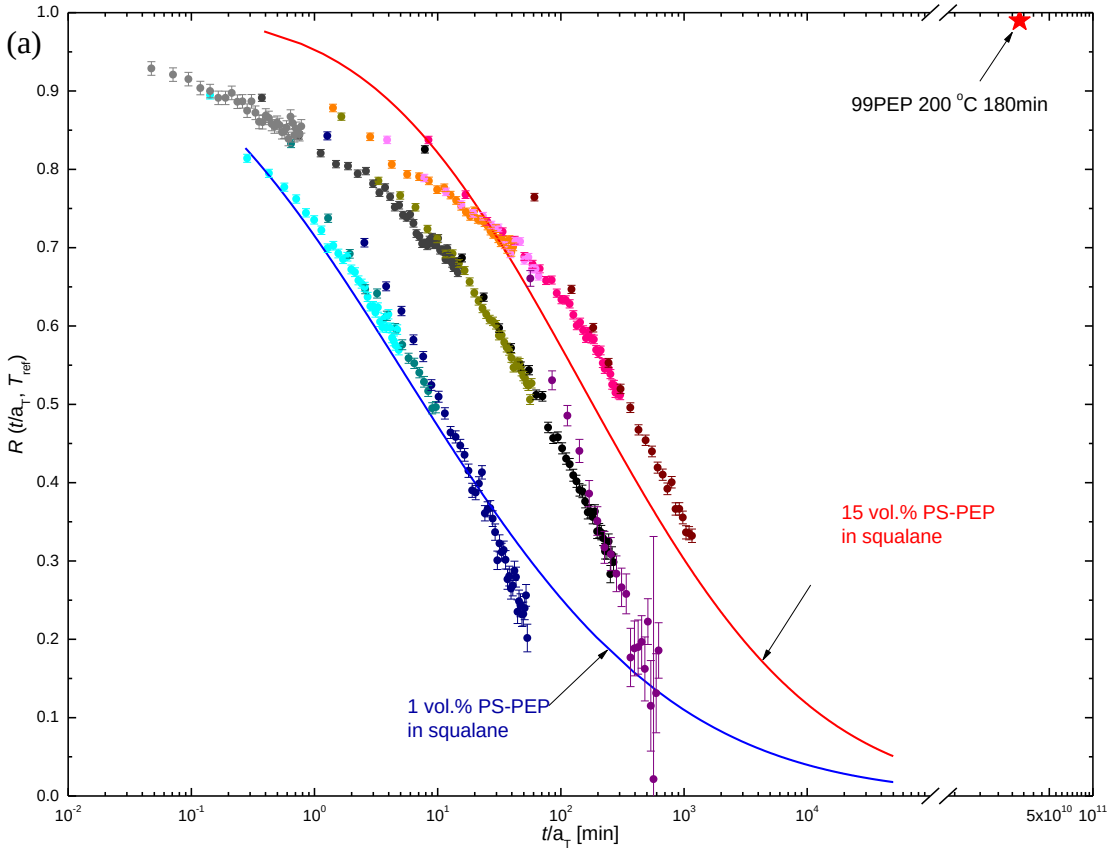

Figure 6.5. (a) $R(t)$ or $R(t/a_T, T_{ref})$ master curves for (left to right) 2PEP, 7PEP, and 15PEP at a reference temperature 110 ºC. The lines are model fits of 1 vol% (left, blue) and 15 vol% (right, red) PS-PEP in pure squalane.[79] The red star corresponds to the 200 ºC measurement with post-mixed 99PEP for 3 hours, where no chain exchange was observed.

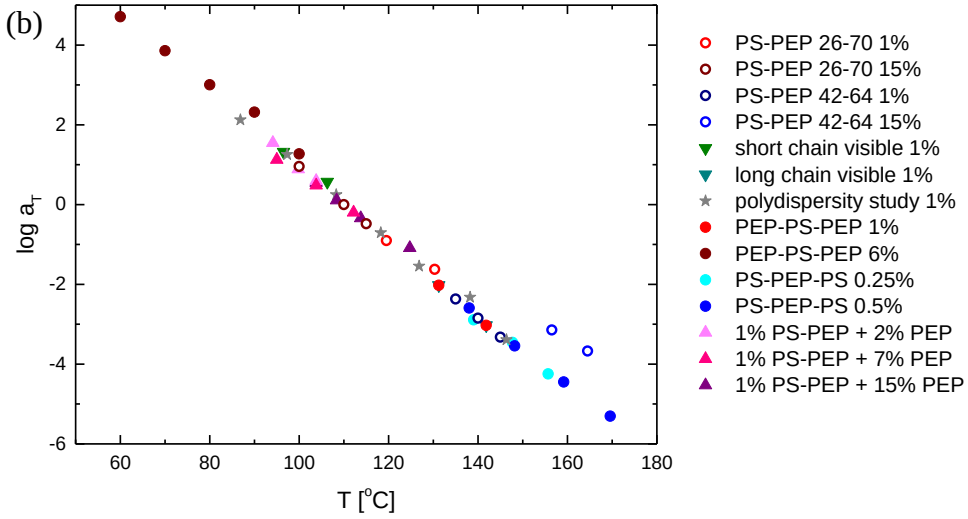

Figure 6.5. (b) Shift factors log(a_T) as a function of temperature at a reference temperature of 110 ºC, for this study, together with the shift factors reported in our previous studies of chain exchange between similar micelles in squalane. As shown in the legend, the open circles represent shift factors for 1 vol%[76] and 15 vol%[79] PS-PEP 26-70 and PS-PEP 42-64 in squalane, reproduced from Choi *et al*. The solid upside-down triangles and stars represent the shift factors for hybridized micelles containing a mixture of PS-PEP 26-70 and PS-PEP 42-64 with designed fractions, reproduced from Chapters 4 and 3, respectively. The filled circles represent shift factors used in the study of triblock copolymer micelle chain exchange, for PEP-PS-PEP and PS-PEP-PS at different concentrations correspondingly, reproduced from Chapter 5.[82] The pink, red, and deep red triangles represent the shift factor used in this study, for the 2PEP, 7PEP, and 15PEP samples.

SAXS

The SAXS data for five 7PEP samples after different thermal treatments are plotted with corresponding fitting curves in Figure 6.6. Samples 1 to 5 correspond to 7PEP micelle solutions with no prior thermal annealing, held at 84 ºC for 3 hours, annealing at 100 ºC for 170 min, at 119 ºC for 60 min, and at 180 ºC for 30 min. Therefore sample 1 corresponds to the initial micelle in a TR-SANS experiment before any chain exchange, while sample 2, 3, 4 each represents the last data point in the TR-SANS trace acquired at each

corresponding temperature, and sample 5 is comparable to the premixed sample used in the SANS experiments. The SAXS pattern of sample 1 (black), and 2 (blue) overlap with each other within experimental error, implying no micelle size change occurs at 84 ºC for up to 3 hours, which corresponds to the longest time data point in the SANS results presented in Figure 3 and 4 for 7PEP at 84 ºC. The SAXS pattern of sample 4 (purple) and 5 (red), on the other hand, suggests a noticeable increase in micelle core size upon annealing at 119 ºC for 60 min or 180 ºC for 30 min, while the SAXS pattern of sample 3 (pink) lies in between those of sample 2 (blue) and sample 4 (purple). The fitted core radius of samples 1, 2, 3, 4 and 5 are 92 Å, 92 Å, 96 Å, 103 Å and 105 Å, respectively, with an error of less than 5%. The fitted core radius of sample 1 is close to the previously reported value (89 Å) for 1 vol% PS-PEP in squalane,[76] due to the fact that the PEP was added at room temperature when the PS cores are frozen.

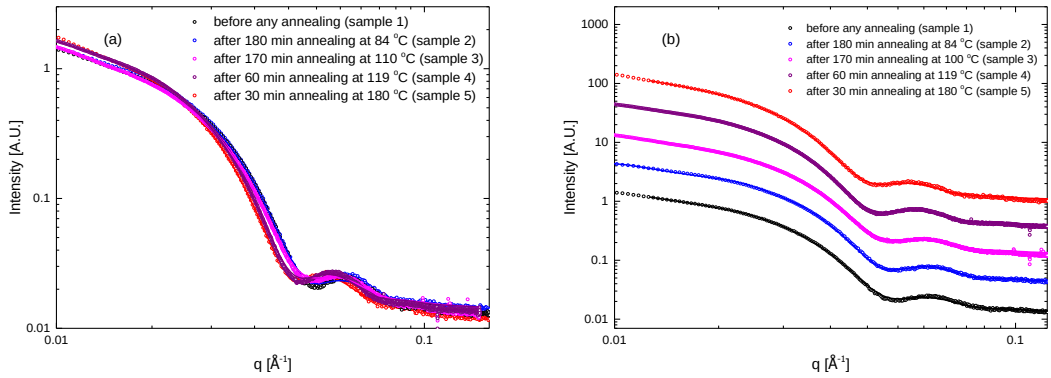

Figure 6.6. (a) SAXS of five 7PEP solutions measured at room temperature: before any annealing (sample 1, black), after 180 min annealing at 84 ºC (sample 2, blue), after 170 min annealing at 100 ºC (sample 3, pink), after 60 min annealing at 119 ºC (sample 4, purple), and after 30 min annealing at 180 ºC (sample 5, red). The open circles are data corresponding to the three samples, as denoted in the legend. The solid lines of the same color are fitting curves for each. (b) Replot of (a) with vertically shifted data and fitting curves to illustrate the fitting. The data and corresponding fitting curves were shifted by multiplying 3^n.

SANS Fitting

The SANS data from a post-mixed 2PEP (red open squares) and 99PEP (blue open circles) taken at room temperature before chain exchange are fitted using equation 6.1 to find the core radius, and the fitting results (solid lines of the same color) are compared with the data in Figure 6.6. The results indicate a significant increase in micelle core radius upon switching the solvent from squalane to PEP. In addition, the fitted core radius for post-mixed 2PEP is close to that from the complete core-shell hard sphere fitting model described in Chapter 2 with SAXS data of a post-mixed 7PEP specimen (Figure 6.5). Both these two fitted core radius are consistent with the reported value of 1 wt% PS-PEP in pure squalane.[125] Since the PEP was added in both 2PEP and 7PEP at room temperature when the PS cores were frozen,[115] the two values should be the same if the assumptions associated with equation 6.1 are satisfied. Therefore the fact that the SANS and SAXS fitting results of the post-mixed solutions match suggest the successful use of contrast matching and that the d- / h- micelles are randomly mixed. We attribute the modest departure of the data from the model fit for $q < 0.02$ Å^{-1} in Figure 6.7 to excess corona scattering, and slight contrast mismatch due to the addition of PEP.

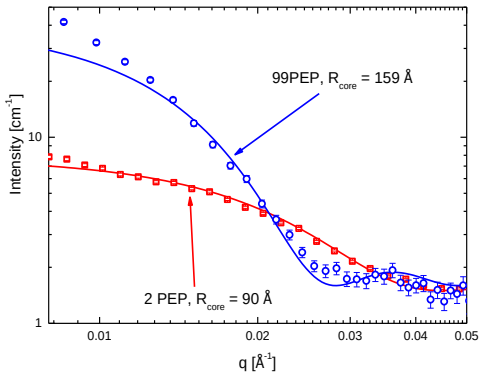

Figure 6.7. SANS data and fitting of post-mixed 2PEP (red) and 99PEP (blue) using equation 6.1. The open symbols are SANS data, and the lines of the same color are fitting curves, respectively. The fitted core radius R_{core} are shown in the plot.

Light Scattering

The mean square scattering intensity $<I_{ave}>^2$, which is directly measured by the DLS instrument, serves as a qualitative test at to whether depletion interaction induced phase separation occurs upon addition of homopolymers. Figure 6.7 summarizes the $<I_{ave}>^2 \times \sin^2\theta$ measured at various angles θ for the three micelle solutions with the same PS-PEP concentration but different PEP contents. Here the square of the average scattering intensity is corrected by multiplying by $\sin^2\theta$ to account for changes in the scattering volume (proportional to $1/\sin\theta$) at different detecting angles. The black, red, and blue rectangular bars in Figure 6.8 identify the average scattering intensity from the three samples, respectively: (1) 1 vol% PS-PEP, (2) 1 vol% PS-PEP + 3 vol% PEP, and (3) 1 vol% PS-PEP + 10 vol% PEP. All scattering intensities here are in arbitrary units.

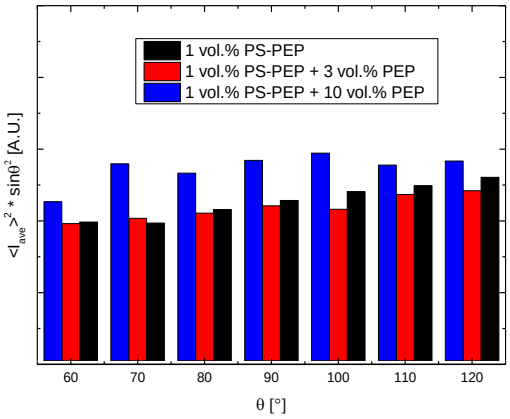

Figure 6.8. Mean square scattering intensity square measured at different angles for three micelle solutions in squalane, as denoted by the legend.

6.4 Discussion

Chain Exchange of PS-PEP in Squalane When a Small Portion of PEP Homopolymers is Added

The first and most important observation from Figure 6.5a is that the chain exchange rate decreases significantly with the addition of PEP (three master curves from left to right). This observation is consistent with the reported slower kinetics in 15 vol% ordered PS-PEP solution, where the corona chains overlap. The model for $R(t)$ reported by Choi *et al.*, which successfully fitted the chain exchange data for several diblocks, cannot explain this result. In this model, $R(t)$ is based on the assumptions that single chain expulsion is the rate-limiting step, and that the activation energy of chain exchange is governed solely by the Flory-Huggins interaction between the core blocks and the corona /solvent matrix. It is well known that the Flory-Huggins interaction parameter χ for a polymer/solvent system governed by simple van der Waals interactions is often greater than χ for a polymer/polymer mixture where the polymerical solvent quality is norminally equivalent to the low molecular weight analogue. While the χ for a polymer/polymer system can be as low as $10^{-2} \sim 10^{-3}$ empirically, the χ between a polymer and a good solvent typically has a lower limit of about 0.34.[118] Milner and co-workers summarized the χ value for polyethylene in 17 *n*-alkanes, demonstrating that χ systematically decreases with increasing *n*.[146] The authors showed by off-lattice Monte Carlo simulations that compared to small molecule solvents of identical chemical species, a polymer chain has the tendency to reduce its free volume due to the bonding constraints, which consequentially leads to a positive contribution to the entropic contribution to the free energy of mixing. Therefore, by substituting part of the solvent squalane with PEP homopolymer, which is essentially a higher molecular weight version of squalane, the χ between the core blocks and solvent matrix should decrease. This should facilitate the chain exchange process, since the enthalpic energy barrier to core block expulsion scaled as χN according to Choi *et al.*[76,79]

and us[80,81] or $\chi N^{2/3}$ according to Lund *et al*.[73,78] Obviously, this argument conflicts with the progressively slower exchanged observed in the 7PEP, 15PEP, and 99PEP micelle solutions.

Three possible explanations for this discrepancy are herein considered: (1) the increase of diffusion time of free chains, due to increased matrix viscosity; (2) the possibility of a larger chain insertion barrier for the core blocks to enter the corona region due to the change of micelle size as a result of the screening effect of PEP homopolymers to PEP blocks, as proposed by Halperin,[113] (3) a favorable corona contribution to the total chain expulsion activation energy, *i.e.*, the relief of stretching of corona blocks upon escaping from a micelle, which favors free chains, is partially screened by the presence of PEP homopolymers.

(1) Matrix Transport Effects

First, we estimate the effect of adding PEP homopolymers on single chain diffusion. As shown in Figure 6.5a, the 2PEP exhibits a chain exchange rate that is comparable to the one without PEP (1 vol% PS-PEP in squalane, blue line). The viscosity of the solvent (squalane + 1 vol% PEP) can be estimated as $\eta_s \approx \eta_{squalane} \times (1 + [\eta] \times c)$. Since squalane is chemically very similar to PEP, the intrinsic viscosity of PEP in squalane can be estimated using the Mark-Houwink equation as $[\eta] = KM^{1/2}$. The value of K is in general below 0.5 $(mL/g)^{1/2}$ for PEP in various theta solvents,[147] which is used as a rough estimation. Therefore the viscosity of solvent with the addition of 2 vol% PEP can be estimated as 6.6 mPa • s, given that the viscosity of squalane is about 2.2 mPa • s at 100 ºC.[148] The fact that increasing the solution viscosity by 3 times does not change the chain exchange rate equivalently suggests that the solution viscosity is not the rate-limiting step, as is expected for the single chain exchange mechanism.[73,81]

This inference is supported by a comparison of the time constant for the expulsion of core blocks from one micelle, with the characteristic time for a polymer chain to diffuse from one micelle to another. Since the PS blocks in the micelle cores are at most weakly entangled, Rouse dynamics can be used to estimate the longest relaxation time constant associated with core blocks expulsion.[149] Combining the longest Rouse relaxation time constant with the core block expulsion energy barrier yields the time constant of core block expulsion:[76] $\tau_{ex} \sim (N^2 b^2 \xi) / (6\pi^2 kT) \times \exp(\alpha\chi N)$. Using the number of repeat units in the PS core blocks N, the fitted $\alpha\chi$ value for 1 vol% PS-PEP (same polymer as used in this study) as 0.041[76], the statistical segment length of the PS blocks b = 0.67 nm,[112] the friction coefficient $\xi = 1.7 \times 10^{-8}$ (N × m × s^{-1}),[111] and the temperature T = 125 ºC, τ_{ex} is estimated to be 3×10^2 s. The characteristic time constant for the diffusion of polymer chain of N repeat units with segment length b, in a solvent of viscosity η_s at temperature T can be expressed as: $t_{diff} \sim L^2 / 6D_t$, where the tracer diffusion coefficient $D_t \approx kT / (6\pi\eta_s \times N^{1/2} b)$, and the micelle to micelle distance L can be roughly estimated as 100 nm for the 1 vol% PS-PEP micelle solution. Here the segment length of PEP blocks is reported as 0.76 nm,[112] the total number of repeat units in a polymer chain is about 1220, and the viscosity of the solvent (squalane + 15 vol% PEP) can be estimated using the same procedure described above as 50 mPa • s. Using these values and recalling that the molecular weight of PEP homopolymers M = 65 kDa, the characteristic diffusion time of a PS-PEP molecule in the 15PEP sample is estimated to be at most 5×10^{-2} s, which is much smaller than τ_{ex}. Both assessment favor chain expulsion over transport through the matrix as the rate-limiting mechanism.

(2) Core Size Evolution

Second, we consider the consequences of the small change in micelle size that was documented upon adding homopolymer. According to Halperin,[113] the rate of chain

exchange is correlated with the micelle size, due to an increased chain insertion barrier for the core blocks to enter corona region, when the micelle core size is larger. Since the PEP homopolymers were added to dilute PS-PEP micelle solutions at room temperature in preparing the 2PEP, 7PEP, and 15PEP samples, all the TR-SANS experiments began with identically sized micelles. Only after sufficient chain exchange at an elevated temperature, could the micelles achieve the larger equilibrated size due to the presence of PEP, at which point the issue of chain insertion might come into play.

We assessed this issue by separately annealing the h- and d- micelle solutions at 180 ºC for 30 min after adding PEP, but before post-mixing (see Figure 6.6 for SAXS data and fits). With those "pre-annealed" samples, the chain exchange rates did not change within experimental error, while the core radius of the micelles did change by approximately 10% (92 Å to 105 Å for 7PEP). In addition, a post-mixed 7PEP specimen was annealed at 84 ºC for 3 hours (the same temperature and time as the first $R(t)$ trace of 7PEP in Figure 6.5a and Figure 6.4b) and subsequently analyzed by SAXS to quantify any change in micelle size in the corresponding SANS experiment. As shown in Figure 6.5, the thermal annealing at 84 ºC does not introduce any noticeable change in micelle size. However, SAXS of two more post-mixed 7PEP specimen annealed at higher temperatures (100 ºC for 170 min and 119 ºC for 60 min, see Figure 6.6) suggest that the core radius of the micelles are gradually increasing (98 Å and 103 Å correspondingly) when chain exchange is relatively more sufficient. In other words, while the chain exchange rate of 7PEP at 84 ºC is not affected by micelle core size change, the micelles do have a tendency to increase their aggregation numbers gradually at higher temperatures (100 ºC and above) during the TR-SANS experiments. Therefore we can conclude that adding PEP homopolymers into dilute PS-PEP micelle solutions can slow down the chain exchange rate even while keeping the micelle size the same, at relatively low temperatures such as 84 ºC and 90 ºC for up to 3 hours. But because the separately annealed 7PEP micelles with a larger size (105 Å

compared to the original 92 Å) possess identical chain exchange rate within experimental error, the micelle size change due to adding homopolymers is not contributing to our primary results here.

(3) Corona Screening Effect

Thirdly, we discuss the screening effect of corona chain stretching due to the corona overlapping in added PEP samples. As shown in Figure 6.5a, chain exchange of 7PEP and 15PEP are both slower than the one without PEP. Similar slower kinetics as a result of increasing concentration of PS-PEP from 1 vol% to 15 vol% has been observed and contributed to the screening of overlapping coronas.[79] The critical concentration for PEP homopolymers to overlap with the PEP corona blocks can be estimated as the concentration of PEP blocks inside the corona: $\rho^* = (N_{agg} \times V_{corona}) / (4/3 \times \pi \times (R_h^3 - R_c^3))$. For the PS-PEP polymers used in this study, the volume of corona block $V_{corona} \approx 1.4 \times 10^5$ Å^3, by assuming the density of PEP blocks is the same as that for the pure PEP homopolymers. The aggregation number N_{agg}, hydrodynamic radius R_h, and core radius R_c are reported for 1 vol% PS-PEP solution in squalane at 100 ºC as:[125] $N_{agg} = 70$, $R_h = 362$ Å, and $R_c = 88$ Å. Therefore the overlapping concentration of PEP in 1 vol% PS-PEP is approximately 5 vol%. Based on this calculation, we expect no corona overlapping in 2PEP but significant overlapping in 7PEP and 15PEP, which is consistent with the observation that no chain exchange rate reduction with 2PEP but significant reduction in 7PEP and 15PEP. The SAXS experiments by Choi *et al.* suggest slight chain stretching ($R_g / <R_g>_0 \approx 1.4$) in the PEP corona blocks in 1 wt.% PS-PEP micelle solutions in squalane.[125] Both our chain exchange study with triblock PEP-PS-PEP in squalane[82] and Halperin's earlier theoretical work[73] imply a facilitating role of corona blocks in chain exchange. In pure squalane, the corona chains experience a relief of stretching by escaping into a good solvent. When the coronas are partially penetrated by homopolymers of the same size or overlapping due to

the increase of concentration of PS-PEP (see Figure 6.1), however, PEP corona blocks remain in semi-dilute solution whether or not they are part of a micelle. Therefore, the observed slower kinetics upon adding PEP to above overlapping concentration is probably a result of the screening effect of homopolymers to coronas.

While consideration of the corona blocks can provide a qualitative explanation for the main feature in Figure 6.4a, it is also true that at early reduced times the $R(t)$ master curves of 7PEP and 15PEP do not follow exactly the model fits of 1 vol% or 15 vol% PS-PEP micelles in pure squalane (the red and blue lines of Figure 6.5a): the initial chain exchange rate seems to be greater than the model prediction. The reason for this is not yet clear.

The possibility of micelle aggregation induced accelerated chain exchange in certain regions due to the depletion effect of added PEP in PS-PEP solutions[145] can be excluded by visually checking the solution (clear) and by measuring the light scattering intensity as a function of added homopolymer concentration. Since even the scattering intensity of the solution containing 10 vol% PEP is not greatly different from the one without PEP (Figure 6.8) at any detector angle, we conclude that any micelle aggregation is very mild, and that macro-phase separation does not occur upon adding PEP up to at least 10 vol%.

In fact, while the addition of PEP does introduce a similar overlapping/stretching in corona chains as increasing the concentration of PS-PEP would, the former does not induce micelle ordering for up to 15 vol% (visually flowing at room temperature, and also no structural factor peak is observed in SANS with d- or h- 15PEP micelles) as the latter.[79] Similar disordering or gel melting has been reported in several other systems of block copolymer micelles when homopolymers with moderate molecular weight were added.[150–153] In addition, it has been found that adding homopolymers to diblock copolymer micelles can introduce a net attraction between micelles due to depletion interaction.[145] Therefore it is reasonable to expect that the corona chains of PS-PEP in squalane with the addition of PEP adopt different conformations than those of micelles in pure squalane. Lack of non-

ordering in 7PEP and 15PEP also enhanced the mobility of these micelles relative to the 15 vol% PS-PEP ordered structure. Both of these issues may contribute to the difference in chain exchange rates compared to concentrated diblock micelle solutions. These issues call for future investigations.

Chain Exchange of PS-PEP in Pure PEP Homopolymers

Chain exchange in 99PEP (1 vol% PS-PEP + 99 vol% PEP) seems to be extremely slow and not detectable at 200 ºC for up to 3 hours in the TR-SANS experiment. This is consistent with the trend shown by 7PEP and 15PEP, and clearly violates predictions of the simple model that only considers core block expulsion activation energy,[76] as discussed above. However, even though in the 99PEP specimens the corona contribution to chain exchange is completely screened, the extremely slow kinetics may not be fully explained if only corona chain overlapping is considered.

In addition to the corona block effect, here we consider another possibility: increased chain insertion activation energy for core blocks to enter the corona region, in both the chain extraction and insertion steps.[113] As shown in Figure 6.7, the 1 vol% PS-PEP micelles in pure PEP are much larger than those in squalane (core radius of 159 Å compared to 90 Å), which can be attributed to the increased screening effect of PEP. This significantly increases the brush density of the PEP corona blocks. According to Halperin, [113] the chain exchange of diblock micelles in homopolymers of the same kind and size as the corona blocks could experience a larger chain insertion barrier ΔF_{ins}, when entering the corona region in the chain extraction step, determined by the bulk osmotic pressure, which leads to slower chain exchange rates compared to diblock micelles of the same concentration in a small molecule selective solvent. As a result, the ratio of the chain exchange rate constant k_{ex} of 99PEP (volume fraction of PEP ϕ_A = 99%, with A being PEP and B being the PS

core block) to that of 0PEP (*i.e.*, 1 vol% PS-PEP in pure squalane, $\phi_A = 0$) can be expressed as:[113]

$$\frac{k_{ex}(\phi_A)}{k_{ex}(\phi_A = 0)} \approx \exp\{-[F_a(\phi_A) - F_a(\phi_A = 0)]\}/kT \approx \exp\{-[F_{ins}(\phi_A) - F_{ins}(\phi_A = 0)]\}/kT\,, \tag{6.3}$$

where

$$\Delta F_{ins}(\phi_A = 0) \approx kTR_{core}^{3/2}(\phi_A = 0)/N_B^{1/2}a^{3/2}, \tag{6.4}$$

and

$$\Delta F_{ins}(\phi_A) \approx kTN_B\phi_A^{9/4}, \text{ when } \phi_A >> \phi^{**}. \tag{6.5}$$

where N_B is the number of repeat units in a PS block, R_{core} is the micelle core radius, and a is the size of one monomer. Here ϕ^{**} is the critical concentration of PEP homopolymers added to introduce screening in the entire corona region and the whole coronal star structure disappears as a consequence. Therefore,

$$\frac{k_{ex}(\phi_A)}{k_{ex}(\phi_A = 0)} \approx \exp\left[R_{core}^{3/2}(\phi_A = 0)/N_B^{1/2}a^{3/2} - N_B\phi_A^{9/4}\right] \tag{6.6}$$

Since for 2PEP, 7PEP and 15PEP, the PEP was added in diblock micelle solutions and not annealed afterwards, R_{core} ($\phi_A = 0$) can be estimated to be 92 Å (Figure 6.7). Using the value of N_B from Table 2.1, a = 2.52Å as estimated by the length of two C-C bonds, and R_{core} ($\phi_A = 0$) = 92 Å (or 90 Å from SAXS fitting, Figure 6.6), equation 6.6 gives the ratio of $k_{ex}(\varphi_A)/k_{ex}(\varphi_A = 0) < \exp(-200)$. Therefore, in addition to the profound screening of

corona chain stretching by added PEP, having such a large micelle in PEP could also significantly increase the chain insertion energy barrier, both of which would contribute to a much slower chain exchange rate.

6.5 Summary

Chain exchange in 1 vol% diblock copolymer PS-PEP micelles in squalane and with varying amounts of added PEP homopolymer has been investigated using TR-SANS. The structure of the micelles was characterized by SANS and SAXS with appropriate fitting models. The results suggest that the addition of PEP slows down the chain exchange rate when sufficient to partially penetrate into the corona region (*i.e.*, when $\rho_{PEP} > \rho^* \approx 5$ vol%), consistent with an earlier study of concentrated diblock micelle solutions.[79] And, the more PEP is added, the slower the chain exchange rate becomes. When the solvent is completely replaced by PEP homopolymer, the chain exchange becomes too slow to be detected, even at substantially elevated temperatures. The influence of both the screening of corona chain stretching and the increasing in micelle core size due to PEP addition are discussed. We herein propose that the relief of corona block stretching upon escaping from a micelle is driving the chain expulsion from one micelle, and that the reduced chain exchange rate upon adding PEP or increasing diblocks concentration is primarily due to the screening effect of PEP homopolymers to PEP corona blocks. On the other hand, the chain exchange of PS-PEP micelles in pure PEP homopolymers, extremely slow kinetics was found. While this observation is consistent with the trend found with 7PEP and 15PEP specimens where squalane was partially substituted with PEP, the significant increase in aggregation number and thus corona chain density could be yet another reason that slows down chain exchange rate.

Chapter 7.

Role of Corona Blocks in Chain Exchange Between Diblock Copolymer Micelles

7.1 Introduction

While the hypersensitivity of the chain exchange rate to core block length has been demonstrated by our experiments with PS-PEP micelles in squalane (Chapter 3), the details about how and how much corona chains affect the chain exchange process is not clear yet. The pioneering theoretical work by Halperin and Alexander suggested that the corona chains could facilitate chain exchange rate by experiencing a relief of stretching state when escaped from a micelle into the solution.[73] In our recent experiments with triblock copolymer micelle chain exchange (see Chapter 5), it was found that the triblocks containing two corona blocks and one core block (*i.e.*, PEP-PS-PEP triblock copolymers) exchange at a much faster rate than the PEP-PS with the same corona block size, and only one corona block (which is comparable to one of the corona blocks in PEP-PS-PEP). The fact that with one additional corona block the chain exchange rate is increased thus implies the corona blocks are significantly affecting the chain exchange process, consistent with Halperin and Alexander's theory.[73] In addition, adding homopolymers PEP of the same size as the PEP corona chains into dilute PS-PEP solutions was found to retard the chain

exchange rate (Chapter 6). This phenomenon could possibly be explained by the screening effect of homopolymers on corona blocks, which reduces the impact of corona chains on chain exchange process. In this study, we intentionally vary the length of corona block in PS-PEP diblock copolymers to investigate the role of corona chain length, which is a more direct approach than to vary polymer architecture or add homopolymers.

7.2 Experiment

Materials Synthesis and Characterization

The PS-PEP diblock copolymers were synthesized using sequential addition of styrene and isoprene, followed by the selective saturation of the polyisoprene blocks to produce PEP using deuterium gas. The deuterated equivalent polymers were also synthesized from perdeuterated styrene monomers and normal isoprene monomers. Deuterated styrene was obtained from Polymer Source, Inc.; all other reagents unless otherwise specified were purchased from Sigma-Aldrich. The saturated PEP blocks contain 2.3 D atoms per repeat unit on average, due to slight H/D exchange, consistent with previous studies (Chapter 5 and Choi *et al.*[76]) The detailed experimental procedures of polymer synthesis have been described in Chapter 2. Table 7.1, reproducing part of Table 2.1, summarizes the molecular weights M_n, the number of repeat units N_n, and the dispersity $Đ$ of the normal and deuterated equivalent PS-PEP (28-40, with the numbers indicating the approximate molecular weight of each block in kDa) polymer. This PEP corona block is considerably shorter than the PS-PEP (26-70) used in our other studies (Chapter 3, 4, 6). The SEC traces of d- and hPS-PEP (28-40) before and after selective saturation were shown in Figure 2.2e and 2.2f, respectively.

Table 7.1. Polymer molecular characteristics.

	M_n / kDa	N_n	$Đ$
hPS-PEP 28-40	28-40	273-550	1.05
dPS-PEP 28-40	30-41	269-560	1.07
hPS-PEP 26-70*	26-70	250-970	1.04
dPS-PEP 26-70*	29-71	260-985	1.10

* The molecular characteristics of hPS-PEP (26-70) and dPS-PEP (26-70) are reproduced from Choi *et al*.[76]

Small Angle X-ray Scattering (SAXS)

SAXS experiments were performed to characterize the structure of PS-PEP (28-40) micelles in squalane at different concentrations and various temperatures. 1 vol%, 3 vol%, 6 vol%, and 10 vol% PS-PEP (28-40) micelles in squalane were prepared following the preparation steps described in Chapter 2. The SAXS experiments were conducted using equipment maintained by the DuPont-Northwestern-Dow Collaborative Access Team at Argonne National Laboratory, using 4 keV radiation (wavelength λ = 0.886 Å) and a sample-to-detector distance of 6 m. Sample solutions were isolated in 1.5 mm quartz capillaries using a high-temperature silicone-based sealant. A 2–20 s exposure to the X-ray beam was used. The 1 vol%, 6 vol%, and 10 vol% samples were heated from 50 ºC ($T_{g,PS}$ ≈ 70ºC[115]) at 30 ºC intervals to 200 ºC. At each temperature, the sample was annealed for at least 5 min before the measurements were taken. The cooling ramp experiments were done with the 1 vol% sample. The 3 vol% sample was only measured at 50 ºC.

Scattered X-rays were collected with a 2-D MAR-CCD detector, and azimuthally averaged to the one-dimensional form of intensity $I(q)$ (arbitrary units) versus the magnitude of the scattering wave vector q, $q = 4\pi\lambda^{-1}\sin(\theta/2)$. Background scattering was

subtracted based on the powder pattern obtained from an empty quartz cell using the Irena macro for Igor Pro, provided by Argonne.[138] The hard sphere fitting model was applied to extract micelle size information for the 1 vol%, 3 vol%, 6 vol%, and 10 vol% micelles at 50 ºC from the corresponding SAXS patterns. The model is described in Chapter 2. At 50 ºC, it was assumed that no solvent penetrates into the micelle core ($T_{g,PS} \approx 70$ ºC[115]), as indicated by the SAXS experiments with PS-PEP (26-70) micelles in squalane.[125] For the 1 vol%, 3 vol% and 6 vol%, the q range for fitting was selected as 0.008 $Å^{-1}$ to 0.15 $Å^{-1}$, which covers the entire features of the data (*i.e.,* both form factor and structure factor). The micelles are closed packed at 10 vol% and a clear Bragg reflection pattern with distinct peaks are shown. The fitting was performed for the q range of 0.035 $Å^{-1}$ to 0.15 $Å^{-1}$, to avoid the complication of the Bragg peaks.

Time Resolved Small Angle Neutron Scattering (TR-SANS)

The TR-SANS experiments were performed with 1 vol%, 2 vol%, and 6 vol% PS-PEP (28-40) micelles in squalane at selected temperatures to investigate the chain exchange rate quantitatively. As discussed in the earlier chapters, when equal amount of dPS-PEP (28-40) micelles are mixed with the hPS-PEP (28-40) micelles in a h/d squalane mixed solvent whose coherent scattering length density matches that of a 50/50 mixed dPS/hPS micelle core, *i.e.*, $\rho_{solvent} = (\rho_{d,core} + \rho_{h,core})/2$, the overall scattering intensity decreases as the isotope labeled chains are exchanging between d/h micelles, which quantitatively characterizes the chain exchange rate in the micelle solution. This situation is illustrated Figure 7.1a, where the deuterated and normal PS blocks/cores are represented by the red and blue lines/circles, the PEP blocks/coronas are shown with the green line/circles, and the purple background indicates the mixed d/h squalane solvent as the purple color equal to a 50/50 mixed red/blue color. Figure 7.1b shows the situation for the PS-PEP (26-70) polymer micelles used by Choi *et al.*[76] The relative size of the corona regions in Figures 7.1a and 7.1b were chosen

based on the ratio of the PEP block sizes in the PS-PEP (28-40) and PS-PEP (26-70) polymers, assuming the corona chains adopt the Gaussian conformation.

The micelle solutions were prepared using the co-solvent method described in Chapter 2. The d and h micelle solutions were separately prepared, and a pre-mixed sample was prepared by co-dissolving equal amount of d and h polymers in contrast matched squalane, to approximate the final state of chain exchange where the isotope labeled chains are completely mixed. The post-mixed samples were prepared by blending equal amounts of d and h micelle solutions at room temperature, where the exchange of PS-PEP molecules are forbidden (as the glass transition temperature of PS blocks is well above room temperature: $T_{g,PS} \approx 70$ ºC[115]). At elevated temperatures above the $T_{g,PS}$, the mixing of isotope labeled chains in the post-mixed sample would make the mean contrast of micelle core with respect to the solvent decrease over time, resulting in the time-resolved scattering intensity.

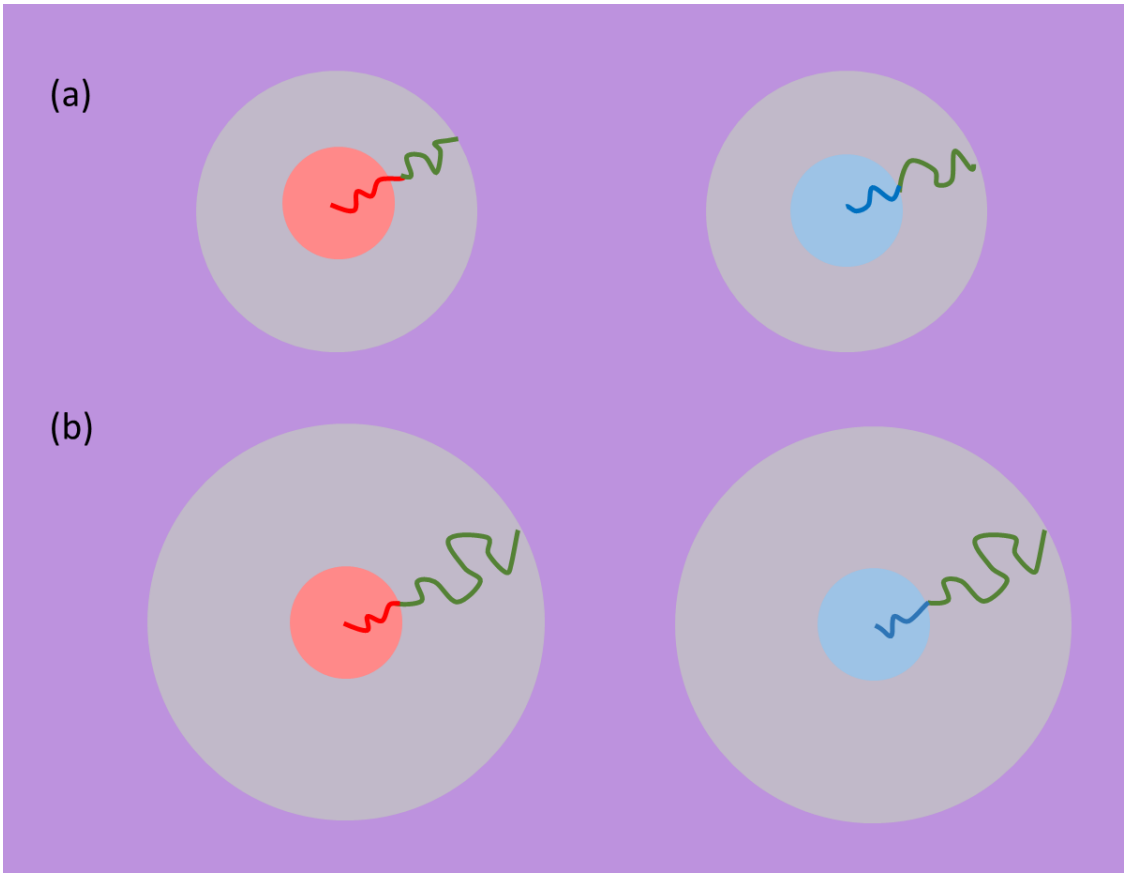

Figure 7.1. (a) A post-mixed sample containing deuterated (red core) micelles and normal (blue core) micelles composed of dPS-PEP (28-40) or hPS-PEP (28-40) polymers correspondingly. The contrast matching solvent mixture is represented by the purple background. Only one representative polymer chain in each micelle is shown. (b) A post-mixed sample containing dPS-PEP (26-70) and hPS-PEP (26-70) micelles, which have a similar micelle core size as the micelles in (a) but a considerably larger corona.

Dynamic Light Scattering (DLS)

DLS experiments were conducted using 1 vol% PS-PEP (28-40) polymer solutions in squalane. The samples were prepared following the procedures described in Chapter 2. A Brookhaven BI-200SM goniometer and a Brookhaven BI-9000AT correlator at $\lambda = 637$ nm were used to make DLS measurements over a range of angles (60°~120°) at room temperature.

7.3 Results and analysis

DLS

As described in Chapter 2, the auto correlation function was fitted using the cumulant method and an average decay rate Γ was obtained. A linear fit of Γ over q^2 for all detector angles was performed to determine the averaged hydrodynamic radius (see Figure 7.2 for data and fitting). Using the average mutual diffusion coefficient D_m as the slope of the linear fit (since $D_m = \Gamma / q^2$), and equation 2.4, the averaged hydrodynamic radius was obtained as 256 Å.

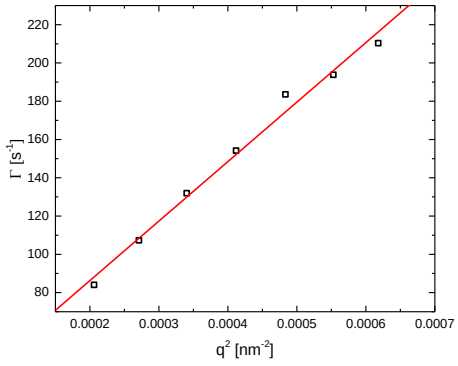

Figure 7.2. Data (black open symbols) and linear fitting line (red) of average decay rate Γ over q^2 for all detector angles.

SAXS Data and Fitting

The SAXS data of 1, 6, and 10 vol% at various temperatures upon heating or cooling are summarized in Figure 7.2. The data obtained at higher temperatures are shifted vertically by factors of 3^n for a clearer view. The intensity shown in the figures are in arbitrary units, and are corrected for empty cell scattering. The heating (red symbols) and subsequent cooling (blue symbols) result in almost identical SAXS patterns for a certain

temperature with the 1 vol% PS-PEP (28-40) sample, as shown by Figures 7.2a and 7.2b. This reproducibility of micelle structures suggests that the micelles prepared with the aforementioned method were at equilibrium. As the temperature increases, all four figures show the smearing of spherical form factor peaks ($q \approx 0.06$ Å for the first peak and 0.09 Å for the second peak), consistent with previous studies (Chapter 5 and Choi *et al.*[125]). In addition, in all four plots, the position of the first minimum (around $q \approx 0.035$ Å^{-1}) of the spherical form factor peaks shifts slightly towards lower q as temperature increases, indicating a minor increase in micelle core size. This observation is consistent with earlier studies for PS-PEP (26-70) micelles[125] as well as the PEP-PS-PEP (approximately 70-24-70) or PS-PEP-PS (approximately 45-140-45) triblock copolymer micelles (Chapter 5), and can be attributed to slight solvent penetration into micelle cores at high temperatures.

Figure 7.2e shows the SAXS patterns obtained from 1, 3, 6, and 10 vol% micelles at 50 ºC, together with corresponding fitting curves in the same color with the SAXS data. A subtle structure peak (at $q < 0.01$ Å^{-1}) can be found in the scattering pattern of 1 vol% at 50 ºC (Figures 7.2a and 7.2b), which becomes significant in the 3 vol% (Figure 7.2e) and 6 vol%. The position of structure peak (q^*) shifts to the right as concentration increases, and the relative intensity of the structure peak increases with concentration, indicating a reduced micelle-to-micelle distance and the subsequent packing of micelles. The 10 vol% sample shows clear Bragg peaks. The position of the primary peak (q^*) and subsequent peaks are (Å^{-1}): 0.01482, 0.02089, 0.02560, 0.02931, 0.03268. The relative peak positions with respect to the primary peak (q_i/q^*) are: 1: 1.4096: 1.7274: 1.9777: 2.2051, and the $(q_i/q^*)^2$ ratios are 1: 2: 3: 4: 4.9. Therefore, at 10 vol%, the micelles close pack into BCC lattice, the same as the PS-PEP (26-70) micelles with longer corona blocks.[125] The closed packed micelle radius R_{nn}, or half the distance between two adjacent micelles in the BCC lattice, can be estimated from the q^* (which corresponds to the first peak [110] in BCC lattice) and lattice parameter a_{bcc}:

$$\boldsymbol{R_{nn} = \frac{\sqrt{3}}{4} a_{bcc} = \frac{\sqrt{6}}{4} \frac{2\pi}{q^*} \approx 260\ \text{Å}} \tag{7.1}$$

Comparing this value to the fitted R_{hs} values for 1, 3, and 6 vol% solutions (see Table 7.2), the micelles in 10 vol% solutions are more closely packed, due to corona overlapping at high concentrations. This result is consistent with the observation of Choi et al.,[125] except that the difference between R_{nn} and R_{hs} is bigger here.

On the other hand, the position of the first minimum of the form factor (around 0.035 $Å^{-1}$) remains roughly the same for 1, 3, 6 and 10 vol%, indicating the micelle core radius R_c (and thus aggregation number N_{agg}) roughly remains the same. The fitted micelle core radius values are summarized in Table 7.2. For the PS-PEP (26-70) diblock copolymer micelles (Choi *et al.*[79]), the aggregation numbers and micelle core radius increased more than 20% as the concentration increases from 1 vol% to 15 vol% when the micelles order. Since the increase in micelle aggregation number at high concentrations could be attributed to the depletion effect of overlapped corona chains,[145] it may be deduced that here with the PS-PEP (28-40) polymers, the depletion effect of micelle corona chains is reduced.

For the 1 vol% PS-PEP (28-40) micelle solutions, a corona thickness, L_{corona} can be estimated from the hydrodynamic radius R_h obtained from DLS measurements as: $L_{corona} = R_h - R_c$ = 256 Å – 101 Å = 155 Å. Because the electron density of the corona blocks and squalane is close (see Table 2.2), the fitting is less sensitive to the corona chain radius of gyration R_g, than R_{hs} which lies in the structure factor. Therefore, instead of directly trusting the R_g from fitting, this important parameter can be estimated as half of the corona thickness, with the assumption of nonpenetration of the corona chains into the core region. The degree of corona chain stretching can be estimated as $S_{corona} = R_g/\langle R_g \rangle_0$ where $\langle R_g \rangle_0$ is the unperturbed radius of gyration. Since the value of $6\langle R_g^2 \rangle_0/MW$ is equal to $0.924 Å^2 \cdot mol \cdot g^{-}$

[1] for *alt*-PEP at 298 K,[112] $\langle R_g \rangle_0$ of PEP with 41,000 g/mol is 79 Å. Therefore $S_{corona} = R_g/\langle R_g \rangle_0 = (155Å /2) /79Å \approx 0.68$. Since the value of S_{corona} is less than one, the corona chains in PS-PEP 28-80 may be unperturbed rather than stretched, while S_{corona} is about 1.4 for 1 wt% PS-PEP (26-70) micelles in squalane at 35 ºC.[125]

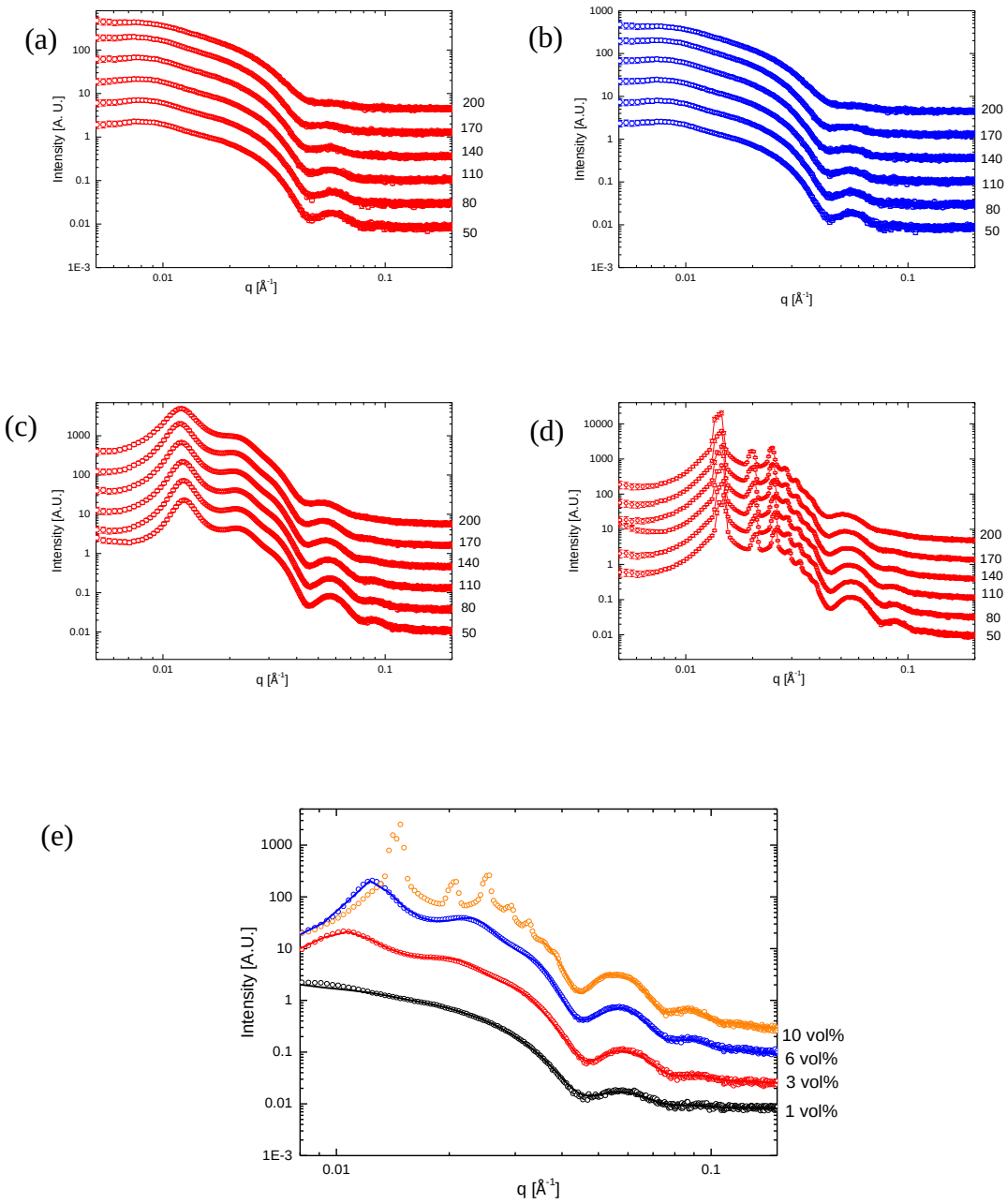

Figure 7.3. SAXS of (a) 1 vol% PS-PEP (28-40) at various temperatures upon heating, (b) 1 vol% PS-PEP (28-40) at various temperatures as the solutions cools down, (c) 6 vol% and (d) 10 vol% PS-PEP (28-40) at the same temperatures upon heating. (e) The SAXS data (open circles) and fitting curves (solid lines of the same color) of PS-PEP (28-40) micelles at 1 vol% (black), 3 vol% (red), 6 vol% (blue), and 10 vol% (orange), measured at 50 ºC.

Table 7.2. SAXS fitting parameters for PS-PEP (28-40) micelles at 1 vol%, 3 vol%, 6 vol%, and 10 vol%. The corresponding fitted curves are shown in Figure 7.3e with the data.

	1 vol%	3 vol%	6 vol%	10 vol%
$\boldsymbol{R_c}$ **/ Å**	101	100	102	104
$\boldsymbol{N_{agg}}$[a]	96	94	101	106

[a] The aggregation number N_{agg} was calculated from the fitted core radius, by assuming no solvent penetration at the experimental temperature 50 ºC, as: $N_{agg} = 4/3 \times \pi \times R_c^3 / \upsilon_{core}$, where υ_{core} is the total volume of one core block.

TR-SANS

Scattering intensities as a function of q from a post-mixed sample recorded during the TR-SANS experiments are shown in Figure 7.3, for the 1 vol%, 2 vol%, and 6 vol% samples, each at one fixed temperature. In each panel, the background scattering associated with a solvent specimen (black stars), the mixed core scattering associated with a pre-mixed specimen (blue circles), and the un-mixed core scattering associated with a post-mixed specimen recorded at room temperature are included as a comparison with the time resolved scattering patterns.

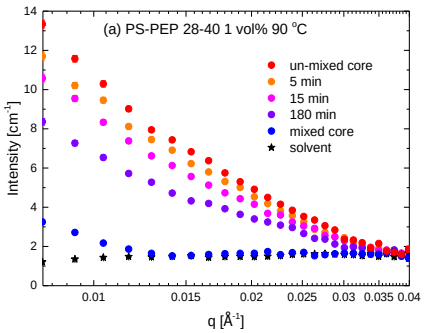
(a) PS-PEP 28-40 1 vol% 90 °C
un-mixed core
5 min
15 min
180 min
mixed core
solvent
Intensity [cm-1]
q [Å-1]

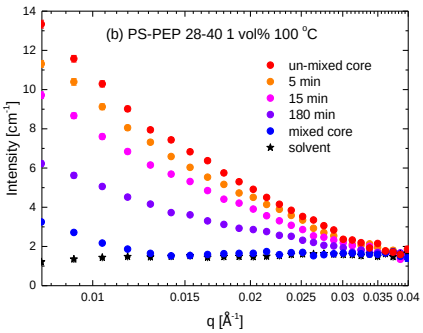
(b) PS-PEP 28-40 1 vol% 100 °C
un-mixed core
5 min
15 min
180 min
mixed core
solvent
Intensity [cm-1]
q [Å-1]

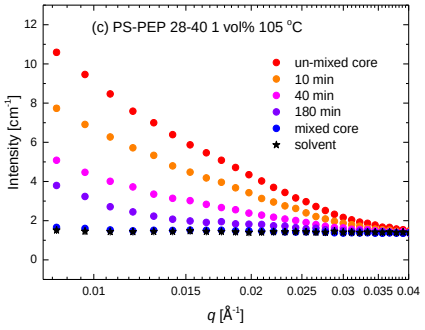
(c) PS-PEP 28-40 1 vol% 105 °C
un-mixed core
10 min
40 min
180 min
mixed core
solvent
Intensity [cm-1]
q [Å-1]

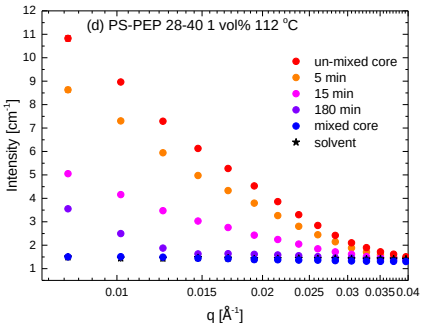
(d) PS-PEP 28-40 1 vol% 112 °C
un-mixed core
5 min
15 min
180 min
mixed core
solvent
Intensity [cm-1]
q [Å-1]

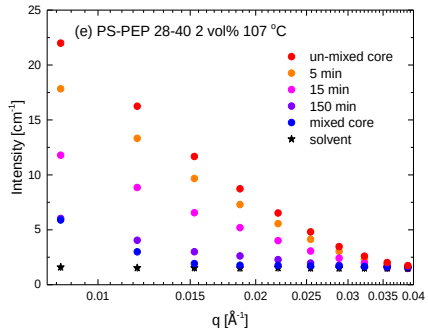
(e) PS-PEP 28-40 2 vol% 107 °C
un-mixed core
5 min
15 min
150 min
mixed core
solvent
Intensity [cm-1]
q [Å-1]

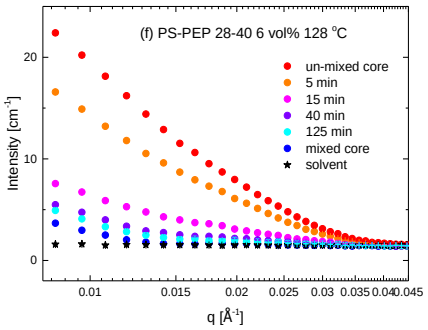
(f) PS-PEP 28-40 6 vol% 128 °C
un-mixed core
5 min
15 min
40 min
125 min
mixed core
solvent
Intensity [cm-1]
q [Å-1]

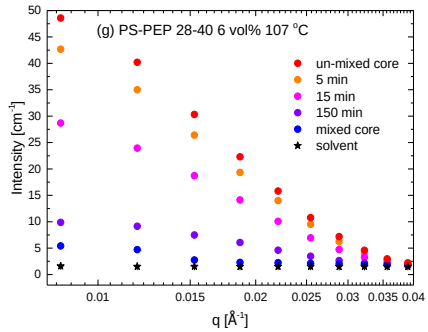
(g) PS-PEP 28-40 6 vol% 107 °C
un-mixed core
5 min
15 min
150 min
mixed core
solvent
Intensity [cm-1]
q [Å-1]

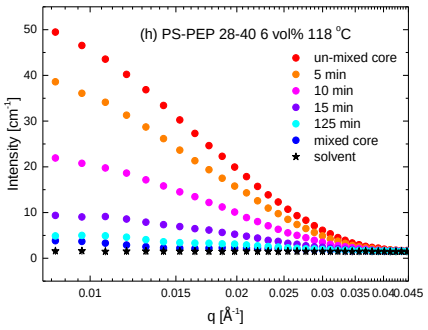
(h) PS-PEP 28-40 6 vol% 118 °C
un-mixed core
5 min
10 min
15 min
125 min
mixed core
solvent
Intensity [cm-1]
q [Å-1]

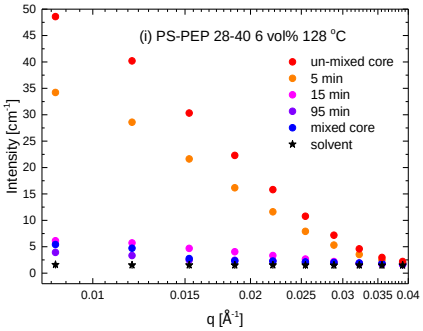

Figure 7.4. $I(q)$ of a post-mixed sample before and during chain exchange, acquired in the TR-SANS experiments of: the 1 vol% PS-PEP (28-40) solutions at (a) 90 ºC, (b) 100 ºC, (c) 105 ºC, and (d) 112 ºC; the 2 vol% PS-PEP (28-40) solutions at (e) 107 ºC, and (f) 118 ºC; the 6 vol% PS-PEP (28-40) solutions at (g) 107 ºC, (h) 118 ºC, and (i) 128 ºC.

As described in the previous chapters, the changes in the SANS intensity were monitored as a function of time at constant temperature over the range $0.09 \leq q \leq 0.04 Å^{-1}$. The relaxation function $R(t)$ that describes the extent of chain mixing is defined via the relative changes in the concentration of dPS blocks in the micelles and has been described in Equation 1.2. $R(t)$ is plotted for each of the measurement temperatures for the 1, 2 and 6 vol% PS-PEP (28-40) in Figure 7.4. The first point of each trace, which corresponds to scattering during the first 5 min exposure, was removed due to the time-dependent temperature.

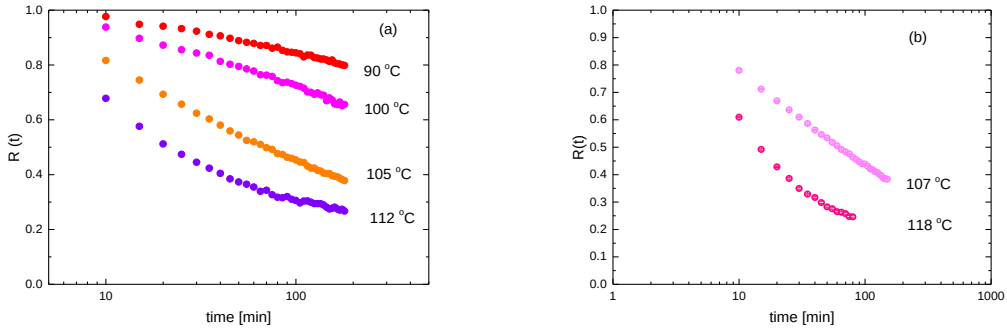

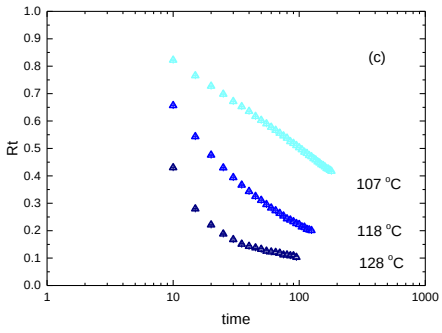

Figure 7.5. The relaxation function $R(t)$ for the chain exchange of (a) 1 vol%, (b) 2 vol% and (c) 6 vol% PS-PEP (28-40) in squalane, at various temperatures as indicated by the different colors and the notations besides.

The time-temperature superposition method has been successfully used in the previous chapters to construct a master curve of $R(t)$ from the individual traces corresponding to different temperatures. The shift factors a_T used in all our past studies follow a straight line on the $\log(a_T)$ vs. T plot (Figure 6.5b). Here we add in the shift factors used in this study to the current shift factors in Figure 7.5d. Figure 7.5c shows only the shift factors used in this study. The master curves corresponding to the three concentrations are constructed using the shift factors. The master curve associated with the 1 vol% micelle chain exchange rate is shown in Figure 7.5a, using the same color scheme as in Figure 7.4a. Figure 7.5b shows the $R(t)$ master curves corresponding to all three concentrations, where the master curve associated with the 1 vol% is shown in grey, to provide a clear comparison between the $R(t)$ of different concentrations. The dashed lines in Figures 7.5a and 7.5b are reproduced from Choi *et al.*[76] where the chain exchange rate of 1 vol% PS-PEP (26-70) is fitted using the model of $R(t)$ developed by the same authors (see Equations 1.3, 1.4). This model assumes the rate limiting step in chain exchange is chain extraction, and the associated activation energy comes only from the enthalpic penalty of pulling the core blocks from the micelle core in to the solution. The length distribution of core blocks is

also considered, but not the corona contribution. The model is described in detail in Chapter 1. Due to the hypersensitivity of core block length to the chain exchange rate, the model was used to generate an estimation of chain exchange rate for PS-PEP (28-40), which has a slightly longer core block, shown by the solid line in Figures 7.5a and 7.5b.

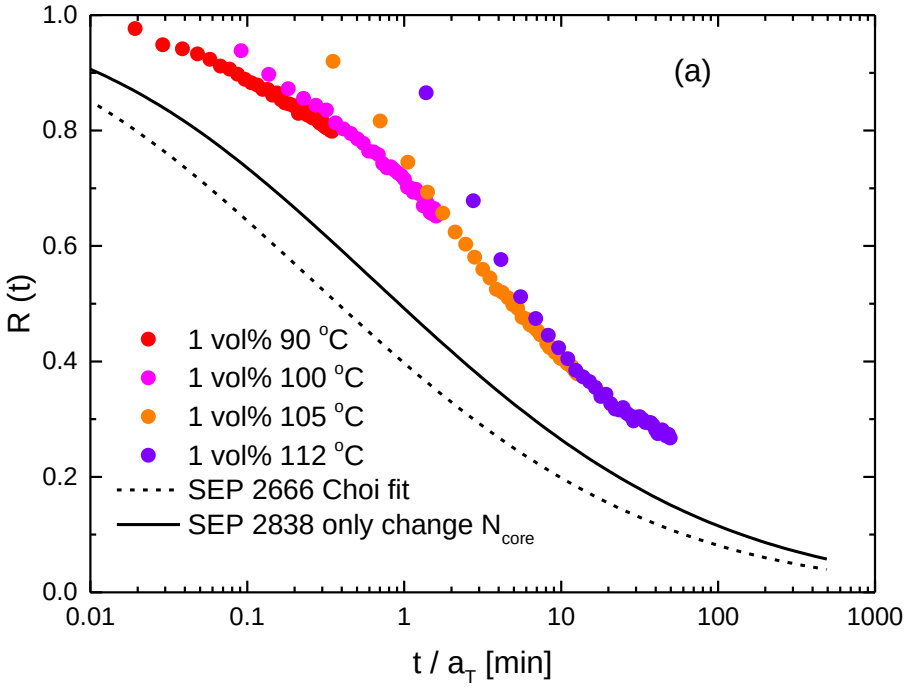
(a)
R (t)
t / a_T [min]
1 vol% 90 °C
1 vol% 100 °C
1 vol% 105 °C
1 vol% 112 °C
SEP 2666 Choi fit
SEP 2838 only change N_core
1.0
0.8
0.6
0.4
0.2
0.0
0.01
0.1
1
10
100
1000

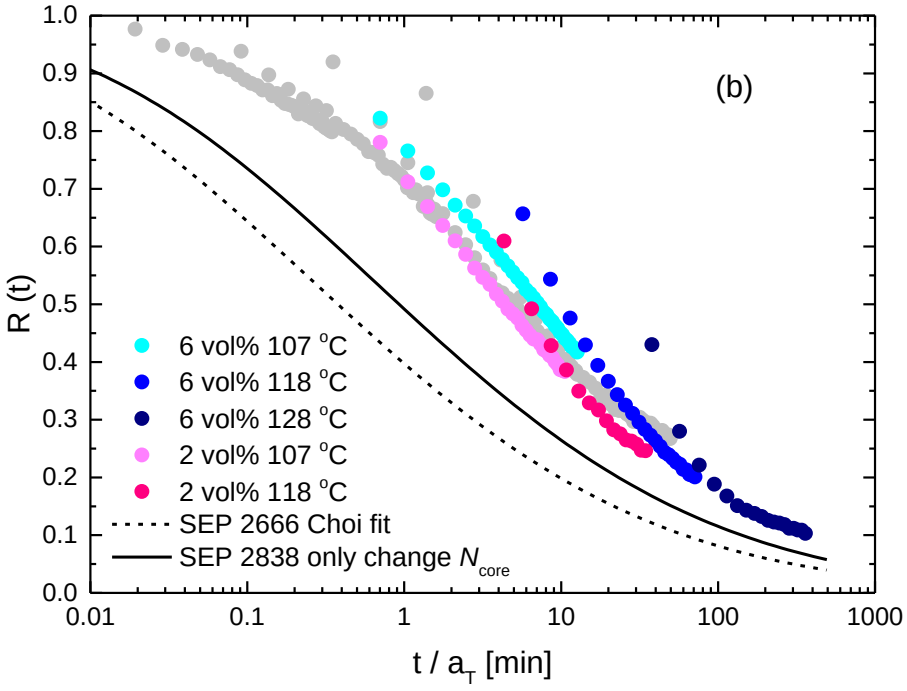
(b)
R (t)
t / a_T [min]
6 vol% 107 °C
6 vol% 118 °C
6 vol% 128 °C
2 vol% 107 °C
2 vol% 118 °C
SEP 2666 Choi fit
SEP 2838 only change N_core
1.0
0.9
0.8
0.7
0.6
0.5
0.4
0.3
0.2
0.1
0.0
0.01
0.1
1
10
100
1000

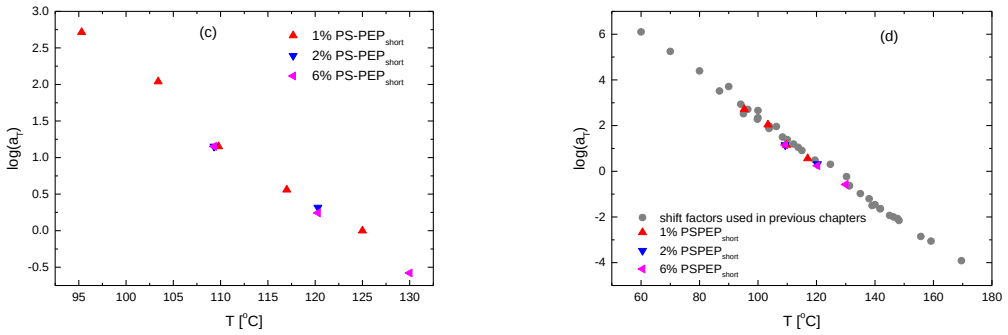

Figure 7.6. (a) The $R(t)$ master curve obtained with 1 vol% PS-PEP micelles (28-40, data points), with the model fit of 1 vol% PS-PEP micelles (26-70, dashed line), reproduced from Choi *et al*.,[76] and the model (Equation 1.3 and 1.4) simulation generated by using the same $\alpha\chi$ and z, but only changing N_{core} from 26 kDa to 28 kDa, at a reference temperature of 125 ºC (b) The $R(t)$ master curve obtained with 2 vol% and 6 vol% PS-PEP (28-40) micelles, combined with the plot shown in (a), where the 1 vol% $R(t)$ master curve is shown in grey in order to clearly illustrate the other two concentrations. (c) The log of shift factors used to obtain the $R(t)$ master curve, for 1 vol%, 2 vol% and 6 vol% PS-PEP (28-40) micelles is plotted against temperature, for a reference temperature 125 ºC. (d) Reproduce of (c), including the comparison with the shift factored used in the previous chapters (represented by the grey symbols).

7.4 Discussion

As shown in Figure 7.5c, the $\log(a_T)$ used in this study generally follows a linear dependence on temperature, similar to what we have seen in the previous chapters, and in the work of Choi *et al*.[76,79] In addition, the overlapping of the new shift factors with the shift factors used in our previous studies (grey symbols in Figure 7.5d) suggests that shorten the corona block length does not change the chain exchange mechanism, which is expected.

One important observation from Figure 7.5a is that the chain exchange between the 1 vol% PS-PEP (28-40) micelles is slower than the 1 vol% PS-PEP (26-70) micelles which have a considerable larger corona (dashed line), even after accounting for the small

difference in core block length (solid line). This observation suggests that the corona blocks may be facilitating the chain exchange of block copolymers, which is also implied by the chain exchange study of triblock copolymer micelles (Chapter 5). On the other hand, upon increasing the concentration of PS-PEP 26-70 from 1 vol% to 15 vol, Choi *et al.*[79] observed an increase in micelle core radius of about 23%. Adding homopolymers of 7 vol% into the 1 vol% PS-PEP 26-70 solutions (Chapter 6) can also introduce an increase in the equilibrium size of micelle cores of about 14%. Both observations can be attributed to the depletion effect of the corona chains.[145] The fitted core radii from SAXS data (Table 7.2) for the 1, 3, 6, and 10 vol% PS-PEP (28-40) micelles, however, generally remain the same, even when the structure factor is significant (Figure 7.2) or the micelles are ordered (10 vol%). In addition, the degree of stretching of the corona chains in the 1 vol% PS-PEP (28-40) micelles is very insignificant, compared to the 1 wt% PS-PEP (26-70) micelles. As discussed in Chapter 6, the corona chains may be facilitating the chain exchange process in two primary ways: (1) the relief of stretching of the corona chains when the molecule escapes the micelle, and (2) the consequences of corona density, which contributes to an additional barrier to the core block extraction and insertion steps. Therefore, the observed lack of depletion induced micelle size increase as well as the reduced degree of corona chain stretching in the PS-PEP (28-40) micelles can both contribute to a slower chain exchange rate, consistent with the TR-SANS results.

In addition to the corona length effect, the concentration dependence in the chain exchange rate of PS-PEP (28-40) micelles is also quantitatively different compared to the PS-PEP (26-70) or PEP-PS-PEP (70-24-70) micelles. As shown in Figure 7.5b, increasing the concentration from 1 vol% to 2 vol%, and then 6 vol%, introduced only a slight slowdown of chain exchange rate. For the PS-PEP (26-70), and PEP-PS-PEP (70-24-70, see Chapter 5), on the other hand, increasing the concentration of polymers from dilute to above the overlapping concentration induced significant changes in the chain exchange

time constant τ: about one order of magnitude difference in τ was reported for the 15 vol% PS-PEP (26-70) micelle solutions compared to the 1 vol% solution,[79] and over one order of magnitude in τ was observed for the 6 vol% PEP-PS-PEP (70-24-70) compared to the 1 vol% solution (Chapter 5). As discussed in Chapters 5 and 6, the overlapping corona chains in concentrated micelle solutions could contribute to slower kinetics for several different reasons, which are all related to the corona chain length. This reduced concentration effect therefore is further evidence of the corona contribution in chain exchange, which is reduced when the corona block length is smaller.

7.5 Summary

In summary, the chain exchange between diblock PS-PEP (28-40) micelles with a relatively smaller corona than the diblock copolymer PS-PEP (26-70) used previous studies was investigated using TR-SANS. Following the procedures (*i.e.*, anionic polymerization with subsequent selective hydrogenation) discussed in Chapter 2, narrowly distributed polymers were synthesized with controlled molecular weights and composition. The structural characteristics of the micelle were obtained by performing a model fitting with the SAXS scattering patterns, by employing a hard sphere fitting model, which was also described in Chapter 2. 1, 3, 6, and 10 vol% micelles were prepared and measured with SAXS. It was found that the micelle core radius in general remains constant with temperature, and that the degree of corona chain stretching in 1 vol% solution is quantitatively less compared to the PS-PEP (26-70) micelles.

TR-SANS experiments were conducted for 1 vol%, 2 vol%, and 6 vol% micelle solutions, to investigate the chain exchange rate. It was found that with a smaller corona block (40 kDa vs. 70 kDa), the chain exchange is slowed down by about one order of magnitude. In addition, a much weaker concentration dependence was found. These observations are consistent with the triblock chain exchange dynamics study (Chapter 5)

and the adding PEP homopolymers study (Chapter 6), where the facilitating role of corona chains are also implied. Additional experiments on the chain exchange between PS-PEP micelles with various PEP corona chain lengths and the same PS core chain lengths are needed, to obtain a quantitative evaluation of the contribution of corona chain length in the chain exchange rate.

Chapter 8.

Hybridization of Diblock Copolymer Micelles

8.1 Introduction

In Chapters 3 to 7, the chain exchange mechanisms were investigated in triblock and diblock copolymer micelles near equilibrium. For the time resolved small angle neutron scattering (TR-SANS) experiments, normal and deuterated equivalent micelles were prepared. The deuterated polymers were of almost identical molecular weight and composition as the normal polymers. In addition, the samples used in these studies were annealed and tested with small angle X-ray scattering (SAXS) during heating and cooling ramps to check for the reproducibility of micelle size. These additional experiments were conducted to establish that the micelles were relatively monodisperse in solution and at or near equilibrium. Yet an interesting question is whether the chain exchange mechanism remains the same when the distribution of initial micelle system is away from equilibrium, *e.g.*, when micelles of different sizes hybridize by chain exchange. The Anniasson and Wall mechanisms[19] and the theoretical analysis of Halperin and Alexander[73] on the chain exchange mechanisms of polymeric micelles suggest that the equilibration time constant of chain exchange in a micelle solution of equilibrium size is much smaller than that of the kinetics for polydispersed micelles to reach the lowest free-energy state.

A primary complication involved in such a micelle hybridization study is that the micelles change in size in an unknown direction, in order to reach their equilibration distritbution. While one might expect the large and small micelles approach an equilibrium size in between the initial dimensions, other mechanisms are possible. For example, some small micelles might dissolve into free chains to facilitate the chain exchange with large micelles. In addition, the path to an exact state of equilibration for the micelle system is not straightforward. It is questionable whether or not the long and short chains will fully hybridize and form monodispersed micelles upon equilibration. As for the contrast matching in TR-SANS, as discussed in the previous chapters, under optimal conditions the deuterated core blocks and normal protonated core blocks must be present in equal volume, *i.e.*, the number of small micelles containing polymer chains with shorter core blocks therefore needs to be larger than that of the large micelles containing polymer chains with longer core blocks. All these factors complicate the investigation of micelle hybridization mechanisms. Despite the difficulties with data interpretation, it is an interesting and important subject, since it is unrealistic to expect micelles are monodisperse and near equilibrium in real applications.

Here we report a TR-SANS study of micelle hybridization in a solution containing a bimodal distribution of micelle sizes. The two types of corresponding polymers are PS-PEP (poly(styrene-*b*-(ethylene-*alt*-propylene))) diblock copolymers, with corona blocks of comparable sizes, but the core block lengths differ by a factor of 1.6. Both the structural characteristics and the chain exchange rates of each micelle component has been characterized by Choi *et al.*[76] Our previous studies have demonstrated that the chain exchange rate is hypersensitive to micelle core block length,[80] and according to Choi *et al.*, [76] that the chain exchange rate constant for the two types of polymers in dilute micelle solution differ by several orders of magnitude. On the other hand, as discussed above, the hybridization of bimodal distributed micelles could involve other micelle size changes.

Therefore here we carefully monitored the micelle size change by performing duplicate TR-SANS experiments in h-squalane when both populations of polymer micelles are deuterated. This design allows the investigation of micelle size change during the micelle hybridization experiments. Since the contrast of micelle does not change during the hybridization process, the observed scattering intensity change is due solely to the change in micelle sizes. Structural information can be extracted by fitting the TR-SANS data with the hard sphere model, which is described in detail in Chapter 2.

7.2 Experiments

Materials

Similar to the other chapters, to quantitatively investigate the chain exchange rate using TR-SANS, deuterated and protonated polymers are needed, together with the contrast matching squalane mixture. In this study, two populations of micelles were separately prepared from dPS-PEP-2 and hPS-PEP-1 diblock copolymers with comparable corona block size but the "2" polymers have a larger core block by a factor of 1.6, in a h/d mixed squalane solvent (58 vol% d-squalane + 42 vol% h-squalane, see Chapter 3 for the determination of the h/d squalane ratios). Another set of TR-SANS experiments were designed to find out the changes in the micelle sizes during the chain exchange with dPS-PEP-2 and dPS-PEP-1 micelles in h-squalane rather than the d/h squalane mixture, in order to enlarge the contrast between micelles and solvents (see Table 2.2 for the corresponding neutron scattering lengths), and to reduce the cost of the expensive d-squalane as well. The molecular characteristics of the three polymers were summarized in Table 2.1.

Time Resolved Small Angle Neutron Scattering (TR-SANS) and Model Fitting

Using the co-solvent method with subsequent thermal annealing, the micelle solutions were prepared in three concentrations, 0.5 vol%, 1 vol% and 3 vol%, as described in

Chapter 2. For the TR-SANS experiments that addressed the chain exchange rate, the post-mixed and pre-mixed samples were prepared from the dPS-PEP-2 and hPS-PEP-1 polymers in the h/d squalane that matches the contrast of a 50/50 hPS/dPS mixed micelle core, following similar procedures described in Chapter 3. The same contrast matching strategy is applied in this study, so that the scattering intensity of the post-mixed specimen decreases over time with the mixing of isotope labeled chains. Figure 8.1a illustrates the chain exchange of dPS-PEP-2 and hPS-PEP-1 micelles in the h/d squalane mixture, where the relative core size of the d and h micelles was determined based on the SANS fitting results from the dPS-PEP-2 and dPS-PEP-1 micelles in h-squalane (Table 8.1). Since the d and h polymers have different core block sizes, the relative amount of the d and h polymer micelles in the post-mixed samples as well as in the micelle cores of the pre-mixed sample was calculated so that the volume of the d and h chains are equal. Bulk densities of PS and PEP were assumed.

To monitor the chain exchange in the post-mixed specimens, TR-SANS experiments were conducted in the same manner as described in previous chapters, where the post-mixed specimen was placed in a pre-heated sample holder at a designated temperature, and the scattering intensity was monitored in 5 min intervals for up to 3.5 hours. The TR-SANS experiments were performed at the Oak Ridge National Laboratory (ORNL) and the National Institute of Standards and Technology (NIST), using the same sample environments and instrumental configurations described in Chapter 6.

To study the micelle size evolution during chain exchange between the big and small micelles, the dPS-PEP-2 and dPS-PEP-1 micelles were prepared in h-squalane at 0.5 vol%, 1 vol% and 3 vol% using the same co-solvent method, followed by thermal annealing, as described in Chapter 2. The corresponding post-mixed and pre-mixed samples were also prepared. The TR-SANS experiments with these post-mixed deuterated polymer micelles in h-squalane were conducted at one temperature (126 ºC) where the chain exchange

kinetics diverges from that observed from micelle solutions containing nearly monodispersed PS-PEP-1 or PS-PEP-2 micelles at equilibrium, as discussed latter in the chapter. Figure 8.1b illustrates the chain exchange between these deuterated micelles. These TR-SANS experiments were conducted at NIST, on the NG-7 30 m beamline. Data were acquired at a sample to detector distance of 4.7 m. The neutron beam had a wavelength $\lambda = 6$ Å and a wavelength spread of $\Delta\lambda/\lambda = 0.11$. The sample environment used was the same as before (Chapter 5). The 2-D scattering data were corrected for empty cell scattering, transmission, and detector sensitivity and reduced to absolute intensity using procedures established by NIST.[134]

The acquired SANS profiles (*i.e.*, scattering intensity I as a function of the wave vector q) for the hybridization of the two populations of d micelles in h squalane were fitted using the hard sphere model described in Chapter 2. The micelle core size during the hybridization process was obtained from the fitted core radius, under the assumption of no solvent penetration into the micelle cores.

Table 8.1. Fitted core radius R_{core} and the calculated N_{agg} values for 0.5 vol%, 1 vol%, and 3 vol% micelle solutions in h-squalane. The corresponding data and the associated fitting curves are shown in Figure 8.6.

Sample	0.5 vol%		1 vol%		3 vol%	
	R_{core}	N_{agg}	R_{core}	N_{agg}	R_{core}	N_{agg}
dPS-PEP-1	102	103	106	117	108	125
dPS-PEP-2	129	120	129	120	133	132
post-mixed	123	146	122	142	122	144
pre-mixed	118	130	130	173	132	180

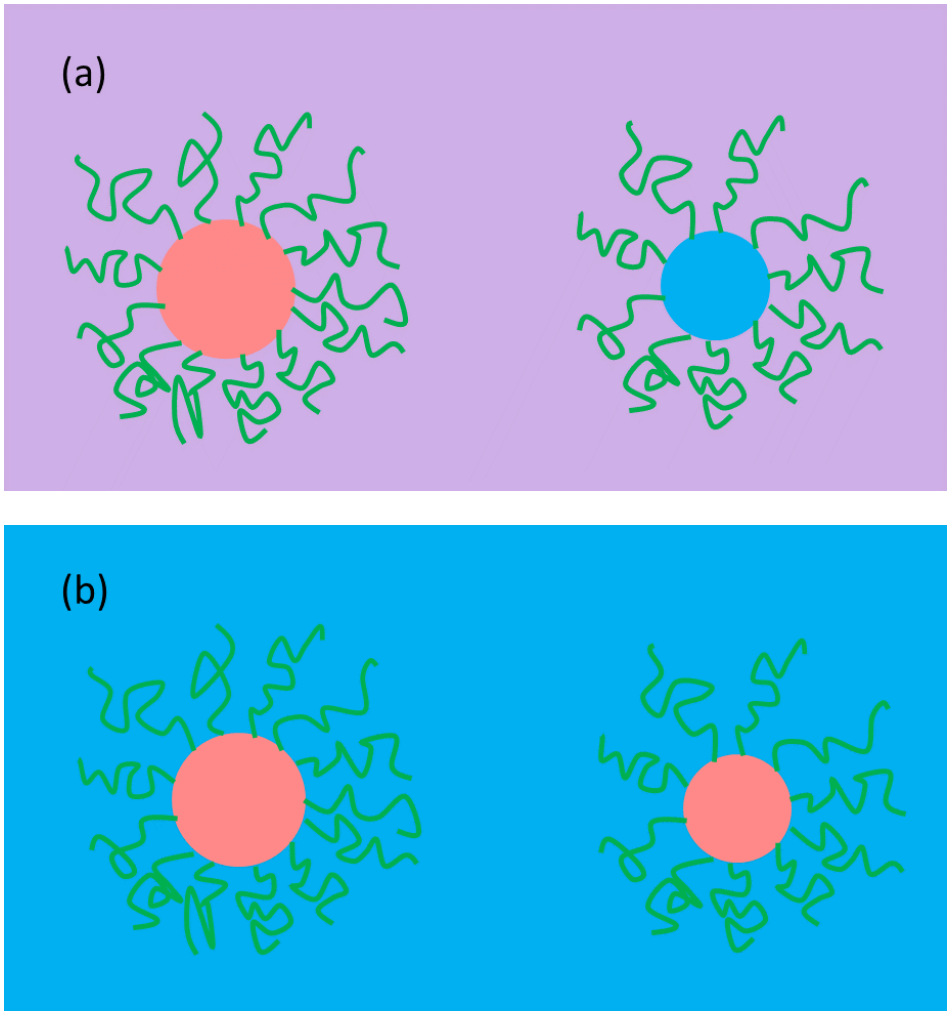

Figure 8.1. Schematic illustration of the big and small micelles in a post-mixed specimen before chain exchange, used in (a) the TR-SANS experiment to investigate micelle hybridization kinetics, and (b) the TR-SANS experiment at 126 ºC to monitor the micelle size evolution. In both figures, the green lines represent the PEP corona chains, while the red and blue filled circles represent the deuterated and normal PS micelle cores, respectively. The purple background in (a) illustrates the d/h mixed squalane, which matches the contrast (or color in the figures) of a 50/50 mixed dPS (red) / hPS (blue) micelle core. The blue background in (b) suggests the solvent is purely h-squalane rather than an isotope labeled mixture.

8.3 Results and Analysis

Micelle Hybridization Kinetics

The TR-SANS data are presented in Figure 8.2, for the three concentrations at several temperature. Each panel shows $I(q)$ recorded as a function of time at a fixed temperature. Similar to the previous chapters, the highest scattering intensities correspond to the post-mixed specimens before chain exchange, which decreases as a function of time due to the mixing of dPS-PEP-2 and hPS-PEP1 chains, and approaches the scattering profile of the pre-mixed specimens. Due to the contrast matching between the micelle cores and the d/h squalane mixture, the pre-mixed scattering profile is close to that of pure solvent, except in the low q region, where the un-matched micelle corona scattering dominates.

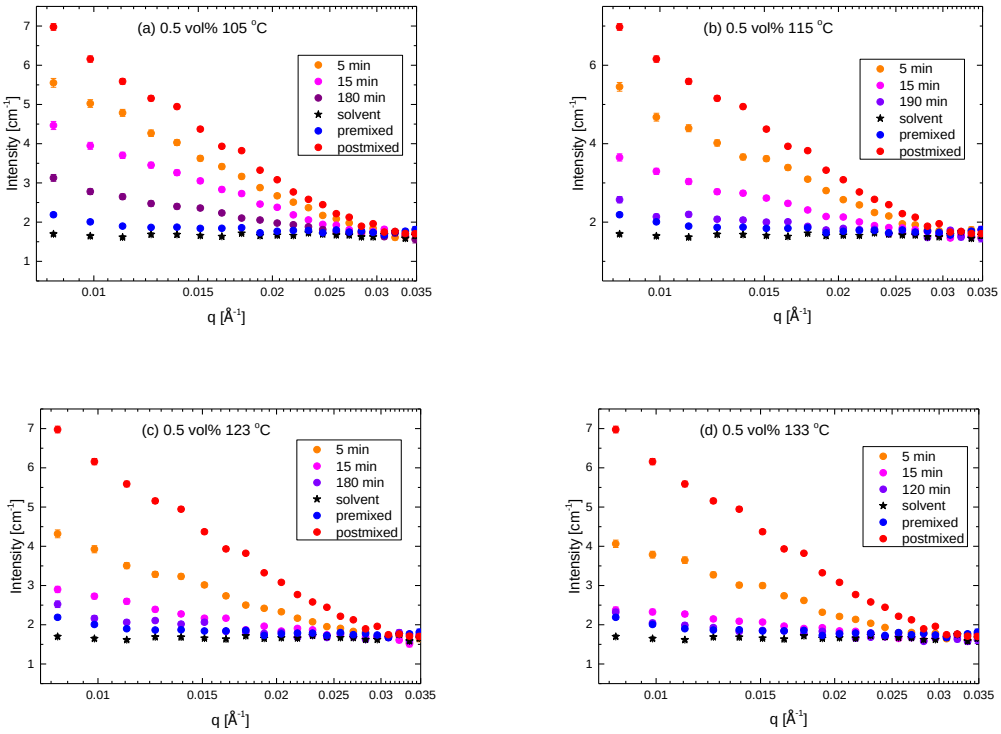

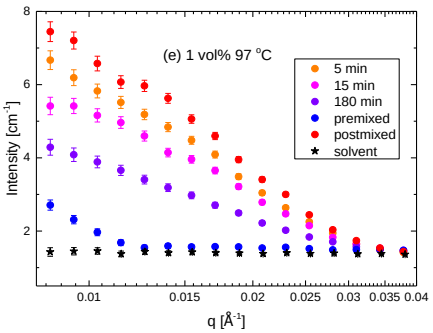
(e) 1 vol% 97 °C
5 min
15 min
180 min
premixed
postmixed
solvent
Intensity [cm-1]
q [Å-1]

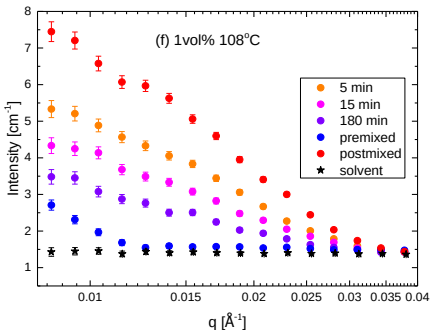
(f) 1vol% 108°C
5 min
15 min
180 min
premixed
postmixed
solvent
Intensity [cm-1]
q [Å-1]

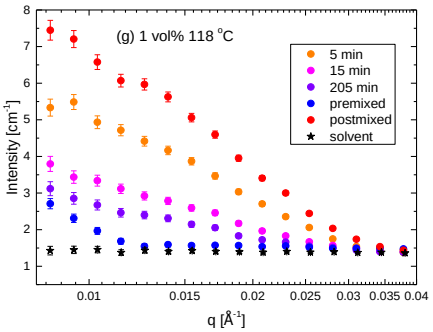
(g) 1 vol% 118 °C
5 min
15 min
205 min
premixed
postmixed
solvent
Intensity [cm-1]
q [Å-1]

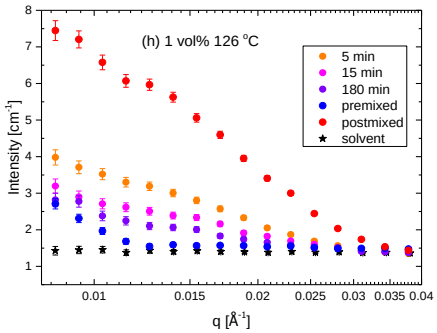
(h) 1 vol% 126 °C
5 min
15 min
180 min
premixed
postmixed
solvent
Intensity [cm-1]
q [Å-1]

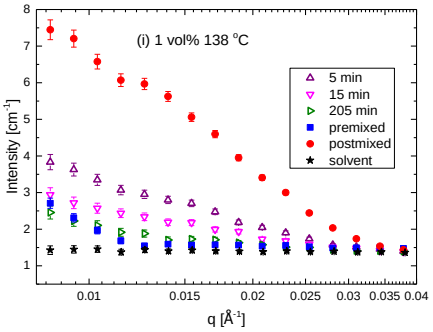
(i) 1 vol% 138 °C
5 min
15 min
205 min
premixed
postmixed
solvent
Intensity [cm-1]
q [Å-1]

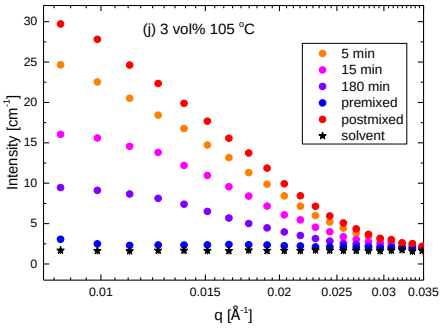
(j) 3 vol% 105 °C
5 min
15 min
180 min
premixed
postmixed
solvent
Intensity [cm-1]
q [Å-1]

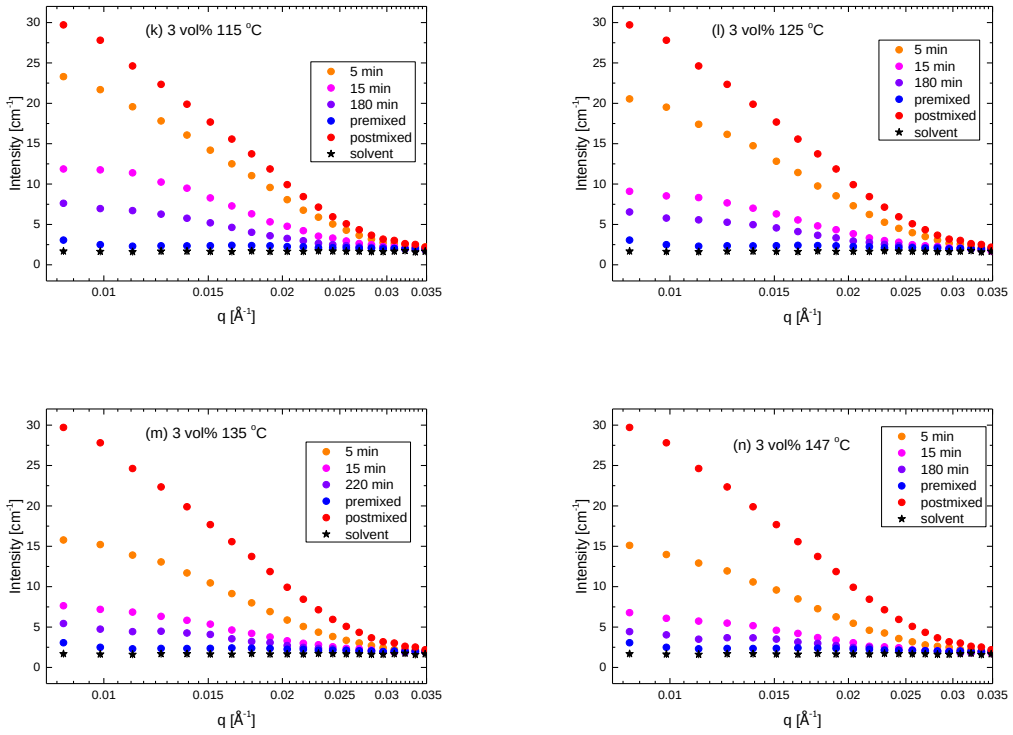

Figure 8.2. Representative TR-SANS patterns recorded in 5 minute increments during the hybridization of: the 0.5 vol% dPS-PEP-2 and hPS-PEP-1 micelles at (a) 105 ºC, (b) 115 ºC, (c) 123 ºC, and (d) 133 ºC; the 1 vol% dPS-PEP-2 and hPS-PEP-1 micelles at (e) 97 ºC, (f) 108 ºC, (g) 118 ºC, (h) 126 ºC, and (i) 138 ºC; the 3 vol% dPS-PEP-2 and hPS-PEP-1 micelles at (j) 105 ºC, (k) 115 ºC, (l) 125 ºC, (m) 135 ºC, and (n) 147 ºC. The corresponding polymer concentration and temperature is identified in each plot. In each plot, the un-mixed core scattering recorded from a post-mixed specimen before chain exchange (red data points), the mixed core scattering recorded from a pre-mixed specimen (blue data points), and the solvent scattering patterns are included to compare with the time resolved scattering patterns (black data points), same as in the previous chapters.

The relaxation function $R(t)$ defined in Equation 1.2 is calculated and plotted in Figure 8.3 for the micelle hybridization experiments conducted at the three concentrations at each temperature. The scattering intensities used in Equation 1.2 were integrated intensities obtained over the q range 0.009 $Å^{-1}$ to 0.035 $Å^{-1}$. The first point corresponding to the measurement at 5 min in each panel was removed due to the transient temperature.

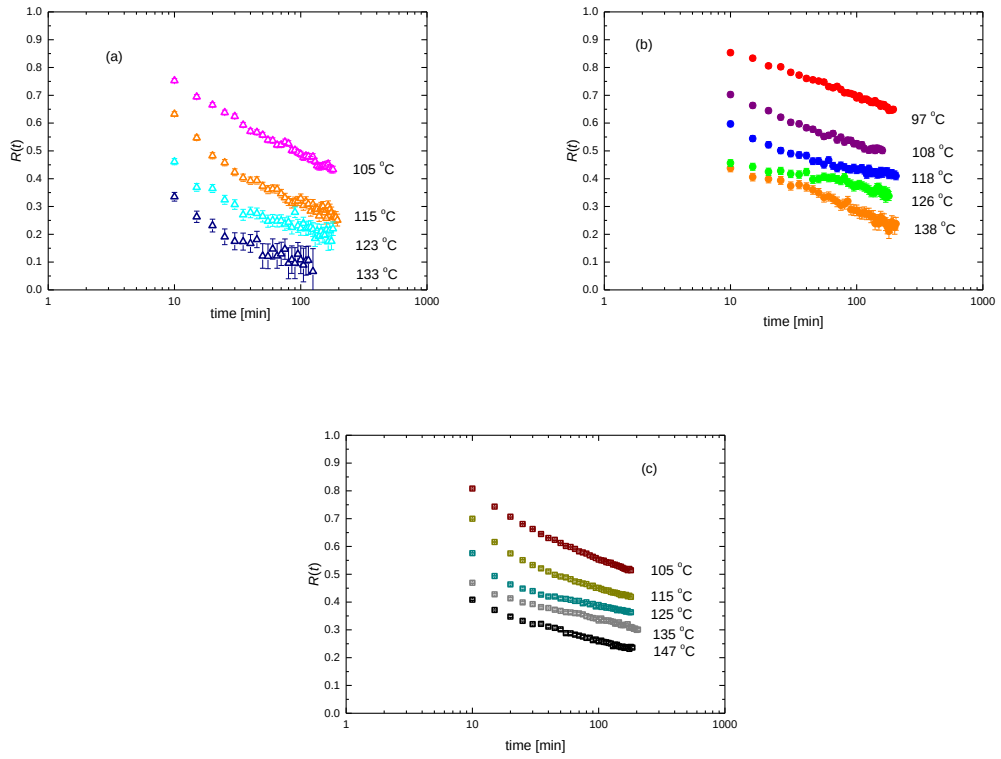

Figure 8.3. R(t) traces obtained at different temperatures for the micelle hybridization between (a) 0.5 vol%, (b) 1 vol%, and (c) 3 vol% dPS-PEP-2 and hPS-PEP-1 micelles. The corresponding temperatures are noted in each figure to the right of each data trace.

In previous chapters, we showed that the $R(t)$ traces obtained at different temperatures can be horizontally shifted using the time-temperature superposition[107]: $R(t/a_T, T_{ref}) = R(t, T)$. Here we adopt the same technique and shift the $R(t)$ traces in Figure 8.3 to construct master curves for the measurements at each concentrations, using a reference temperature T_{ref} = 125 ºC. The shift factors used in this study are summarized and compared with the shift factors used by Choi *et al.* with nearly monodispersed PS-PEP-2 or PS-PEP-1 micelles at 1 vol%[76] in Figure 8.4. The master curves obtained using those shift factors are shown in Figure 8.5a, 8.5b, 8.5c, and Figure 8.6, where the data corresponding to the three concentrations are plotted individually in the first three figures, and together in the last one. In Figure 8.6, the $R(t)$ master curves associated with the micelle hybridization at the three

difference concentrations are compared. The fitting curves of the $R(t)$ master curves of nearly monodispersed 1 vol% PS-PEP-1 and 1 vol% PS-PEP-2 micelles are reproduced from Choi *et al.*,[76] and also plotted in Figure 8.6. The corresponding fitting model functions are described in Chapter 2, equation 1.3 and 1.4.

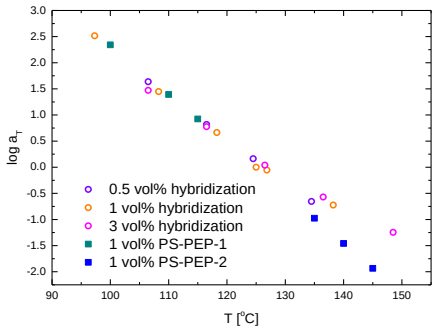

Figure 8.4. The shift factors used in this micelle hybridization study (open round symbols) where the initial post-mixed specimen contains two populations of micelles, the PS-PEP-2 and PS-PEP-1, are compared with the shift factors for the micelle chain exchange between nearly monodispersed PS-PEP-2 or PS-PEP-1 micelles near equilibrium (solid squares), reproduced from Choi *et al.*[76] The color logics are shown in the legend.

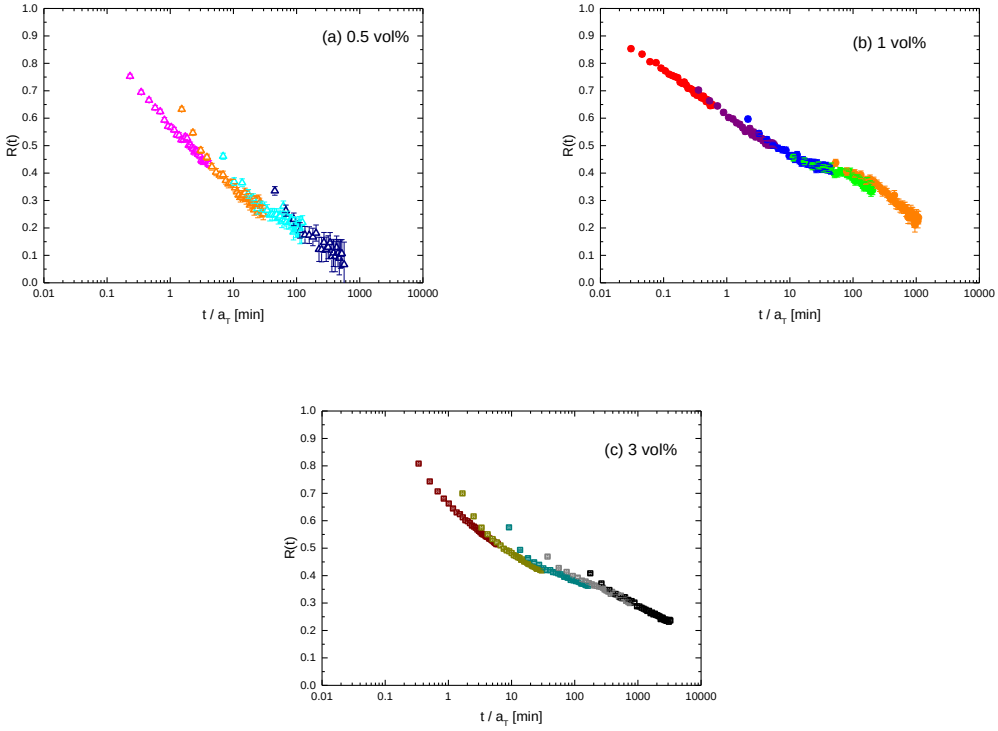

Figure 8.5. The $R(t)$ master curves constructed using the shift factors shown in Figure 8.4 for the micelle hybridization of (a) 0.5 vol%, (b) 1 vol%, and (c) 3 vol% PS-PEP micelle solutions. Each of the $R(t)$ traces shown in plot (a), (b) and (c) correspond to the unshifted $R(t)$ traces in Figure 8.3a, 8.3b, and 8.3c of the same color, respectively.

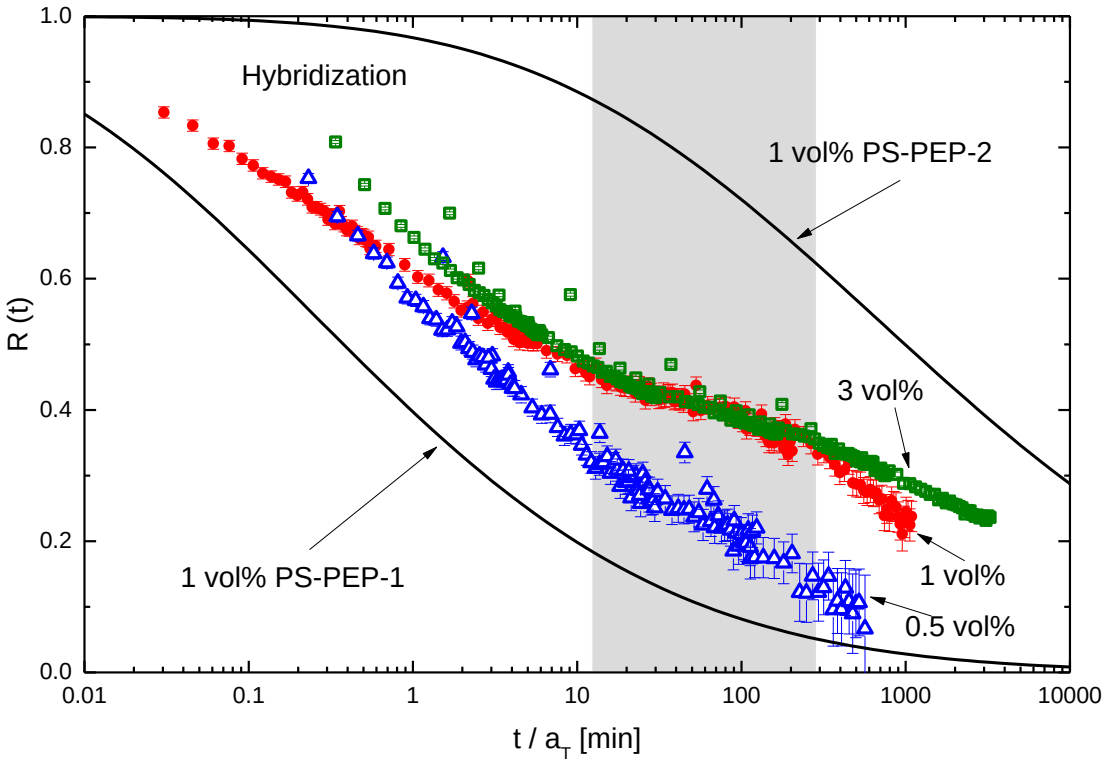

Figure 8.6. The $R(t)$ master curves associated with the hybridization of 0.5 vol% (blue), 1 vol% (red), and 3 vol% (green) micelle solutions are reproduced from Figure 8.5a, 8.5b, and 8.5c, respectively, on the same plot. The reference temperature T_{ref} = 125 °C. The two black lines represent the model fitting curves for the $R(t)$ master curves of nearly monodispersed 1 vol% PS-PEP-1 (left) and 1 vol% PS-PEP-2 (right), and are reproduced from Choi *et al*.[76] The shaded region identifies the time range where the shapes of the $R(t)$ master curves associated with the micelle hybridization of 1 vol% and 3 vol% solutions are different from the two black lines.

Micelle Hybridization Size Evolution during Hybridization Process at the Plateau Temperature

As briefly discussed in the introduction section, while the hybridization of micelles must involve micelle size change, as the system is away from equilibrium, how the micelle size changes during the process is not clear. The shaded region in Figure 8.6 identifies a time range where the shape of $R(t)$ master curves are different from the model fitting curves,

for the 1 vol% and 3 vol% micelle solutions. In the previous chapters, we showed that the shape of the $R(t)$ master curves obtained using several different micelle systems near equilibrium in general followed the same model. Since the micelle size evolution is a slow process compared to chain exchange, this observation in micelle hybridization is possibly connected with the change in micelle sizes during the experiment. The corresponding temperature of the shaded t/a_T region is approximately 126 ºC. Therefore, we selected this temperature and conducted another set of almost identical TR-SANS experiments with d-PS-PEP-2 and d-PS-PEP-1 micelles in h-squalane, where the dPS-PEP-1 polymers have almost identical molecular weight and composition as the hPS-PEP-1 polymers used in the previous TR-SANS experiments (see Table 2.1). The scattering patterns obtained in these TR-SANS experiments are summarized in Figure 8.7, for the 0.5, 1, and 3 vol% micelle solutions. In each panel, the time resoled scattering patterns acquired from a post-mixed specimen at 126 ºC are compared with the scattering of a pre-mixed specimen, a post-mixed specimen before chain exchange, a d-PS-PEP-1 and a d-PS-PEP-2 micelle solution at corresponding concentration. A zoomed in plot for each concentration is shown beside each corresponding plot, to illustrate the position of the first minimum in $I(q)$, which is associated with the form factor of the micelle cores, and thus is a reflection of micelle core size. Clearly, the position of the first minimal in $I(q)$ changes during the experiment, during the hybridization of micelles at all the concentrations. This implies change of micelle size during the hybridization process.

These SANS data associated with the pre-mixed and post-mixed specimens, as well as those associated with the separately prepared dPS-PEP-2 and dPS-PEP-1 micelle solutions before mixing, were fit with the hard sphere model described in Chapter 2. The aggregation numbers N_{agg} were calculated by assuming no solvent in the cores, based on this relation: N_{agg} × core block volume = core volume = $3/4\times\pi\times R_{core}^3$. The corresponding fitting curves are compared with the SANS data in Figure 8.8. The time resolved SANS data of the post-

mixed specimen at 126 ºC were also fitted with the model, and the core radius was found to change during the 3 hours associated with the measurement. However, the size distribution of the core radius R_{core} was found to be at least 15%, comparable with the changes in the fitted values of R_{core} during this process. The uncertainties associated with fitting results increase significantly from less than 2% to around 10% when the distribution of R_{core} is considerable. Therefore, the core radius evolution during the hybridization at 126 ºC suggested by the fitting results is not a reliable evidence. For the d-PS-PEP-1, d-PS-PEP-2, as well as the pre-mixed and post-mixed specimens, the distribution of R_{core} is always less than 10%, and the fitting uncertainties are always below 2% of R_{core} at all three concentrations. The fitted R_{core} and the corresponding N_{agg} values for these four specimens are summarized in Table 8.1.

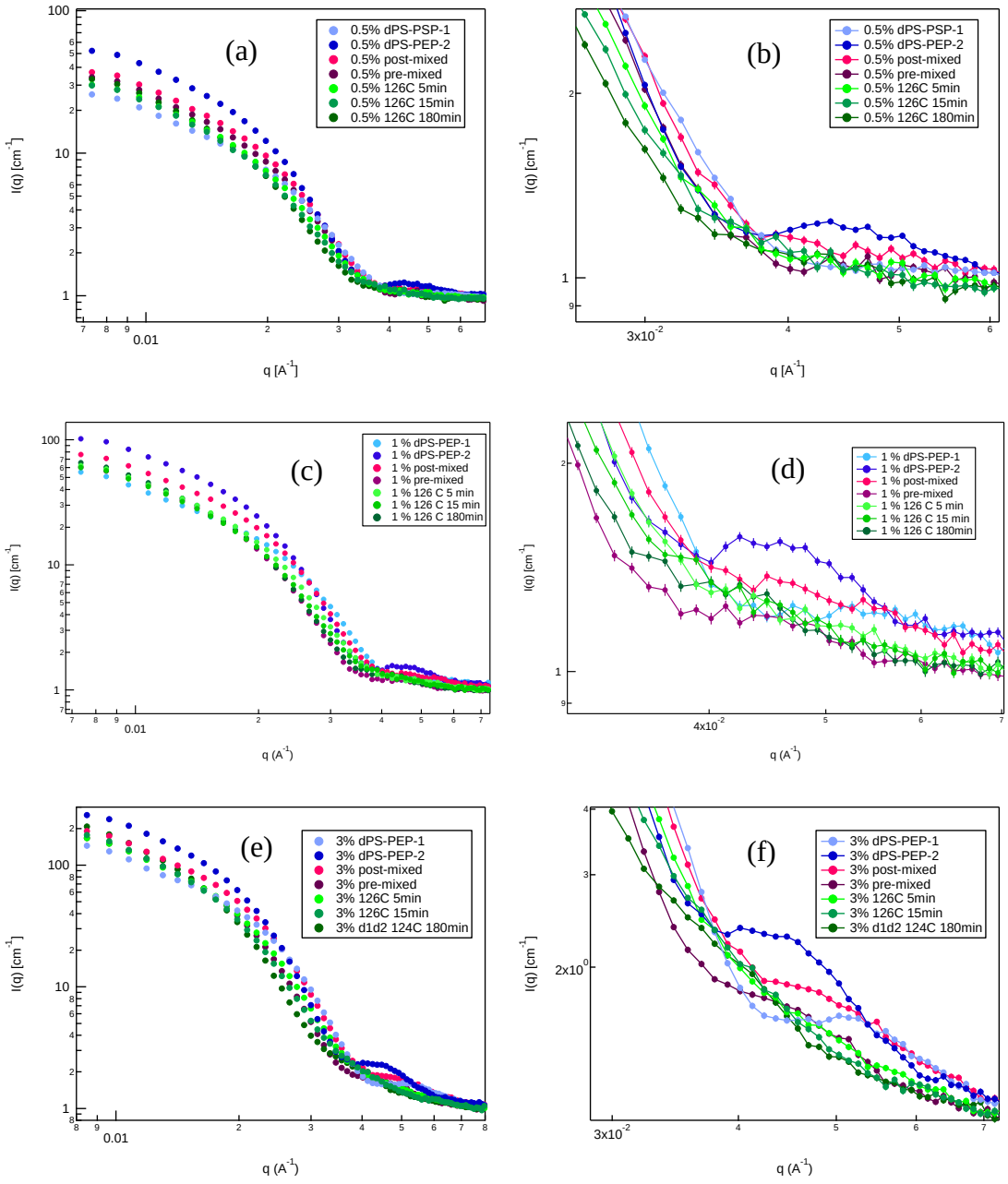

Figure 8.7. Representative scattering intensity profile measured in the TR-SANS experiments dealing with the hybridization of deuterated big and small polymer micelles in h-squalane for (a) 0.5 vol%, (c) 1 vol%, and (e) 3 vol% solutions. The (b), (d) and (f) show the zoomed in plots of scattering data shown in (a), (c), and (e), respectively, to illustrate the shift in the first minimal, which is a reflection of the averaged micelle core radius. In each panel, the scattering from a post-mixed sample before chain exchange, a pre-mixed sample which approximate the equilibrium state after sufficient amount of chain exchange, and the time dependent scattering pattern obtained with the post-mixed sample at the plateau temperature suggested by Figure 8.5, 126 ºC.

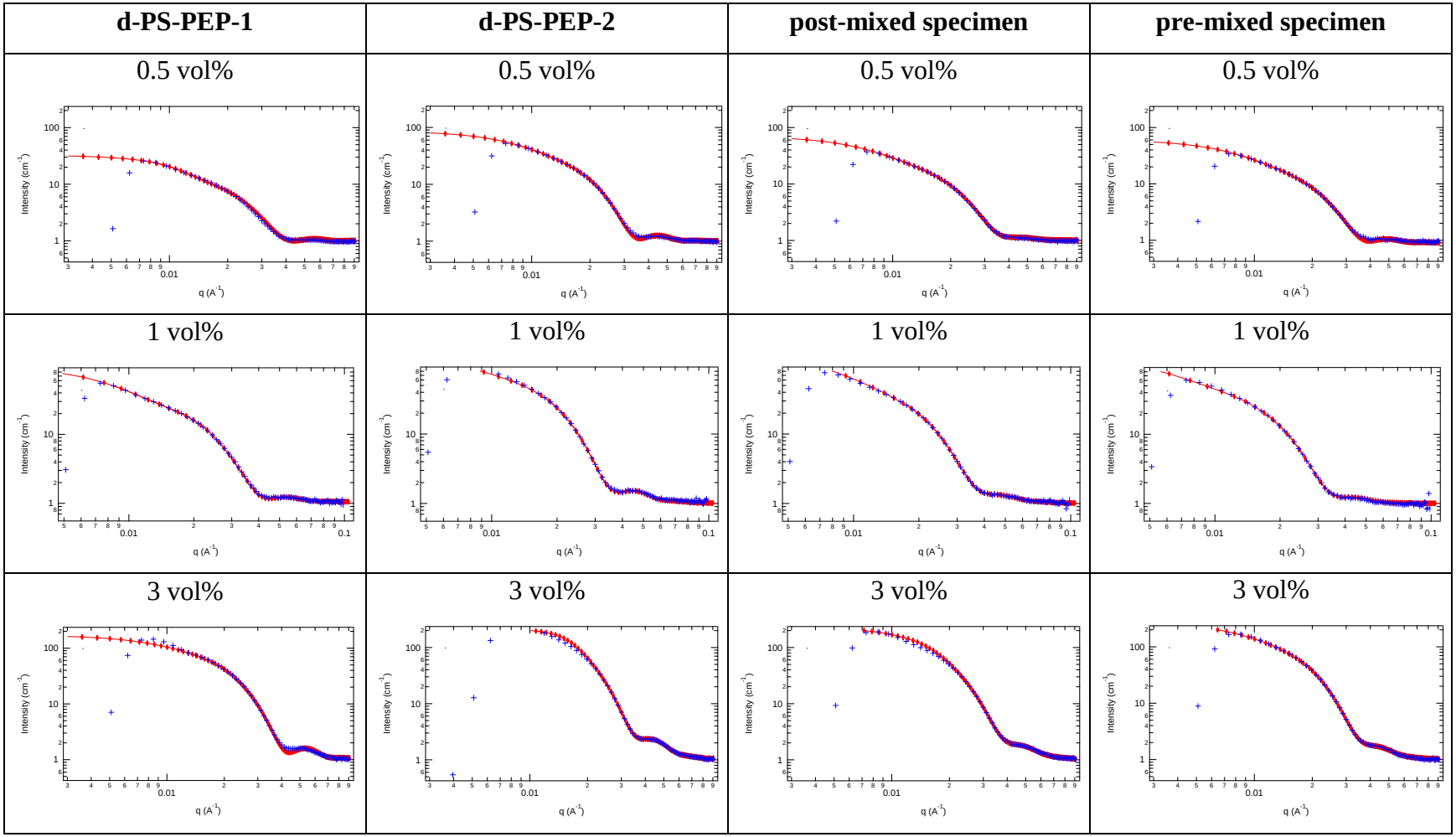

Figure 8.8. Fitting curves (red symbol connected with lines) and data (blue markers) for the d-PS-PEP-1, d-PS-PEP-2, post-mixed, and pre-mixed specimens at 0.5 vol%, 1 vol%, and 3 vol%.

8.5 Discussions

In the previous chapters, we found the $\log(a_T)$, when plotted versus T, in general follows a straight line with a slope and magnitude that is independent of polymer concentration, molecular weights, distribution, composition, and architecture. As shown in Figure 8.4, the shift factors used in this study in general follow the same dependence on temperature as the shift factors reported by Choi *et al.*[76] for nearly monodispersed PS-PEP-2 or PS-PEP-1 micelles near equilibrium. However, the four shift factors associated with the micelle hybridization in 0.5 vol%, 1 vol% and 3 vol% solutions at temperatures higher than 130 ºC seem to be outliers. This observation implies that the chain exchange mechanism is changing during micelle hybridization process when temperature is above 130 ºC.

As shown in Figure 8.6, the $R(t)$ master curves associated with the micelle hybridization between PS-PEP-2 and PS-PEP-1 micelles lie between the two model fitting curves corresponding to the chain exchange rate of dilute PS-PEP-2 micelle solutions and dilute PS-PEP-1 micelle solutions, respectively. This observation is expected due to the hypersensitivity of chain exchange rate to the core block lengths. However, the $R(t)$ master curves associated with the micelle hybridization in the 1 vol% and 3 vol% solutions adopt a different shape compared to the two fitting curves for chain exchange in micelles near equilibrium. It seems that the slope of the $R(t)$ master curves decreases at around 126 ºC, which then is resumed at around 138 ºC for the 1 vol% and 147 ºC for the 3 vol%, forming a "plateau" region as identified by the shaded region in Figure 8.6. This "plateau" appeared in the $R(t)$ master curves associated with the 1 vol% and 3 vol% solutions during micelle hybridization suggests another process of with a larger relaxation time constant is operative at an intermediate temperature. According to Annianson and Wall,[19] and Halperin and Alexander,[73] the chain exchange between micelles away from equilibrated sizes involves a slower process of micelle size change, and therefore may gradually come into play during the experiments. The corresponding temperature of the "plateau" is comparable to the onset

temperature where the shift factors no longer follow the previously observed the linear dependence in the log(a_T) versus T plot (*i.e.*, the outlier data points in Figure 8.4). As a matter of fact, time-temperature superposition fails whenever two or more processes coincide with different temperature dependence. Therefore both observations evidence a change in chain exchange mechanism during the micelle hybridization process at relatively higher temperatures.

As shown in Figure 8.6, the 0.5 vol% micelles hybridized at a faster rate than the 1 vol% and 3 vol%. If the micelle fusion/fission process is involved, the chain exchange rate should increase with micelle concentration.[16,99,154] In the micelle fusion process, two micelles need to approach and merge with each other, and therefore the sparser the micelles are in the solution, the less possible it is for them to meet each other. Clearly, this is contradictory to the observation that the micelle hybridization in the most dilute 0.5 vol% solution is the fastest among the three.

On the other hand, the micelle core radius R_{core} of the post-mixed specimens lie between the R_{core} associated with the d-PS-PEP-1 and d-PS-PEP-2 solutions, at all three concentrations (see Table 8.1). The fitted micelle core radius R_{core} of the pre-mixed specimens, however, are closer to the post-mixed micelle core radius only when the solution is sufficiently dilute (0.5 vol%). When the concentration is relatively higher (1 vol% and 3 vol%), these values are closer to that of the dPS-PEP-2 micelles. Since no structure factor peaks are present in the scattering patterns associated with 3 vol% dPS-PEP-2 or 3 vol% dPS-PEP-1 solutions (Figure 8.8), all the three concentrations used in this study should be within the dilute solution region where the corona chain overlapping is insignificant. Therefore this observed differences in R_{core} for the pre-mixed specimens at different concentrations are not due to the depletion effect of corona chains, which was discussed in Chapters 6 and 7. Rather, this result suggests a different equilibration core size are associated with the relatively dilute micelle solution at 0.5 vol% compared to the 1 vol%

and 3 vol% solutions. This difference in the final state of chain exchange may contribute to the different micelle hybridization kinetics between the 0.5 vol% and the 1 vol% or 3 vol% micelle solutions. Future investigations are necessary to determine the detailed mechanisms.

8.6 Summary

In this chapter, micelle hybridization kinetics is studied using a blend of two populations of separately prepared micelles of comparable corona sizes but different core sizes (Figure 8.1), using TR-SANS and the contrast matching strategy, similar to the procedures described in the previous chapters. The rate of micelle hybridization was found to be faster than the chain exchange rate of the bigger micelles, and slower than that of the smaller micelles. The shape of the relaxation function $R(t)$ is, however, different from the $R(t)$ of monodispersed big (PS-PEP-2) or small (PS-PEP-1) micelle solutions, or any $R(t)$ master curves obtained in the previous chapters, which are associated with the chain exchange between micelles at equilibrium. A plateau at around 126 ºC was observed in the $R(t)$ master curves corresponding to the 1 vol% and 3 vol% solutions, but not in the 0.5 vol% solution. Since in the initial blend, the micelle sizes follow a bimodal distribution, the system is away from equilibrium, and to achieve the equilibrated structures, the size of the micelles is required to change too. This situation is different from the ones in our other studies where the micelle sizes remain the same throughout the chain exchange experiment. We monitored the micelle size change by performing a similar TR-SANS experiment but with deuterated big and small micelles, so that the hybridization between them do not involve contrast change and the micelle size change can been seen from the time dependent scattering intensity. The acquired SANS data were fit with the spherical form factor. It was found that the core radius R_{core} of the pre-mixed micelles at 1 vol% and 3 vol% is significantly larger than the averaged R_{core} of the big and small micelle, and is close to the

size of the big micelles. For the 0.5 vol%, however, the R_{core} of the pre-mixed micelles is in between that of the big and small micelles, and is close to the averaged mean core radius of the two. Future investigations are necessary to establish a detailed mechanism for the micelle hybridization kinetics.

Chapter 9.

Summary and Future Work

9.1 Research summary

In this thesis, the chain exchange mechanisms in block copolymer micelles are investigated in detail. A model micelle system composed of poly(styrene-*b*-(ethylene-*alt*-propylene)) (PS-PEP) or corresponding symmetric PS-PEP-PS and PEP-PS-PEP triblock copolymer micelles in squalane (selective for the PEP blocks) was selected and studied. The polymers were synthesized using sequential anionic polymerization of styrene and isoprene, followed by the selective saturation of the polyisoprene blocks with homogeneous Ni/Al catalyst. Several narrowly distributed polymers were prepared with controlled molecular weights and distributions, together with the corresponding deuterated equivalents. The molecular characteristics of the polymers were determined using SEC (size exclusion chromatography) and ^{1}H NMR (nuclear magnetic resonance) spectrums. The micelles were prepared using a co-solvent method, where the polymers were dissolved in a mixed squalane and neutral solvent dichloromethane, followed by the removal of the latter, and subsequent thermal annealing. The structure of the polymer micelles was characterized using synchrotron small angle X-ray scattering (SAXS) located in Argonne National Laboratory, as well as dynamic light scattering (DLS). The chain exchange kinetics was quantitatively investigated using time-resolved small angle neutron scattering (TR-SANS). The TR-SANS experiments were conducted in the Oak Ridge National

Laboratory (ORNL) or the National Institute of Standards and Technology (NIST). A contrast matching strategy was employed so that the chain exchange rate can be monitored by the time dependent scattering intensity.

In the thesis, each chapter from Chapter 3 to Chapter 8 provided an investigation of one aspect of the micelle chain exchange mechanisms. First, Chapter 3 and 4 conclusively demonstrated the hyposensitivity of chain exchange rate, and the single chain exchange mechanism, respectively, using dilute PS-PEP diblock copolymer micelles with carefully designed components. The discussions in the following chapters are all based on these two results.

Then, Chapter 5 extended the scope of chain exchange study to triblock copolymer micelles, to investigate the effect of polymer architecture. The chain exchange rate of PS-PEP-PS was found to be slower than the PEP-PS-PEP micelles by about nine orders of magnitude, while the two polymers were of comparable size and the micelle solution is dilute. In addition, this study suggested an accelerating effect of the corona chains, which was not observed in our previous experiments. The effect of corona blocks is studied in the following two chapters, 6 and 7.

In Chapter 6, we replaced a fraction of the solvent with homopolymers PEP of comparable size as the PEP blocks, in a 1 vol% PS-PEP diblock copolymer micelle solution. Our TR-SANS experiments showed that the chain exchange rate between the micelles is reduced with the addition of PEP when the concentration of PEP is sufficient so that the PEP chains and the PEP corona chains overlap. This overlapping of corona chains also exist in concentrated PS-PEP micelle solutions where no PEP is added. In 15 vol% PS-PEP solution, the chain exchange rate was also found to be reduced.[79] Our observation in this chapter thus confirms the role of corona chains overlapping in chain exchange.

In Chapter 7, we directly measured the impact of corona block length, using synthesized PS-PEP (28-40, numbers indicating molecular weight of each block) diblocks

with similar core block length but a considerably smaller corona block, compared to the PS-PEP 26-70 used in the previous chapters. It was found that the chain exchange in PS-PEP micelle solutions is slower when the PEP corona block is smaller. In addition, the concentration dependence of chain exchange rate is also weaker when the PEP corona block is smaller. These observations, together with those made in Chapter 6 and Chapter 5, suggest a significant impact of corona chains in micelle chain exchange. Two primary hypotheses were considered in this study, one being the stretching of corona chains inside a micelle and the subsequent relief when the molecule escapes, and the other being the corona density, which contribute to an extra barrier for the core block extraction and insertion steps. In general, our results suggest combined effect of the two, and the detailed mechanism is to be explored in future research.

In the last chapter, Chapter 8, we studied the micelle hybridization kinetics in a mixed micelle solution containing two populations of PS-PEP micelles with distinct micelle core size. Using TR-SANS, the micelle hybridization was investigated at different concentrations. While still within dilute regime, the chain exchange rate was observed to be different when the solution is relatively more dilute (0.5 vol% compared to 1 vol% and 3 vol%). In addition, the chain exchange relaxation function in micelle hybridization process was found to be different from that in our previous chain exchange studies when micelles were at equilibrium. Another set of TR-SANS experiments were designed to investigate micelle size evolution during the hybridization process. Although the reason is not yet clear, our results suggest that the equilibrium state of the 0.5 vol% solution is different from the rest two solutions, and that a slower micelle size change process in addition to the chain exchange between micelles are involved in the micelle hybridization process.

9.2 Proposed Future Work

Several possible directions for future work are suggested by this thesis research. First, the detailed role of corona blocks should be investigated and a quantitative understanding of the chain exchange rate dependence on the corona block length should be established. This can be done by synthesizing a series of PS-PEP polymers with identical core block length and various corona block length. The investigation can start with 1 vol% micelle solutions, and the effect of corona block length on chain exchange rate can be revealed by TR-SANS experiments. The micelle structural characteristics (*e.g.*, core radius, aggregation number, corona thickness) is equally important in such a study, to exclude other factors that could impact chain exchange process, which can be evaluated using DLS and SAXS. As discussed above, the concentration dependence of the chain exchange rate can be regarded as one measurement of the effect of corona blocks on chain exchange rate. Therefore, it is also necessary to measure the chain exchange rate, as well as the change in micelle size due to the depletion effect of overlapping corona blocks[145] in concentrated solutions using PS-PEP of different corona block length. In Chapter 7, it was found that the difference in chain exchange rate between 6 vol% and 1 vol% PS-PEP 28-40 is much smaller than that between 15 vol% and 1 vol% PS-PEP26-70. To make a better comparison of the two, it may be necessary to measure the chain exchange rate in a 15 vol% solution of the PS-PEP 28-40 and / or that in a 6 vol% solution of the latter PS-PEP 26-70.

Second, the results in Chapter 5 suggest that the chain exchange in dilute PEP-PS-PEP 70-24-70 is about four orders of magnitude faster than that in dilute PS-PEP 26-70. Since our results suggest a significant accelerating effect of the corona blocks, it is an interesting question that whether or not the chain exchange in the triblock copolymer micelles with the same composition and molecular weight as a diblock copolymer micelles would be different. In other words, it is not yet clear that whether only changing polymer architecture from diblock to triblock while keeping the molecular weight and core/corona chain ratio

the same is going to affect the chain exchange rate. To answer this question, it is necessary to synthesize PS-PEP 24-140 or PEP-PS-PEP 35-26-35, and measure the chain exchange rate of corresponding micelles using TR-SANS. Similarly, the PS-PEP-PS 45-140-45 used in Chapter 5 can be compared with PS-PEP 90-140, or a PS-PEP-PS 21-67-21 can be compared with PS-PEP 42-67, which was investigated by Choi *et al*.[76]

Third, our study of PEP-PS-PEP triblock copolymer micelles in Chapter 5 suggest no molecular crossover ("knots") inside the micelle cores. Since these triblocks contain a large fraction of corona chains (volume fraction of corona chains ≈ 88%) and the core blocks are at most weakly entangled ($M_{e,PS}$ ≈ 13 kDa at 413 K[112]), the situation of PEP-PS-PEP triblocks containing a significant longer and larger fraction of PS blocks could be quantitatively different. If there were molecular crossovers of PS blocks in the micelle cores, the chain extraction would have been much more difficult as one of the PEP blocks has to be pulled into the core first. For asymmetric PEP-PS-PEP containing a shorter PEP block, this effect may be reduced. The chain exchange kinetics in asymmetric triblock copolymer micelles is interesting in other ways as well. For example, the packing in asymmetric PEP-PS-PEP triblock micelles and therefore packing induced corona chain overlapping / micelle size change may be quite different due to the different (and less dense) corona profiles. Similarly, the concentration dependence could be different too. For asymmetric PS-PEP-PS, on the other hand, the chain exchange may be easier, since the shorter PS end which comes out first, can help the extraction of the other PS block, as suggested by the results in Chapter 5.

Last, the relation between the CMT (critical micelle temperature) (and thus the free chain concentration) and the chain exchange rate is not yet clear. For all the experiments varying the polymer molecular weights, composition, and architecture, it is expected that the CMT is also changed.[125] Therefore the CMT change is correlated with polymer structural parameter change. To investigate the impact of CMT separately, we can tune the

solvent quality by mixing the squalane with a neutral solvent, which dissolves both PS and PEP blocks and is also thermally stable at below 200 ºC. In that way the interaction between micelle core blocks and the solvent can also be controlled by tuning the fraction of neutral solvent. The CMT of these micelle system can be measured by DLS and SAXS.

Bibliography

(1) Bates, F. S.; Fredrickson, G. H. *Annu. Rev. Phys. Chem.* **1990**, *41*, 525–557.

(2) Halperin, A.; Tirrell, M.; Lodge, T. P. In *Macromolecules: Synthesis, Order and Advanced Properties*; Advances in Polymer Science; Springer Berlin Heidelberg, 1992; pp 31–71.

(3) Gohy, J.-F. In *Block Copolymers II*; Abetz, V., Ed.; Advances in Polymer Science; Springer Berlin Heidelberg, 2005; pp 65–136.

(4) Huggins, M. L. *J. Am. Chem. Soc.* **1942**, *64*, 1712–1719.

(5) Flory, P. J. *J. Chem. Phys.* **1942**, *10*, 51–61.

(6) Kataoka, K.; Harada, A.; Nagasaki, Y. *Adv. Drug Deliv. Rev.* **2001**, *47*, 113–131.

(7) Gaucher, G.; Dufresne, M.-H.; Sant, V. P.; Kang, N.; Maysinger, D.; Leroux, J.-C. *J. Controlled Release* **2005**, *109*, 169–188.

(8) Anderson, W. Block copolymers as viscosity index improvers for lubricating oils. US3763044 A, October 2, 1973.

(9) Schouten, M.; Dorrepaal, J.; Stassen, W. J. M.; Vlak, W. A. H. M.; Mortensen, K. *Polymer* **1989**, *30*, 2038–2046.

(10) Ruzette, A.-V.; Leibler, L. *Nat. Mater.* **2005**, *4*, 19–31.

(11) Li, T.; Heinzer, M. J.; Redline, E. M.; Zuo, F.; Bates, F. S.; Francis, L. F. *Prog. Org. Coat.* **2014**, *77*, 1145–1154.

(12) Baines, F. L.; Dionisio, S.; Billingham, N. C.; Armes, S. P. *Macromolecules* **1996**, *29*, 3096–3102.

(13) Hirzinger, B.; Helmstedt, M.; Stejskal, J. *Polymer* **2000**, *41*, 2883–2891.

(14) Willner, L.; Poppe, A.; Allgaier, J.; Monkenbusch, M.; Richter, D. *Europhys. Lett.* **2001**, *55*, 667–673.

(15) Won, Y.-Y.; Davis, H. T.; Bates, F. S. *Macromolecules* **2003**, *36*, 953–955.

(16) Meli, L.; Santiago, J. M.; Lodge, T. P. *Macromolecules* **2010**, *43*, 2018–2027.

(17) Jain, S.; Bates, F. S. *Macromolecules* **2004**, *37*, 1511–1523.

(18) Hayward, R. C.; Pochan, D. J. *Macromolecules* **2010**, *43*, 3577–3584.

(19) Aniansson, E. A. G.; Wall, S. N.; Almgren, M.; Hoffmann, H.; Kielmann, I.; Ulbricht, W.; Zana, R.; Lang, J.; Tondre, C. *J. Phys. Chem.* **1976**, *80*, 905–922.

(20) Wennerström, H.; Lindman, B. *Phys. Rep.* **1979**, *52*, 1–86.

(21) Hamley, I. W. *Block Copolymers in Solution: Fundamentals and Applications*; John Wiley & Sons, 2005.

(22) Hamley, I. W. *The Physics of Block Copolymers*; Oxford Science Publications; Oxford University Press: Oxford, 1998.

(23) Riess, G. *Prog. Polym. Sci.* **2003**, *28*, 1107–1170.

(24) Zhulina, E. B.; Adam, M.; LaRue, I.; Sheiko, S. S.; Rubinstein, M. *Macromolecules* **2005**, *38* (12), 5330–5351.

(25) Halperin, A. *Macromolecules* **1987**, *20*, 2943–2946.

(26) Gennes, P.-G. de. *Scaling Concepts in Polymer Physics*; Cornell University Press, 1979.

(27) Noolandi, J.; Hong, K. M. *Macromolecules* **1983**, *16*, 1443–1448.

(28) Leibler, L.; Orland, H.; Wheeler, J. C. *J. Chem. Phys.* **1983**, *79*, 3550–3557.

(29) Nagarajan, R.; Ganesh, K. *Macromolecules* **1989**, *22*, 4312–4325.

(30) Hurter, P. N.; Scheutjens, J. M. H. M.; Hatton, T. A. *Macromolecules* **1993**, *26*, 5592–5601.

(31) Webber, S. E.; Munk, P.; Tuzar, Z. *Solvents and Self-Organization of Polymers*; Springer Science & Business Media, 2012.

(32) Tuzar, Z.; Kratochvíl, P. *Adv. Colloid Interface Sci.* **1976**, *6*, 201–232.

(33) Lee, H.-N.; Lodge, T. P. *J. Phys. Chem. Lett.* **2010**, *1*, 1962–1966.

(34) Lee, H.-N.; Lodge, T. P. *J. Phys. Chem. B* **2011**, *115*, 1971–1977.

(35) Lee, H.-N.; Newell, N.; Bai, Z.; Lodge, T. P. *Macromolecules* **2012**, *45*, 3627–3633.

(36) Alexandridis, P.; Lindman, B. *Amphiphilic Block Copolymers: Self-Assembly and Applications*; Elsevier, 2000.

(37) Chen, S.; Guo, C.; Liu, H.-Z.; Wang, J.; Liang, X.-F.; Zheng, L.; Ms, J.-H. *Mol. Simul.* **2006**, *32*, 409–418.

(38) Su, Y.; Wang, J.; Liu, H. *Langmuir* **2002**, *18*, 5370–5374.

(39) Booth, C.; Attwood, D. *Macromol. Rapid Commun.* **2000**, *21*, 501–527.

(40) Pispas, S.; Hadjichristidis, N.; Potemkin, I.; Khokhlov, A. *Macromolecules* **2000**, *33*, 1741–1746.

(41) Moffitt, M.; Khougaz, K.; Eisenberg, A. *Acc. Chem. Res.* **1996**, *29*, 95–102.

(42) Cohen Stuart, M. A.; Hofs, B.; Voets, I. K.; de Keizer, A. *Curr. Opin. Colloid Interface Sci.* **2005**, *10*, 30–36.

(43) Harada, A.; Kataoka, K. *Macromolecules* **1995**, *28*, 5294–5299.

(44) Kabanov, A. V.; Batrakova, E. V.; Alakhov, V. Y. *J. Controlled Release* **2002**, *82*, 189–212.

(45) Kakizawa, Y.; Kataoka, K. *Adv. Drug Deliv. Rev.* **2002**, *54*, 203–222.

(46) Zhu, Z.; Sukhishvili, S. A. *ACS Nano* **2009**, *3*, 3595–3605.

(47) He, C.; Kim, S. W.; Lee, D. S. *J. Controlled Release* **2008**, *127*, 189–207.

(48) Lee, H.-N.; Bai, Z.; Newell, N.; Lodge, T. P. *Macromolecules* **2010**, *43*, 9522–9528.

(49) Lin, H.-H.; Cheng, Y.-L. *Macromolecules* **2001**, *34*, 3710–3715.

(50) Hiemenz, P. C.; Rajagopalan, R. *Principles of Colloid and Surface Chemistry, Third Edition, Revised and Expanded*; CRC Press, 1997.

(51) He, Y.; Li, Z.; Simone, P.; Lodge, T. P. *J. Am. Chem. Soc.* **2006**, *128*, 2745–2750.

(52) Bang, J.; Jain, S.; Li, Z.; Lodge, T. P.; Pedersen, J. S.; Kesselman, E.; Talmon, Y. *Macromolecules* **2006**, *39*, 1199–1208.

(53) Khandpur, A. K.; Macosko, C. W.; Bates, F. S. *J. Polym. Sci. Part B Polym. Phys.* **1995**, *33*, 247–252.

(54) Higgins, J. S.; Benoît, H. *Polymers and Neutron Scattering*; Clarendon Press Oxford, 1994.

(55) Roe, R.-J.; Roe, R.-J. *Methods of X-Ray and Neutron Scattering in Polymer Science*; OXFORD UNIV PR, 1999.

(56) Pedersen, J. S. *Adv. Colloid Interface Sci.* **1997**, *70*, 171–210.

(57) Debye, P. *J. Phys. Colloid Chem.* **1947**, *51*, 18–32.

(58) Zimm, B. H. *J. Chem. Phys.* **1948**, *16*, 1093–1099.

(59) Berry, G. C. *J. Chem. Phys.* **1966**, *44*, 4550–4564.

(60) Brown, W. *Dynamic Light Scattering: the Method and Some Applications*; Oxford University Press, USA, 1993; Vol. 49.

(61) Chu, B.; Wang, Z.; Yu, J. *Macromolecules* **1991**, *24*, 6832–6838.

(62) Schmitz, K. S. *An Introduction to Dynamic Light Scattering of Macromolecules*; Academic Press Inc., 1990.

(63) Pecora, R. *Dynamic Light Scattering: Applications of Photon Correlation Spectroscopy*; Springer Science & Business Media, 2013.

(64) Schärtl, W. *Light Scattering from Polymer Solutions and Nanoparticle Dispersions*; Springer Science & Business Media, 2007.

(65) Berne, B. J.; Pecora, R. *Dynamic Light Scattering: With Applications to Chemistry, Biology, and Physics*; Courier Corporation, 2000.

(66) Feigin, L. A.; Svergun, D. I. *Structure Analysis by Small-Angle X-Ray and Neutron Scattering*; Taylor, G. W., Ed.; Springer US: Boston, MA, 1987.

(67) Wennerström, H.; Evans, D. F. *The Colloidal Domain: where Physics, Chemistry, Biology, and Technology Meet*; Wiley-VCH: New York, 1999.

(68) Larsson, K. *Lipids: Molecular Organization, Physical Functions and Technical Applications*; Oily Press Dundee, UK, 1994.

(69) Bates, F. S.; Hillmyer, M. A.; Lodge, T. P.; Bates, C. M.; Delaney, K. T.; Fredrickson, G. H. *Science* **2012**, *336*, 434–440.

(70) Aniansson, E. A. G.; Wall, S. N. *J. Phys. Chem.* **1975**, *79*, 857–858.

(71) Lessner, E.; Teubner, M.; Kahlweit, M. *J. Phys. Chem.* **1981**, *85*, 3167–3175.

(72) Lessner, E.; Teubner, M.; Kahlweit, M. *J. Phys. Chem.* **1981**, *85*, 1529–1536.

(73) Halperin, A.; Alexander, S. *Macromolecules* **1989**, *22*, 2403–2412.

(74) Dormidontova, E. E. *Macromolecules* **1999**, *32*, 7630–7644.

(75) Lund, R.; Willner, L.; Richter, D.; Dormidontova, E. E. *Macromolecules* **2006**, *39*, 4566–4575.

(76) Choi, S.-H.; Lodge, T. P.; Bates, F. S. *Phys. Rev. Lett.* **2010**, *104*, 047802.

(77) Zinn, T.; Willner, L.; Lund, R.; Pipich, V.; Richter, D. *Soft Matter* **2012**, *8*, 623.

(78) Lund, R.; Willner, L.; Stellbrink, J.; Lindner, P.; Richter, D. *Phys. Rev. Lett.* **2006**, *96*, 068302.

(79) Choi, S.-H.; Bates, F. S.; Lodge, T. P. *Macromolecules* **2011**, *44*, 3594–3604.

(80) Lu, J.; Choi, S.; Bates, F. S.; Lodge, T. P. *ACS Macro Lett.* **2012**, *1*, 982–985.

(81) Lu, J.; Bates, F. S.; Lodge, T. P. *ACS Macro Lett.* **2013**, *2*, 451–455.

(82) Lu, J.; Bates, F. S.; Lodge, T. P. *Macromolecules* **2015**, *48*, 2667–2676.

(83) Lund, R.; Willner, L.; Richter, D. In *Controlled Polymerization and Polymeric Structures*; Abe, A., Lee, K.-S., Leibler, L., Kobayashi, S., Eds.; Advances in Polymer Science; Springer International Publishing, 2013; pp 51–158.

(84) Rharbi, Y. *Macromolecules* **2012**, *45*, 9823–9826.

(85) Špaček, P.; Kubín, M. *J. Appl. Polym. Sci.* **1985**, *30*, 143–150.

(86) Price, C.; Hudd, A. L.; Booth, C.; Wright, B. *Polymer* **1982**, *23*, 650–653.

(87) Špaček, P. *J. Appl. Polym. Sci.* **1986**, *32*, 4281–4283.

(88) Wang, Y.; Kausch, C. M.; Chun, M.; Quirk, R. P.; Mattice, W. L. *Macromolecules* **1995**, *28*, 904–911.

(89) Wang, Y.; Balaji, R.; Quirk, R. P.; Mattice, W. L. *Polym. Bull.* **1992**, *28*, 333–338.

(90) Underhill, R. S.; Ding, J.; Birss, V. I.; Liu, G. *Macromolecules* **1997**, *30*, 8298–8303.

(91) Prochazka, K.; Kiserow, D.; Ramireddy, C.; Tuzar, Z.; Munk, P.; Webber, S. E. *Macromolecules* **1992**, *25*, 454–460.

(92) van Stam, J.; Creutz, S.; De Schryver, F. C.; Jérôme, R. *Macromolecules* **2000**, *33*, 6388–6395.

(93) Prochazka, K.; Bednar, B.; Mukhtar, E.; Svoboda, P.; Trnena, J.; Almgren, M. *J. Phys. Chem.* **1991**, *95*, 4563–4568.

(94) Gehlen, M. H.; De Schryver, F. C. *Chem. Rev.* **1993**, *93*, 199–221.

(95) Tian, M.; Qin, A.; Ramireddy, C.; Webber, S. E.; Munk, P.; Tuzar, Z.; Prochazka, K. *Langmuir* **1993**, *9*, 1741–1748.

(96) Pacovská, M.; Procházka, K.; Tuzar, Z.; Munk, P. *Polymer* **1993**, *34*, 4585–4588.

(97) Lund, R.; Willner, L.; Stellbrink, J.; Radulescu, A.; Richter, D. *Phys. B Condens. Matter* **2004**, *350*, E909–E912.

(98) Lund, R.; Willner, L.; Richter, D.; Iatrou, H.; Hadjichristidis, N.; Lindner, P. *J. Appl. Crystallogr.* **2007**, *40*, s327–s331.

(99) Kelley, E. G.; Murphy, R. P.; Seppala, J. E.; Smart, T. P.; Hann, S. D.; Sullivan, M. O.; Epps, T. H. *Nat. Commun.* **2014**, *5*.

(100) Murphy, R. P.; Kelley, E. G.; Rogers, S. A.; Sullivan, M. O.; Epps, T. H. *ACS Macro Lett.* **2014**, *3*, 1106–1111.

(101) Hlavatá, D.; Stejskal, J.; Pleštil, J.; Koňák, Č.; Kratochvíl, P.; Helmstedt, M.; Mio, H.; Laggner, P. *Polymer* **1996**, *37*, 799–805.

(102) Stejskal, J.; Hlavatá, D.; Sikora, A.; Konňák, Č.; Pleštil, J.; Kratochvíl, P. *Polymer* **1992**, *33*, 3675–3685.

(103) Smith, C. K.; Liu, G. *Macromolecules* **1996**, *29*, 2060–2067.

(104) Haliloğlu, T.; Bahar, I.; Erman, B.; Mattice, W. L. *Macromolecules* **1996**, *29*, 4764–4771.

(105) Lund, R.; Willner, L.; Lindner, P.; Richter, D. *Macromolecules* **2009**, *42*, 2686–2695.

(106) Ferry, J. D. *Viscoelastic Properties of Polymers*; John Wiley & Sons, 1980.

(107) Williams, M. L.; Landel, R. F.; Ferry, J. D. *J. Am. Chem. Soc.* **1955**, *77*, 3701–3707.

(108) Yokoyama, H.; Kramer, E. J. *Macromolecules* **1998**, *31*, 7871–7876.

(109) Cavicchi, K. A.; Lodge, T. P. *Macromolecules* **2003**, *36*, 7158–7164.

(110) Barrat, J. L.; Fredrickson, G. H. *Macromolecules* **1991**, *24*, 6378–6383.

(111) Chapman, B. R.; Hamersky, M. W.; Milhaupt, J. M.; Kostelecky, C.; Lodge, T. P.; von Meerwall, E. D.; Smith, S. D. *Macromolecules* **1998**, *31*, 4562–4573.

(112) Fetters, L. J.; Lohse, D. J.; Richter, D.; Witten, T. A.; Zirkel, A. *Macromolecules* **1994**, *27*, 4639–4647.

(113) Halperin, A. *Macromolecules* **2011**, *44*, 5072–5074.

(114) Lund, R.; Willner, L.; Pipich, V.; Grillo, I.; Lindner, P.; Colmenero, J.; Richter, D. *Macromolecules* **2011**, *44*, 6145–6154.

(115) Lai, C.; Russel, W. B.; Register, R. A. *Macromolecules* **2002**, *35*, 841–849.

(116) Hsieh, H.; Quirk, R. P. *Anionic Polymerization: Principles and Practical Applications*; CRC Press, 1996.

(117) Morton, M. *Anionic Polymerization: Principles and Practice*; Elsevier, 2012.

(118) Hiemenz, P. C.; Lodge, T. P. *Polymer Chemistry, Second Edition*; CRC Press, 2007.

(119) Hadjichristidis, N.; Pitsikalis, M.; Pispas, S.; Iatrou, H. *Chem. Rev.* **2001**, *101*, 3747–3792.

(120) Szwarc, M. *Nature* **1956**, *178*, 1168–1169.

(121) Gehlsen, M. D. *Catalytic Hydrogenation of Polymers : Synthesis and Characterization of Model Polyolefins*; Ph.D. dissertation, University of Minnesota: United States -- Minnesota, 1993.

(122) Habersberger, B. M.; Lodge, T. P.; Bates, F. S. *Macromolecules* **2012**, *45*, 7778–7782.

(123) Matsubara, S.; Yokota, Y.; Oshima, K. *Chem. Lett.* **2004**, *33*, 294–295.

(124) Hahn, S. F. *J. Polym. Sci. Part Polym. Chem.* **1992**, *30*, 397–408.

(125) Choi, S.-H.; Bates, F. S.; Lodge, T. P. *J. Phys. Chem. B* **2009**, *113*, 13840–13848.

(126) Eckert, R. J. A. Hydrogenated star-shaped polymer. US4156673 A, May 29, 1979.

(127) Lapporte, S. J. *Ann. N. Y. Acad. Sci.* **1969**, *158*, 510–525.

(128) VonNiederhausern, D. M.; Wilson, G. M.; Giles, N. F. *J. Chem. Eng. Data* **2000**, *45*, 157–160.

(129) Jakeš, J. *Czechoslov. J. Phys. B* **1988**, *38*, 1305–1316.

(130) Bang, J.; Viswanathan, K.; Lodge, T. P.; Park, M. J.; Char, K. *J. Chem. Phys.* **2004**, *121*, 11489–11500.

(131) Castelletto, V.; Hamley, I. W.; Pedersen, J. S. *J. Chem. Phys.* **2002**, *117*, 8124–8129.

(132) Pedersen, J. S.; Svaneborg, C.; Almdal, K.; Hamley, I. W.; Young, R. N. *Macromolecules* **2003**, *36*, 416–433.

(133) Choi, S.-H. Block copolymer self-assembly in solution: Structure and dynamics. Ph.D. dissertation, University of Minnesota: United States -- Minnesota, 2010.

(134) Kline, S. R. *J. Appl. Crystallogr.* **2006**, *39*, 895–900.

(135) Sakurai, S.; Hashimoto, T.; Fetters, L. J. *Macromolecules* **1995**, *28*, 7947–7949.

(136) Lund, R.; Willner, L.; Stellbrink, J.; Lindner, P.; Richter, D. *Phys. Rev. Lett.* **2006**, *96*, 068302.

(137) Balsara, N. P.; Tirrell, M.; Lodge, T. P. *Macromolecules* **1991**, *24*, 1975–1986.

(138) Ilavsky, J.; Jemian, P. R. *J. Appl. Crystallogr.* **2009**, *42*, 347–353.

(139) Renou, F.; Nicolai, T.; Benyahia, L.; Nicol, E. *J. Phys. Chem. B* **2009**, *113*, 3000–3007.

(140) Chassenieux, C.; Nicolai, T.; Benyahia, L. *Curr. Opin. Colloid Interface Sci.* **2011**, *16*, 18–26.

(141) Nguyen-Misra, M.; Mattice, W. L. *Macromolecules* **1995**, *28*, 1444–1457.

(142) Dalvi, M. C.; Eastman, C. E.; Lodge, T. P. *Phys. Rev. Lett.* **1993**, *71*, 2591–2594.

(143) Yokoyama, H.; Kramer, E. J. *Macromolecules* **2000**, *33*, 954–959.

(144) Yokoyama, H.; Kramer, E. J.; Fredrickson, G. H. *Macromolecules* **2000**, *33*, 2249–2257.

(145) Abbas, S.; Lodge, T. P. *Phys. Rev. Lett.* **2007**, *99*, 137802.

(146) Milner, S. T.; Lacasse, M.-D.; Graessley, W. W. *Macromolecules* **2009**, *42*, 876–886.

(147) Mays, J. W.; Fetters, L. J. *Macromolecules* **1989**, *22*, 921–926.

(148) Poole, C. F.; Pomaville, R. M.; Dean, T. A. *Anal. Chim. Acta* **1989**, *225*, 193–203.

(149) Rouse Jr, P. E. *J. Chem. Phys.* **1953**, *21*, 1272–1280.

(150) Malmsten, M.; Lindman, B. *Macromolecules* **1993**, *26*, 1282–1286.

(151) Yamazaki, R.; Numasawa, N.; Nose, T. *Polymer* **2004**, *45*, 6227–6234.

(152) Yamazaki, R.; Nose, T. *Polymer* **2003**, *44*, 6505–6511.

(153) Renou, F.; Benyahia, L.; Nicolai, T. *Macromolecules* **2007**, *40*, 4626–4634.

(154) Li, Z.; Dormidontova, E. E. *Macromolecules* **2010**, *43*, 3521–3531.

Appendices

A.1 Shift Factors

In this thesis, the time-temperature superposition principle[107] was employed in order to construct a master curve of the relaxation function $R(t)$ from individual $R(t)$ traces measured at different temperatures. The shift factors used in our studies from Chapter 3 to Chapter 8, in general, follow a linear dependence on temperature on a log-linear scale, except for a few outliers which are associated with micelle size change(Chapter 8). Figure 10.1 summarizes all the shift factors used in this thesis at the reference temperature T_{ref} = 110 ºC, including a comparison with the shift factors reported by Choi *et al.*, for PS-PEP 26-70 and PS-PEP 42-67 (poly(styrene-*b*-(ethylene-*alt*-propylene)), numbers indicating molecular weight for each block) diblock copolymer micelles at 1 vol%[76] and 15 vol%.[79] The temperature dependence of the shift factors using the WLF (Williams-Landel-Ferry) model, which is widely applicable to the rheology measurements of polymer systems, is expressed as:[107]

$$\log(a_T) = -\frac{C_1\left(T - T_{ref}\right)}{C_2 + \left(T - T_{ref}\right)}. \qquad (A.1)$$

C_1 and C_2 can be estimated from the documented values measured at the glass transition temperature of bulk polystyrene ($C_{1,g}$ = 13.7, $C_{2,g}$ = 50 ºC, for $T_{g,PS}$ = 100 ºC).[106] Using these values for C_1 and C_2, and the glass transition temperature of PS in squalane ($T_{g,PS\ in\ squalane} \approx 70$ ºC[115]), log(a_T) at a reference temperature of 70 ºC can be calculated. The log(a_T)

at T_{ref} = 110 ºC can simply be estimated by vertically shift in the plot so that $\log(a_T) = 0$ at T = 110 ºC. The plot of $\log(a_T)$ at T_{ref} = 110 ºC is therefore generated, and is shown in Figure 10.1 by the black line. The data follows a quite different trend compared to the WLF curve. As suggested by Chapter 5, 6, and 7, the PEP corona chains are facilitating the chain exchange process, which makes the chain exchange not a single relaxation process of the PS core blocks. On the other hand, it is also possible that as the temperature increases, the solvent starts to penetrate into micelle cores, which makes the glass transition temperature of PS a function of temperature.

Alternatively, the shift factors data can be fitted to the Arrhenius law for small molecules:

$$\log(a_T) = \frac{E_a}{2.303R}\left(\frac{1}{T} - \frac{1}{T_{ref}}\right), \qquad (A.2)$$

where R is the universal gas constant (R = 8.314 $J \cdot K^{-1} \cdot mol^{-1}$), and both T and T_{ref} are in Kelvin. The fitting curve is shown in Figure 10.2 by the red line. The fitted activation energy E_a is 268 kJ/mol, which is on the same order to the bonding energy between C–C bonds (348 kJ/mol) and that between C-H bonds (413 kJ/mol), suggesting that the process is unlikely a single relaxation event that follows the Arrhenius law.

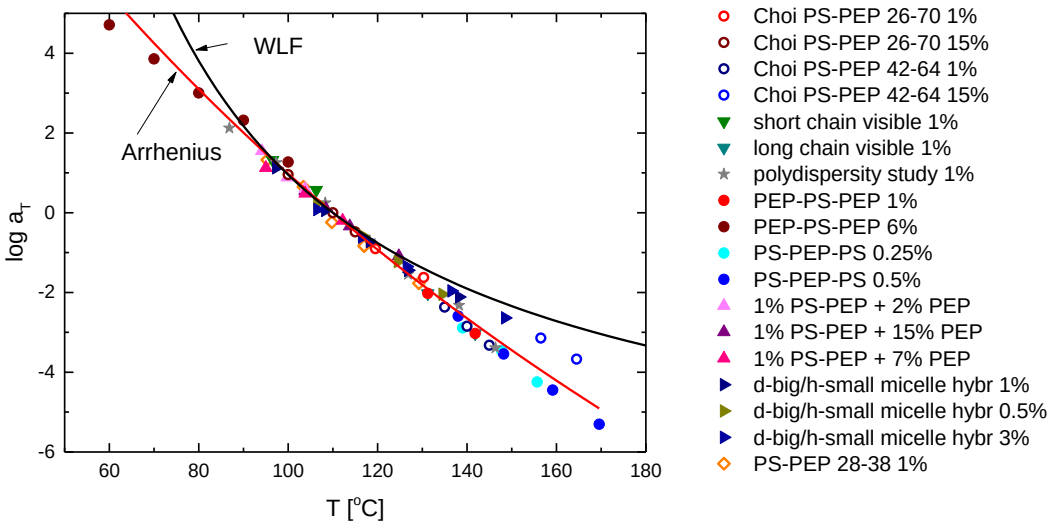

Figure A.1. Summary of shift factors used in this thesis, at a reference temperature 110 ºC. The data points and corresponding micelle systems are as noted in the legend. The open circles of four different colors are reproduced from Choi et al., for 1 vol% PS-PEP (26-70) and PS-PEP (42-67) micelle solutions,[76] and 15 vol% PS-PEP (26-70), and PS-PEP (42-67) ordered micelle solutions.[79] The stars represent the shift factors used in Chapter 3, reproduced from Figure 3.4b. The up-side-down triangles represent the shift factors used in Chapter 4, reproduced from Figure 4.4b. The solid circles represent the shift factors used in Chapter 5, reproduced from Figure 5.6. The upwarding triangles represent the shift factors used in Chapter 6, reproduced from Figure 6.4b. The open diamonds represent the shift factors used in Chapter 7, reproduced from Figure 7.6c. The triangles pointing to the right represent the shift factors used in the micelle hybridization study discussed in Chapter 8, reproduced from Figure 8.4a. The black line is generated from the WLF equation, and the red line is fitting curve from the Arrhenius law, as discussed above.

A.2 Estimation of Uncertainties in *R*(*t*)

The relaxation function *R*(*t*) is used in every chapter of this thesis, as a quantitative evaluation of the chain exchange rate as a function of time at a certain reference temperature. *R*(*t*) is defined in Equation (1.2) as:[78]

$$R(t) = \left(\frac{I(t) - I(\infty)}{I(0) - I(\infty)} \right)^{1/2}$$

In the previous chapters, $R(t)$ is calculated using integrated intensity over a proper range of q from corresponding post-mixed, pre-mixed, and time resolved measurements. We can regard the value of $R(t)$ at each time point t_i, R_i, as a function of $I(t_i)$, $I(0)$, and $I(\infty)$. According to the error propagation principle for a function containing several independent variables, the uncertainty of R_i can be estimated as:

$$S_{R_i} = \sqrt{\left(\frac{\partial R(t)}{\partial I(t)}\Big|_{t=t_i}\right)^2 S^2_{I(t_i)} + \left(\frac{\partial R(t)}{\partial I(0)}\Big|_{t=t_i}\right)^2 S^2_{I(o)} + \left(\frac{\partial R(t)}{\partial I(\infty)}\Big|_{t=t_i}\right)^2 S^2_{I(\infty)}}, \qquad (\mathrm{A}.3)$$

where

$$\frac{\partial R(t)}{\partial I(t)}\Big|_{t=t_i} = \frac{1}{2} \times \big(I(0) - I(\infty)\big)^{-1/2} \times \big(I(t_i) - I(\infty)\big)^{-1/2}, \qquad (A.4)$$

$$\frac{\partial R(t)}{\partial I(0)}\Big|_{t=t_i} = \big(I(t_i) - I(\infty)\big)^{1/2} \times \left(-\frac{1}{2}\right) \times \big(I(0) - I(\infty)\big)^{-3/2}, \qquad (A.5)$$

and

$$\frac{\partial R(t)}{\partial I(\infty)}\Big|_{t=t_i} = \frac{1}{2} \times \big(I(t_i) - I(\infty)\big)^{1/2} \times \big(I(0) - I(\infty)\big)^{-3/2} - \frac{1}{2} \times \big(I(t_i) - I(\infty)\big)^{-1/2} \times \big(I(0) - I(\infty)\big)^{-1/2}. \qquad (A.6)$$

Using the same error propagation principal, the square of the uncertainties of the integrated scattering intensities, $S^2_{I(t_i)}$, $S^2_{I(0)}$, and $S^2_{I(\infty)}$ were calculated as the sum of the square of the

scattering intensity uncertainty at a certain q_k, while q_k is between the integration lower limit q_{min} and higher limit q_{max}.

10.3 Scattering Intensity Calibration due to Thermal Expansion

As suggested by the expression of $R(t)$, when the time resolved scattering intensity $I(t)$ is close to $I(0)$ or $I(\infty)$, the value of $R(t)$ is sensitive to either $I(0)$ or $I(\infty)$, respectively. Due to the thermal expansion of solutions with increasing temperature, the incoherent scattering intensity decreases, making the overall observed scattering intensity decrease with temperature. Therefore, to obtain a better estimation of $R(t)$, it is necessary to use the $I(0)$ and $I(\infty)$ measured at the same temperature as the corresponding $I(t)$, especially when $I(t)$ is close to $I(0)$ or $I(\infty)$. Experimentally, the post-mixed samples before chain exchange were measured at room temperature or around 60 ºC, when the chain exchange kinetics of the system is known and 60 ºC was determined to be a safe temperature that won't induce chain exchange. It is not possible to directly measure $I(0)$ at a temperature where molecules start to exchange. The $I(\infty)$, on the other hand, was measured from the pre-mixed specimen, where the chain exchange is complete. Therefore we measured $I(\infty)$ at different temperatures, up to the highest temperature used in time-resolved experiments. A thermal expansion coefficient of scattering intensity can then be calculated. Since the pre-mixed and post-mixed specimens contain the same fraction of deuterated and normal polymers, the same thermal expansion coefficient should apply to $I(0)$. Using this method, we can estimate $I(0)$ at each temperature used in time-resolved chain exchange measurements, and use these calibrated values to obtain a better estimation of the relaxation function $R(t)$.

Figure A.2 compares the $R(t)$ calculated using $I(0)$ and $I(\infty)$ at room temperature, with that calculated using calibrated $I(0)$ or $I(\infty)$ at the corresponding temperatures of each $R(t)$ trace. The data were acquired from the chain exchange TR-SANS experiments discussed in Chapter 7, using the 1 vol% PS-PEP 28-40 micelle solutions in squalane. The two $R(t)$

traces shown in Figure 10.2c and 10.2d associated with 90 ºC and 100 ºC were reproduced from Figure 7.5a and Figure 7.5b. The other two traces corresponding to the higher temperatures were not shown in Chapter 7, due to the large uncertainties, and possible mis-position of the cells, which could have contributed to the slower temperature equilibration process, and subsequently the upturn in $R(t)$ traces at the beginning of experiment. The same shift factors were used in constructing the master curve shown in Figure A.2b and A.2d, as well as in Figure 7.6a for the first two traces.

Comparing Figure 10.2a with 10.2c, and 10.2b with 10.2d, it is clear that the thermal expansion calibration leads to more obvious changes in $R(t)$ when it is close to 1 and 0. The shape of the $R(t)$ master curves after thermal expansion correction is closer to that of the model simulation / fitting lines. This correction for thermal expansion is thus necessary to obtain a better estimation of $R(t)$ from experimentally measured scattering intensities, especially when $I(t)$ is closer to $I(0)$ and $I(\infty)$, and when the experimental temperature is significantly higher than room temperature.

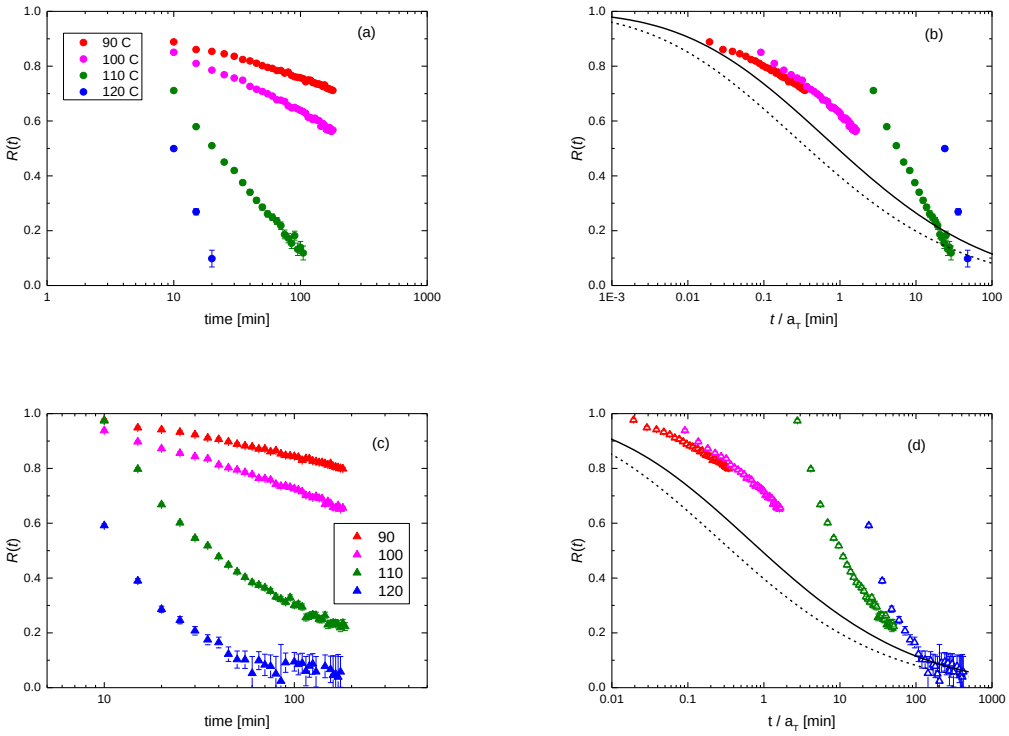

Figure A.2. The $R(t)$ traces (a) and corresponding master curve (b) calculated using the $I(0)$ and $I(\infty)$ measured at room temperature are compared with the $R(t)$ traces (c) and corresponding master curves (d) calculated using the $I(0)$ and $I(\infty)$ calibrated or measured at each temperature associated with the traces. The solid line and dashed line are model simulation or model fitting curves, reproduced from Figure 7.6a.

A.4 Fitting Parameter Sensitivity in the Hard Sphere Model

The hard sphere model is used in this thesis to extract micelle structural characteristics from SANS or SAXS measurements. The model is described in Chapter 2 in detail, from Equation 2.7 to Equation 2.12. Since the model contains nine variables, simply varying all the nine variables and trying to get a best fit for the data will only produce infinite numbers of fitting parameter combinations, when all of them can be reasonable numbers. In order to obtain a more "controlled" fitting, it is necessary to test the sensitivity of fitting parameters in the model, and allow the least possible parameters to vary when obtaining a

fit. The data were fitted in Igor Pro, using modified fitting functions provided by the NIST data reduction package.[134] Figure A.3 shows an example of determining fitting parameter sensitivities for one set of SANS data obtained with 1 vol% d-PS-PEP 26-67 micelle solutions in squalane. A best fit (solid red line in Figure 10.3) was first obtained with the data (blue markers in Figure A.3), and then each of the nine fitting parameters was reduced by 10% individually while keeping other parameters the same. The resulting curves are shown in Figure 10.3 with the dashed red lines. From Figure A.3a to A.3i, the parameters under test are: the volume fraction of hard spheres η_{hs}, the aggregation number N_{agg}, the micelle core radius R_c, the interfacial thickness between core and corona region σ_{int}, the radius of gyration of corona chains R_g, the hard sphere radius R_{hs}, the two parameters describing corona profile a_1 and s, and the core radius standard deviation σ_R.

As shown in Figure A.3, the more the dashed red line deviates from the solid red line, the more sensitive the fitting is to the parameters. In some circumenstances, the insensitive parameters can be fixed to a reasonable value when performing the first fitting tials. In addition, such a test of individually varing the fitting parameters suggests the range of q where one parameter is contributing most. For example, as shown in Figure A.3c and A.3h, reducing the core radius R_c changes mostly the intensity at $q > 0.01$ Å^{-1} (which is associated with the form factor of scattering intensity), while reducing the corona profile parameter s changes mostly the intensity at $q < 0.01$ Å^{-1}. This allows for the individual fitting of some parameters such like R_c, by limiting the q range of input data. A final fitting result will be obtained using initial values very close to the best fit values, which can be estimated by performing several fitting trials, and when all nine parameters are allowed to vary.

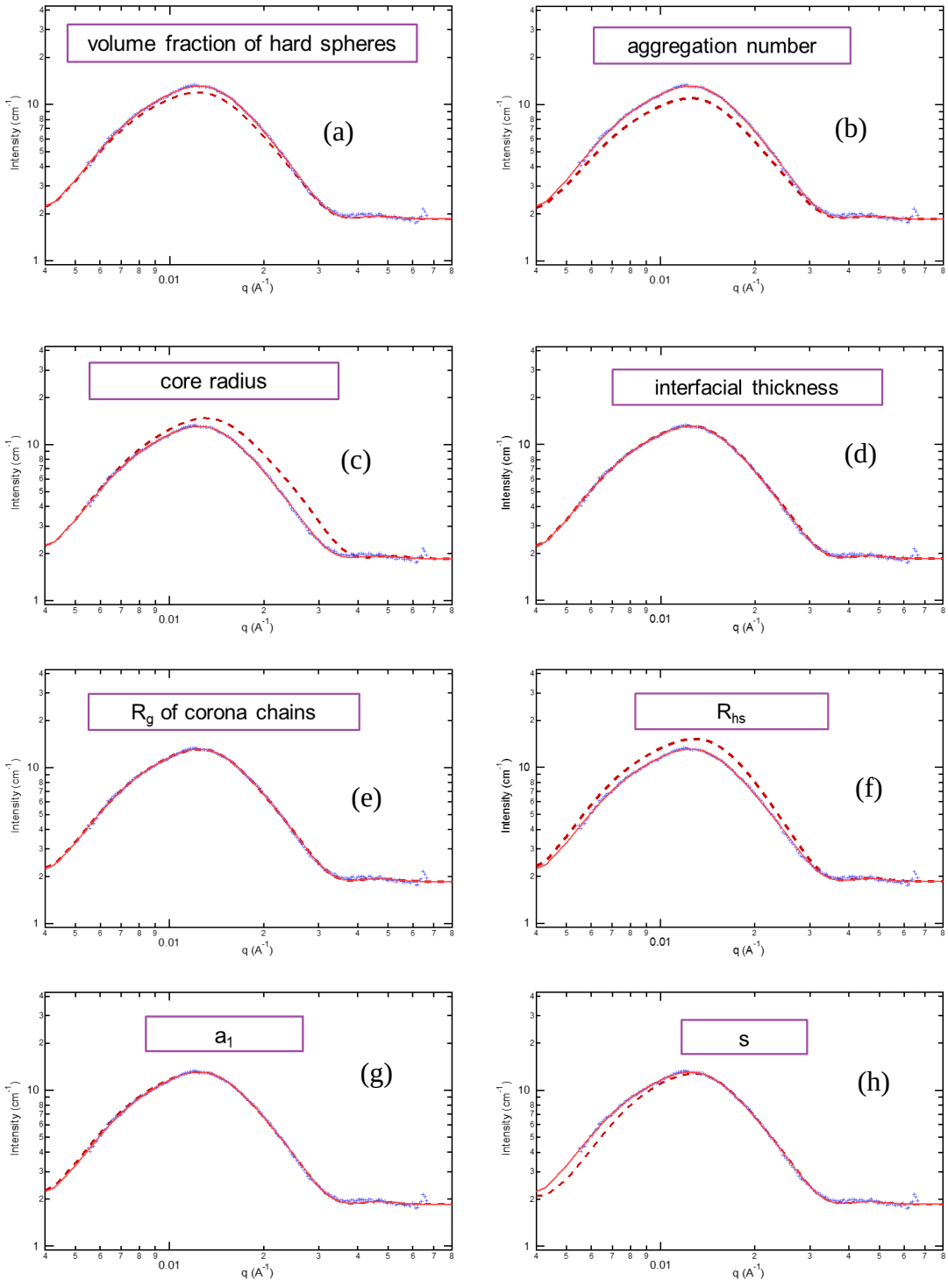
volume fraction of hard spheres
(a)
aggregation number
(b)
core radius
(c)
interfacial thickness
(d)
R_g of corona chains
(e)
R_{hs}
(f)
a_1
(g)
s
(h)
Intensity (cm^{-1})
q (A^{-1})
0.01

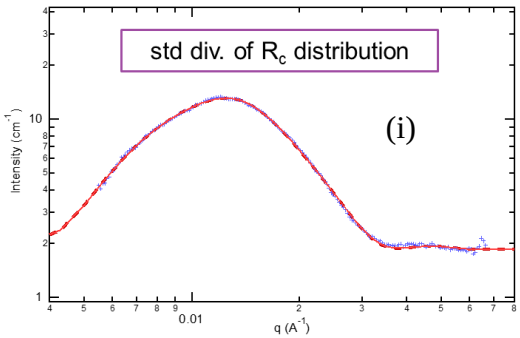

Figure A.3. Example $I(q)$ plots of a fitting parameter sensitivity test using the hard sphere model, and SANS data obtained from 1 vol% d-PS-PEP 42-67. In each panel, one of the nine parameters were reduced by 10%. The resulting model generated curve is shown by the red dashed line, while the data and the best fit to the data are represented by the blue markers and the red solid line. Corresponding fitting parameter under sensitivity test is noted in each plot.

A.5 Distribution of Isotope Labeled Chains in the Premixed Micelle Solutions

An interesting phenomenon seen in the $R(t)$ master curves is the sharp decrease of $R(t)$ compared to the model when approaching the complete stage of chain exchange (*i.e.*, as $R(t) \rightarrow 0$). This was observed for both dilute[76] and concentrated[79] PS-PEP solutions, as well as in PEP-PS-PEP solutions (Figure 5.5), and PS-PEP solutions with added PEP homopolymers (Figure 6.5a). As discussed in section A.2, the uncertainties in $R(t)$ calculation increases as $R(t)$ decreases, since the scattering intensity decreases and approaches to the scattering intensity of a corresponding premixed specimen, which blurred the differences between the $R(t)$ master curves with the model for small $R(t)$s. This increased uncertainties in $R(t)$, however, cannot fully explain this differences, as it seems the chain exchange is faster than the model predictions, consistently for all the micelle chain exchange mentioned above.

Here we discuss the influence of fluctuations in isotope composition in the mixed micelle cores, which can lead to the overestimation of $I(\infty)$, the scattering intensity of a fully mixed core composed of 50/50 dPS/hPS chains, and subsequently the underestimation

of $R(t)$. Experimentally, $I(\infty)$ is approximated by the SANS scattering intensity of a premixed specimen, which is made by co-dissolving equal amounts of isotope labeled polymers in squalene and the co-solvent dichloromethane, followed by the removal of the co-solvent and thermal annealing. Ideally, complete chain exchange should lead to the even (50/50) distribution of isotope labeled chains, the micelles in a premixed specimen will always contain a distribution of isotope composition, with the averaged composition 50/50. Therefore, the scattering intensity measured from a premixed specimen is always higher than the ideal case of micelles cores composed of exact 50/50 dPS/hPS chains. As shown in equation 1.2, an overestimation of $I(\infty)$ leads to the underestimation of the differences between $I(t)$ and $I(\infty)$, as well as that between $I(0)$ and $I(\infty)$. If the differences in the denominator has a larger impact on $R(t)$, this overestimation of $I(\infty)$ can result in smaller $R(t)$ values compared to model fitting / prediction curves, as $t \rightarrow \infty$ and $I(t) \rightarrow I(\infty)$.

This influence of the fluctuation in the composition of dPS/hPS labeled chains in the premixed specimen can be accounted for by subtracting the composition fluctuation induced scattering I_{fluc} from the measured $I(\infty)$.As the dPS-PEP and hPS-PEP polymers have essentially the same corona block length, the corona scattering terms that appear in $I(0)$, $I(\infty)$, and $I(t)$ are identical, which cancels out in the subtraction operation and do not have impact on the $R(t)$ (see equation 1.2). Therefore, I_{fluc} can be estimated from a $I(q)$ curve simulated using the hard sphere model described in Chapter 2, but only considering the core scattering parts. The last $R(t)$ trace (119 °C) of chain exchange in a postmixed 7PEP specimen (*i.e.*, 1% PS-PEP + 7% PEP in squalene, see Chapter 6) was chosen to be an example. To simulate the $I(q)$ induced by dPS/hPS composition fluctuation, micelle structural parameters (core radius, core radius standard distribution, etc.) obtained by fitting SAXS patterns of a premixed 7PEP specimen were used. Instead of a perfect 50/50 dPS/hPS mixed micelle cores, the I_{fluc} was accordingly calculated for 35/65 dPS/hPS mixed micelle cores. The $R(t)$ was then calculated as:

$$\mathrm{R(t)} = \left(\frac{I(t) - I(\infty) + I_{fluc}}{I(0) - I(\infty) + I_{fluc}}\right)^{1/2} \qquad (A.7)$$

Figure A.4 compares the original $R(t)$ (grey solid symbols) and the corrected $R(t)$ traces (purple open symbols) calculated from the above equation, for 7PEP postmixed solutions chain exchange at 119 °C. The two $R(t)$ traces are plotted using the same shift factors shown in Figure 6.5b. Five other $R(t)$ traces corresponding to lower temperatures are reproduced from Figure 6.5a and also shown in Figure A.4. The blue and red dashed curves are model fits for chain exchange between 1 vol% PS-PEP[76] and 15 vol% PS-PEP[79] micelles in pure squalene, respectively. As shown in Figure A.4, The purple and grey symbols overlap within experimental errors, suggesting that the fluctuation of dPS/hPS composition in the mixed micelle cores of the premixed specimen does not have a significant impact on the $R(t)$ values.

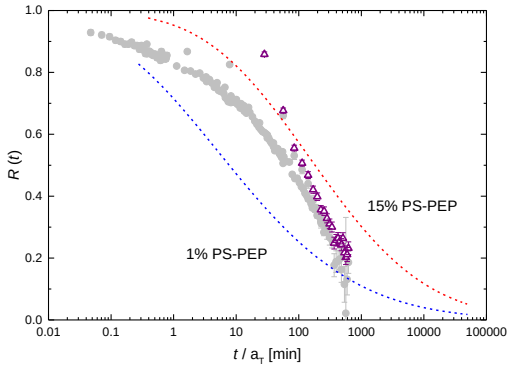

Figure A.4. $R(t)$ master curves for chain exchange in 7PEP postmixed solution, at a reference temperature 110 °C, and shifted using the shift factors shown in Figure 6.5b. The grey traces are reproduced from Figure 6.5a, while the purple trace corresponds to the R(t) calculated using equation A.7 by correcting for the isotope fluctuation induced extra scattering for a micelle core composed of 35/65 dPS/hPS chains. The dashed lines are model fits for 1 vol%, and 15 vol% PS-PEP micelle chain exchange, also reproduced from Figure 6.5a.